

UNIVERSITY OF OKLAHOMA

GRADUATE COLLEGE

EXPERIMENTAL, ANALYTICAL, AND NUMERICAL INVESTIGATIONS OF
GAS LEAKAGE THROUGH ANNULAR CEMENT

A DISSERTATION

SUBMITTED TO THE GRADUATE FACULTY

in partial fulfillment of the requirements for the

Degree of

DOCTOR OF PHILOSOPHY

By

MUSTAFA ABDULSAMAD H. AL RAMADAN

Norman, Oklahoma

2020

EXPERIMENTAL, ANALYTICAL, AND NUMERICAL INVESTIGATIONS OF
GAS LEAKAGE THROUGH ANNULAR CEMENT

A DISSERTATION APPROVED FOR THE
MEWBOURNE SCHOOL OF PETROLEUM AND GEOLOGICAL ENGINEERING

BY THE COMMITTEE CONSISTING OF

Dr. Saeed Salehi, Chair

Dr. Catalin Teodoriu, Co-Chair

Dr. Harold L. Stalford

Dr. Ramadan Ahmed

Dr. Deepak Devegowda

© Copyright by MUSTAFA ABDULSAMAD H. AL RAMADAN 2020
All Rights Reserved.

Dedication

All praise and gratitude go to the almighty Allah for bringing me this far. This dissertation is dedicated to my parents, who have been a source of motivation, inspiration, and encouragement. Also, I would like to dedicate it to my wife (Sarah), my daughter (Yara), my brothers, and my sister for their patience, love, support, and help.

Acknowledgement

I would like to express my appreciation and gratitude to the almighty Allah for showering his blessings on me throughout my life. My deepest gratitude goes to the chair of my committee, Dr. Saeed Salehi. Dr. Salehi was not only my advisor, but also a brother, a friend, and a mentor to me. He was always present whenever I faced any problems and needed help. He taught me how to think out of the box, be resilient, proactive, and professional. I learned so many things under his supervision. From the bottom of my heart, thank you so much Dr. Salehi.

I would like to express gratitude to my co-advisor Dr. Catalin Teodoriu for his help in designing and fabricating the wellbore model. Dr. Teodoriu motivated and supported me during this time. Also, my gratitude is extended to Dr. Ramadan Ahmed for his support and valuable feedback. I am very thankful to Dr. Deepak Devegowda for his help and feedback on the development of the numerical model. Special thanks go to Dr. Harold Stalford for his valuable feedback and support.

I am also grateful to Mr. Jeff McCaskill at the University of Oklahoma Well Construction Technology Center for his help and support during my experiments. My gratitude goes to Dr. Murtada Aljawad, Dr. Chinedum Ezeakacha, Dr. Raj Kiran, Dr. Harshkumar Patel, Dr. Shawgi Ahmed, Mr. George Kwatia, and my friends for their support and consultations.

I would like to extend my appreciation to King Fahd University of Petroleum and Minerals (KFUPM) and Saudi ARAMCO for sponsoring me to earn this PhD. Special thanks to Dr. Abdulaziz O. Al-Kaabi and Dr. Dhafer A. Al Shehri for their help, support, and encouragement. I would like to express my sincere thanks to my brother Dr. Khalid Al Ramadan for his support and encouragement. I am also indebted to the person whom I learned a lot from, Dr. Sidqi Abu Khamsin.

Last, but certainly not least, I would like to extend my deepest gratitude to my wonderful family for their patient, love, support, encouragement, understanding, and help. Thank you for everything you did for me. This academic degree would not have been possible without your support and help.

Table of Contents

Dedication.....	iv
Acknowledgement.....	v
Table of Contents	vii
List of Tables.....	x
List of Figures.....	xi
Abstract.....	xv
1 Chapter 1: Introduction.....	1
1.1 Background.....	1
1.2 Problem Statement and Motivation	2
1.3 Research Objectives	4
1.4 Research Hypotheses.....	5
1.5 Research Scope and Methodology	5
1.6 Dissertation Structure	8
2 Chapter 2: Literature Review	9
2.1 Gas Migration.....	9
2.2 Overview of Well Integrity and Potential Wellbore Leakage Pathways.....	11
2.3 Review of Well Integrity and Potential Wellbore Leakage Pathways According to Current Regulations and Standards	17
2.3.1 NORSOK D-010 (2013): Well Integrity in Drilling and Well Operations	17
2.3.2 International Organization for Standardization ISO 16530-1 (2017): Petroleum and Natural Gas Industries—Well Integrity. Part 1: Life Cycle Governance.	18
2.3.3 API Standards.....	18
2.4 Development of Potential Wellbore Leakage Pathways on the Short and Long Terms	22

2.5	Review of Experimental Studies of Gas Leakage through Cement Column	25
2.6	Review of Wellbore Leakage Models (Analytical, Numerical, and Empirical)	32
3	Chapter 3: Experimental Investigation.....	39
3.1	Scope of Work	39
3.2	Experimental Setup	39
3.3	Test Matrix & Procedure	42
3.3.1	Test Matrix	42
3.3.2	Test Procedure	42
3.3.3	Data Preparation and Calculation.....	43
3.4	Results and Discussions	47
3.4.1	Specimen 1: Class H Cement Without Additives (24hrs of WOC)	47
3.4.2	Specimen 2: Class H Cement Without Additives (12hrs of WOC)	50
3.4.3	Specimen 3: Class H Cement, Latex, and Bentonite (24hrs of WOC).....	52
3.4.4	Specimen 4: Class G Cement Without Additives (24hrs of WOC)	56
4	Chapter 4: Analytical Investigation of the Critical Length of Casing-Liner Overlap	60
4.1	Overview	60
4.2	Methodology.....	60
4.2.1	Model and Leakage Scenarios Assumptions	62
4.3	Results and Discussions	63
4.3.1	First Case (Differential Pressure of 250 psi)	63
4.3.2	Second Case (Differential Pressure of 500 psi).....	64
4.3.3	Third and Fourth Case (Differential Pressures of 1000 and 1500 psi).....	65
4.3.4	Fifth Case (Fixed Permeability and Varying Differential Pressures).....	67

5	Chapter 5: Development of Numerical Gas Leakage Model	69
5.1	Overview	69
5.2	Methodology.....	69
5.3	Model Validation & Verification	75
5.4	Results and Discussions	77
	5.4.1 Parametric Study	79
	5.4.2 Field Case Study.....	91
6	Chapter 6: Summary, Conclusions, and Recommendations	96
6.1	Summary.....	96
6.2	Conclusions	96
6.3	Recommendations and Future Work	98
	Nomenclature	101
	References	105
	Appendix A: Microannulus Gap Sizes in The Experimental Investigation	117
	Appendix B: Data used to Generate the Leakage Scenarios in the Analytical Investigation...	119
	Appendix C: Governing Equations for the Numerical Model.....	128
	Appendix D: Leakage Scenarios Developed by the Numerical Model.....	134

List of Tables

Table 2-1: Standards that have been reviewed in this section.....	17
Table 2-2: Cement systems (Bannister et al. 1984).....	26
Table 2-3: Summary of test results (Stormont et al. 2018)	29
Table 2-4: Results summary of experiments (Kwatia et al. 2019)	31
Table 3-1: Pipe dimensions used to fabricate the wellbore setup	40
Table 3-2: Test matrix for the experimental investigation	42
Table 3-3: Summary of findings from the first tests performed on each specimen	59
Table 4-1: Input data for studying the effect of cement matrix permeability.....	63
Table 5-1: Input data used for model validation	75
Table 5-2: Input data used for model verification	76
Table 5-3: Input data for studying the effect of cement matrix permeability.....	80
Table 5-4: Input data for studying the impact of cement porosity on leakage time	84
Table 5-5: Input data for studying the impact of microannulus gap size	86
Table 5-6: Input data for investigating the impact of cement length on the leakage time	90
Table 5-7: Input data used to simulate the field case scenario	93

List of Figures

Figure 1-1: Leakage pathways in the cement sheath.....	2
Figure 1-2: Well design showing gas invasion into casing-liner overlap (Ahmed et al. 2020)	4
Figure 1-3: Workflow for investigating gas leakage in annular cement	7
Figure 2-1: Major contributing parameters during the cementing process, after (Bonett and Pafitis 1996).....	11
Figure 2-2: Number of wells reported to have had integrity issues (reproduced after Vignes and Aadnoy 2008)	15
Figure 2-3: Number of well integrity failures per 100 drilled wells (Carlsen 2019).....	16
Figure 2-4: Degree of hydration with time (reproduced after Icheim 2017).....	22
Figure 2-5: Mechanical failure modes of cement (Patel and Salehi 2019)	25
Figure 2-6: Flow rate and applied differential pressure with time (Opedal et al. 2018)	28
Figure 2-7: Flow rate against pressure gradient for different casing pipe roughness (Corina et al. 2020).....	32
Figure 2-8: SCP incidents by casing type (Xu and Wojtanowicz 2017)	34
Figure 2-9: Schematic of gas migrating through cemented annulus causing SCP (Xu and Wojtanowicz 2017)	35
Figure 3-1: The schematic of the wellbore setup used in this study	41
Figure 3-2: The real experimental system	41
Figure 3-3: Specimen 1 results using Forchheimer’s equation	46
Figure 3-4: Specimen 1 results using the pulse-decay approach.....	47
Figure 3-5: Specimen 1 results of leakage time at different cement age (Class H w/o additives, WOC: 24 hours)	49

Figure 3-6: Specimen 1 results of wellbore permeability using three methods at different cement age (Class H w/o additives, WOC: 24 hours)..... 49

Figure 3-7: A microannulus bubbling from the cemented annulus in specimen 1..... 50

Figure 3-8: Specimen 2 results of leakage time at different cement age (Class H w/o additives, WOC: 12 hours) 51

Figure 3-9: Specimen 2 results of wellbore permeability using three methods at different cement age (Class H w/o additives, WOC: 12 hours)..... 51

Figure 3-10: Specimen 3 results of leakage time at different cement age (Class H cement with Latex and Bentonite, WOC: 24 hours)..... 52

Figure 3-11: Different bubble sizes from microannuli within the cement sheath in specimen 353

Figure 3-12: Gas transit time for cement slurries formulated with Latex and Bentonite at different temperatures 54

Figure 3-13: Specimen 3 results of wellbore permeability using three methods at different cement age (Class H cement with Latex and Bentonite, WOC: 24 hours)..... 55

Figure 3-14: Bubble size and intensity in specimens 1, 2, and 3 56

Figure 3-15: Specimen 4 results of leakage time at different cement age (Class G, WOC: 24 hours)..... 58

Figure 3-16: Specimen results of wellbore permeability using two methods at different cement age (Class G, WOC: 24 hours)..... 58

Figure 4-1: Schematic of gas migration through liners and liner hangers with different lengths of casing-liner overlap 62

Figure 4-2: First case results of leakage time for different lengths of casing-liner overlap for various permeability values at 250 psi pressure differential. 64

Figure 4-3: Second case results of leakage time for different lengths of casing-liner overlap for various permeability values at 500 psi pressure differential.	65
Figure 4-4: Third case results of leakage time for different lengths of casing-liner overlap for various permeability values at 1000 psi pressure differential.	66
Figure 4-5: Fourth case results of leakage time for different lengths of casing-liner overlap for various permeability values at 1500 psi pressure differential.	66
Figure 4-6: Fifth case results of leakage time for different lengths of casing-liner overlap for a permeability value of 0.5 mD at various differential pressures.....	67
Figure 5-1: Leakage model (a) 3D annular casing cement; (b) side view of the simulated stripe with logarithmic grid system; and (c) top view of the system	74
Figure 5-2: Normalized flow rate for analytical and numerical solutions versus pressure	76
Figure 5-3: Pressure decline match of the experimental data.....	77
Figure 5-4: Pressure profile within the cement sheath at different gas injection times	78
Figure 5-5: Impact of cement matrix permeability on leakage time for $K_c=0.00001$ mD (flow rate at 1000 psi and 110 °F).....	81
Figure 5-6: Impact of cement matrix permeability on leakage time for $K_c=0.0001$ mD (flow rate at 1000 psi and 110 °F).....	81
Figure 5-7: Impact of cement matrix permeability on leakage time for $K_c=0.001$ mD (flow rate at 1000 psi and 110 °F).....	82
Figure 5-8: Impact of cement matrix permeability on leakage time for $K_c=0.01$ mD (flow rate at 1000 psi and 110 °F).....	82
Figure 5-9: Impact of cement matrix permeability on leakage time for $K_c=0.1$ mD (flow rate at 1000 psi and 110 °F).....	83

Figure 5-10: Impact of cement porosity on leakage time (flow rate at 1000 psi and 110 °F)....	85
Figure 5-11: Impact of microannulus gap size on leakage time for $\omega=10 \mu\text{m}$ (flow rate at 1000 psi and 110 °F).....	87
Figure 5-12: Impact of microannulus gap size on leakage time for $\omega=25 \mu\text{m}$ (flow rate at 1000 psi and 110 °F).....	87
Figure 5-13: Impact of microannulus gap size on leakage time for $\omega=50 \mu\text{m}$ (flow rate at 1000 psi and 110 °F).....	88
Figure 5-14: Impact of microannulus gap size on leakage time for $\omega=75 \mu\text{m}$ (flow rate at 1000 psi and 110 °F).....	88
Figure 5-15: Impact of microannulus gap size on leakage time for $\omega=100 \mu\text{m}$ (flow rate at 1000 psi and 110 °F).....	89
Figure 5-16: Leakage scenarios for different overlap lengths and microannulus gap sizes.....	91
Figure 5-17: Actual wellbore schematic at the time of loss of well control (BSEE 2014)	92
Figure 5-18: Gas flow rate with time during the pressure test conducted on the casing-liner overlap (flow rate at 900 psi and 110 °F).....	94
Figure 5-19: Gas flow rate with time during the pressure test conducted on the casing-liner overlap for $K_c=0.01 \text{ mD}$ (flow rate at 900 psi and 110 °F)	95

Abstract

Cementing operations present many difficulties worldwide attributable to shallow flows. Cement sheath integrity and durability play key roles in the oil and gas industry, particularly during the drilling and completion stages. Cement sealability aids in ensuring the well integrity by mitigating/preventing leakage of fluids to surface and adjacent formations. Failure of cement to seal the annulus can lead to serious dilemmas that may result in loss of well integrity.

The use of liners instead of full casings is one of the most common practices for drilling offshore wells. In field applications, the length of a casing–liner overlap is selected randomly. In some cases, shorter overlaps (50 to 200 ft) are chosen because of the lower cost and easy identification of leaks during pressure tests. However, some loss of well control incidents (particularly the incident that motivated this study) has been linked to gas leakage along with the casing–liner overlap.

In this research, cement sealability is investigated experimentally. A novel wellbore model was designed and fabricated to serve the objective of this study. Class H and Class G cements were used. Also, anti-gas migration additives were used to study their impact on the cement sealability. This experimental study showed that cement without anti-gas migration additives cannot seal the annular space nor prevent gas migration. In addition, the wellbore permeability of Class H and Class G cements ranged between 10^{-3} to 10^{-1} mD. Furthermore, wellbore permeability of annular cement increases as cement age increases.

This research also investigated the critical length of the casing–liner overlap and the current casing pressure test duration by modeling gas leakage through the cement placed within the overlap using experimental, analytical, and numerical approaches. Leakage scenarios were developed to mimic gas migration within the cement in the casing–liner overlap.

The modeling results revealed that having longer casing–liner overlap will increase the leakage time of gas to reach the end of the overlap. The results also showed that the current casing pressure test duration of 30 minutes not adequate to verify the cement's integrity within the overlap. Also, the results suggest that the length of the casing–liner overlap should not be less than 300 ft to maintain the integrity of the well in the case of gas influx. Further details are highlighted in the results section. In practice, the rationale behind selecting a casing–liner overlap length is not sustainable. Thus, this study's major advantage is that with field data, it provides both scientific and research-based evidence that can be used to inform the decision behind the selection of the casing–liner overlap length, especially in gas migration-prone zones.

This research's novelty is the development of a numerical model that accounts for gas flow through cement sheath and microannulus. There is no numerical model that considers the flow of gas through cement and microannulus. The model developed in this study is efficient and allows for optimizing design parameters to assess well-design risks. More importantly, the optimum length of casing-liner overlap can be determined for certain particular well conditions.

Chapter 1: Introduction

1.1 Background

Cement integrity is of critical importance to maintaining the integrity of a wellbore throughout the well life cycle. During the drilling and completion phases, cement integrity becomes more crucial due to the dangerous consequences that might occur when the cement integrity fails. The ability of cement to seal the annular space plays a critical role in maintaining the well's integrity by preventing the movement and migration of subsurface fluid to surface and adjacent formations. Cement sealability strongly depends on the cement sheath properties such as, but not limited to, permeability, thickening time, static gel strength, and unconfined compressive strength. Some of these properties are more important than the others during the setting phase of the cement. Cement permeability is a crucial property to resist fluid movement through the cement sheath. An ultra-low permeable cement is desired to prevent fluid flow through the cement and provide excellent zonal isolation.

Annular gas flow through and around the cement can occur during the setting phase of the cement, especially in gas prone zones, and this phenomenon known as gas migration. Annular gas flow can result in catastrophes (i.e., loss of well control, breaching of shallow formation, or a blowout). Annular gas flow is sometimes encountered before installing the blowout preventer (Murray et al. 1995). Gas molecules can migrate through a cemented annulus if the cement is permeable and has poor bonding with formation or casing. In other words, the existence/development of microannuli, induced fractures, and channels (even with an ultra-low permeable cement matrix) allow the gas to migrate through these features rather than the cement matrix itself. Hence, permeable cemented annulus poses many challenges as it endangers the well's integrity. Therefore, wellbore leakage pathways of uncontrolled formation fluids need to be

identified since they provide information on how they can be managed. Potential wellbore leakage pathways can be developed due to defective completion operation or changes in the well over a long period (Ajayi and Gupta 2019). Crow et al. (2010) claimed that the faulty completion operation could result from poor cement placement, poor bonding of cement to casing/rock surface, and cement degradation. More causes for the potential leakage pathways are discussed in the next section. The leakage pathways allow gas to migrate through the cement, even if the cement matrix has a low permeability. Some of these leakage pathways are shown in Figure 1-1.

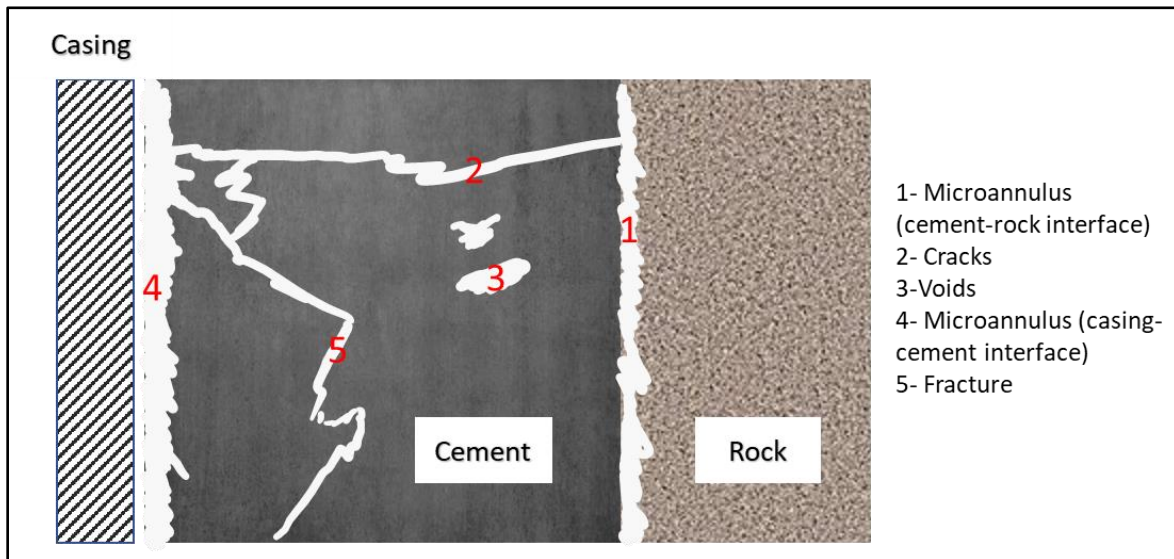


Figure 1-1: Leakage pathways in the cement sheath

1.2 Problem Statement and Motivation

The gas migration phenomenon has been of significant concern since the 1960s. Gas migration has been considered one of the root causes of most loss of well control incidents in the oil & gas industry. This phenomenon, particularly in shallow formations, can endanger the integrity of wells. In offshore drilling operations, liners and liner-hangers in shallow formations, instead of full casing strings, are more susceptible to gas migration. Liner-hangers consist of sealing assembly, which

acts as a barrier to prevent fluid entry from the wellbore. Liners are hung above the last casing shoe, and they are cemented in place. The distance between the top of the liner and casing shoe is known as liner/casing overlap length. In field application, the casing-liner overlap length is chosen arbitrarily, and there is no physical rationale behind this length.

Cement sheath within the casing-liner overlap and the liner hanger's seal assembly are considered a dual barrier system for maintaining a well's integrity (Ahmed et al. 2020). Moore et al. (2002) reported that 30 to 50% of the seal assembly in the overlap failed, and that is according to a survey conducted in 1999 on operators working in the Gulf of Mexico (GoM).

The motivation of this study is stemmed from a well control incident. The incident took place in Main Pass Block (MP-295) in the GoM in 2013 (BSEE 2014). This incident triggered the attention of regulators, companies, and academia to perform more studies on cement and liners. The well had a dual barrier system in the annulus (seal assembly and cement). The crew encountered a gas kick, and the dual barrier system failed, allowing the gas kick to pass through the seal assembly and the cement within the casing/liner overlap. The gas flowed into a shallow sand formation below the conductor casing, as shown in Figure 1-2. Therefore, the seal assembly can fail, but the cement sheath can fail, too, especially if the cement has flaws such as channels or microannulus. Both the cement placed within the casing-liner overlap and the cement placed behind the previous casing leaked. Casing cement can leak through the cement matrix and cement flaws, causing gas accumulation above the cement column, which results in sustained casing pressure.

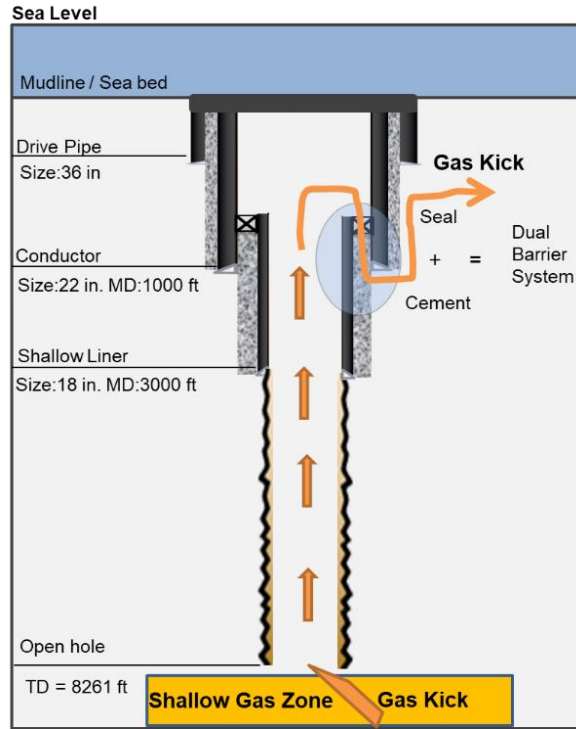


Figure 1-2: Well design showing gas invasion into casing-liner overlap (Ahmed et al. 2020)

Limited experimental and modeling studies have been conducted to investigate the cement sealability and to understand the leak through the developed pathways (Tao et al. 2010a; Rocha-Valadez et al. 2014; Aas et al. 2016; Xu and Wojtanowicz 2017; Stormont et al. 2018; Ahmed et al. 2019a; Corina et al. 2019; Al Ramadan et al. 2019a; Al Ramadan et al. 2019b). Therefore, more experimental and numerical studies are needed to confirm oil well cement's ability to seal the annulus. It is supposed to form a barrier that can prevent fluid propagation and movement. Also, further studies are required to investigate the critical length of casing-liner overlap.

1.3 Research Objectives

One critical benefit of oil well cement is maintaining well integrity by preventing fluid movement and providing zonal isolation for vertical, deviated, and horizontal wells. Therefore, oil well

cement needs to be evaluated thoroughly to maintain wells' integrity and prevent well control incidents. The objectives of this dissertation include:

- Evaluate the ability of the cement to seal as a primary barrier.
- Evaluate the effect of anti-gas migration additives on the cement sealability.
- Evaluate the impact of wait on cement (WOC) time on the cement sealability.
- Investigate the critical casing-liner overlap length using analytical and numerical approaches.
- Investigate the impact of cement matrix permeability, cement porosity, casing-liner overlap length, and microannulus gap size on the leakage time.

1.4 Research Hypotheses

Based on the challenges raised by industry and regulators in terms of primary barrier identification in liner hanger dual barrier systems, the following hypotheses are considered for this research:

- Cement can be considered as a primary barrier if it is properly designed, placed, and tested.
- The critical casing-liner overlap length should be at least 300 ft.
- Casing pressure test duration should be at least 60 min.

1.5 Research Scope and Methodology

The workflow that is used to address the research objectives is shown in Figure 1-3. The methods that have been utilized to conduct this study are categorized into four study methodologies, and they are:

1. *Literature Study*: The aim of the literature study performed in this research is to provide a comprehensive and thorough review of literature on gas leakage through cement sheath. An in-depth revision of gas migration, development of wellbore leakage pathways, experimental and modeling studies of gas leakage in cement sheath was conducted. Also, identification of gaps in the current standard regarding gas migration was performed. The outcome of the literature review provided the baseline for integrating the experimental and modeling studies to achieve this research's objectives.
2. *Experimental Investigation*: Large setups were designed and fabricated to investigate cement sealability. Four major experiments were conducted which composed of 30 tests. Class H and Class G cement were used. Also, anti-gas migration additives were used to study their effect on cement sealability.
3. *Analytical Investigation*: Analytical model was used to investigate the critical casing-liner overlap length. Gas leakage scenarios were developed using an analytical model to assess the reliability of the current requirement of the liner lap length and current regulations regarding pressure test duration.
4. *Numerical Modeling*: A new numerical gas leakage model was developed, and it was validated and verified using the experimental data. This model considered both the cement matrix and microannulus. Leakage scenarios using the numerical model were developed to investigate the critical length of casing-liner overlap.

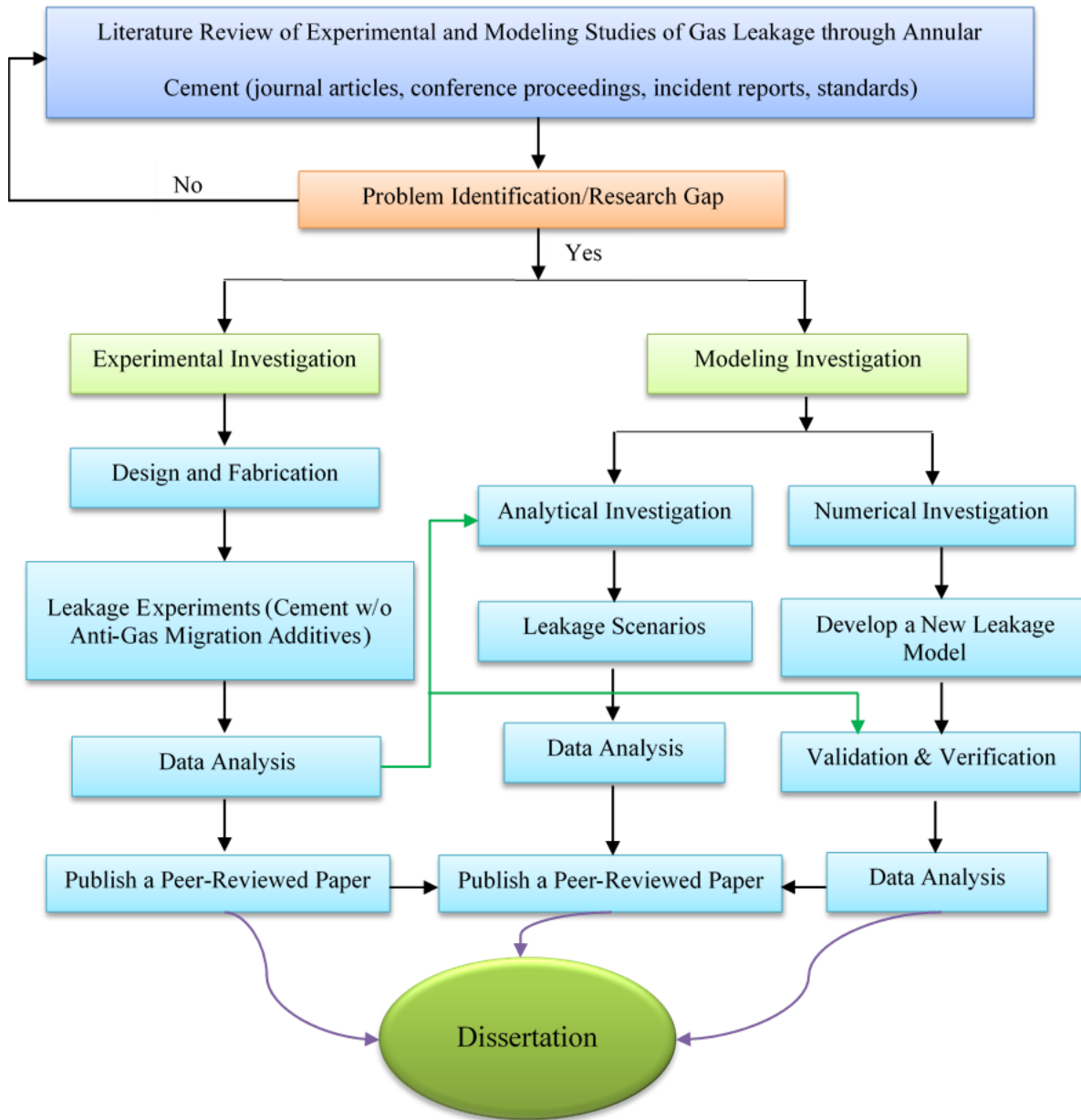


Figure 1-3: Workflow for investigating gas leakage in annular cement

1.6 Dissertation Structure

This dissertation is organized into six chapters. Chapter 1 starts with providing the background for cement integrity and gas migration. It also includes the problem statement and the study's motivation, followed by the research objectives, the research hypotheses, the research scope, and the methodology used to address the hypotheses and objectives. According to the current standards and regulations, chapter 2 provides an in-depth literature review for gas migration, well integrity, and potential wellbore leakage pathways. Also, it describes how the possible wellbore leakage pathways can develop during the life span of the well. Finally, a comprehensive review of experimental and modeling investigations is presented.

Chapter 3 discusses the experimental work performed in this study. The experimental system is described in detail in section **3.2**. The test matrix, test procedure, and data preparation are considered in section **3.3**. Section **3.4** discusses the results of the experimental investigation. Chapter 4 summarizes the analytical analysis of the critical length of casing-liner overlap. Section 4.2 describes the methodology used to develop the leakage scenarios, and it provides the assumption made for the model and leakage scenarios. The results of this investigation are discussed in section **4.3**.

Chapter 5 describes the development of the numerical gas leakage model to investigate the critical length of the casing-liner overlap. The methodology of developing the numerical leakage model is described in detail in section **5.2**. Model validation and verification are discussed in section **5.3**. Then, the findings of this numerical model are discussed in section **5.4**. This section includes parametric study of different variables and their impact on the leakage time. Also, it investigates the critical length of casing-liner overlap by developing leakage scenarios. Finally, it presents a field case study based on the developed numerical model. Chapter 6 includes the summary of this study, conclusions drawn based on all investigations, and future work that should be considered.

Chapter 2: Literature Review

2.1 Gas Migration

Gas migration can be defined as “*Gas entry into a cemented annulus with the potential to provide a flow path into the wellbore for gas, water, and hydrocarbons*” (Kwatia 2018). During primary cementing, gas migration is considered one of the critical issues in the oil and gas industry for many years (Abbas et al. 2014). If not detected, such an issue might lead to loss of zonal isolations, loss of well control, and disasters such as blowouts and groundwater contamination.

Several factors can cause gas to migrate through the cemented annulus. According to Nelson and Guillot (2006), there are two root causes of gas migration: i) annular hydrostatic pressure reduction; and ii) pathways in annulus resulting in gas intrusion. Talabani et al. (1997) categorized gas migration into three types. Void generated between the cement sheath and the casing is considered the first type of gas migration where the gas can flow through that void. To mitigate this type of gas migration, the optimum amount of magnetite is added to the cement mixture. The second type takes place via the void developed between the cement and the wellbore wall caused by the formation of filter cake. A buildup of filter cakes leads to poor bonding between the cement and the wellbore. This type can be mitigated by adding Anchorage Clay that will improve the bonding between the cement and the wellbore. The third type of gas migration is caused by the reduction of cement hydrostatic pressure during the cement transition from a liquid phase to a solid phase. This type is also known as primary gas migration.

Figure 2-1 shows the main parameters that cause gas to migrate in a cemented annulus. Bonett and Pafitis (1996) reported three essential practices that are to be considered to achieve better cementing and mitigate gas intrusion, i) density control; ii) mud removal; and iii) slurry design. Slurry density is vital since it is controlling the cement hydrostatic pressure. During cement placement, gas migration can occur if the cement hydrostatic pressure is lower than the formation

pore pressure. Therefore, slurry density must be designed appropriately to overcome gas migration during cement placement.

On the other hand, designing high slurry density might lead to loss circulation and fracturing the formation if it is higher than the formation fracture pressure. Therefore, the slurry design should consider both the formation pore pressure and fracture pressure. Drilling mud removal is an essential step before cementing operation to achieve good cementing and prevent gas migration. Poor mud cake removal will create pathways for gas to migrate; therefore, mud cake must be removed properly to mitigate gas migration. Appropriate cement slurry design is another essential key for attaining effective cementing operation. Several gas migration control additives can be mixed with cement to resist gas migration. The use of fluid loss control additive in cement slurry is also crucial to prevent gas migration. Fluid loss from the cement slurry into the formation leads to volume reduction that will cause the annular hydrostatic pressure to decrease, allowing gas to migrate.

Throughout the years, several additives have been formulated and developed to address gas migration issues. Anti-gas migration additives include microsilica, nanomaterials, latex, etc. The oil and gas industry is exploring nanotechnology to improve cement sealability and material properties. For example, Nanosilica additives have been identified to provide various benefits such as early strength development, final compressive strength, fluid loss characteristics, and acceleration of hydration (Patel 2016; Ahmed et al. 2018; Fakoya et al. 2018; Kimanzi et al. 2019). Expanding cement has also emerged as a promising solution to improve cement bonding by compensating volume shrinkage and microannulus formation after the cement has set. Expanding cement has also been shown to improve the cement sheath's mechanical integrity by minimizing risk of structural failure (Patel et al. 2019). Also, the use of geopolymers as a substitution of

Portland cement to enhance the cement slurry was discussed in the literature (Salehi et al. 2017; Khalifeh et al. 2018).

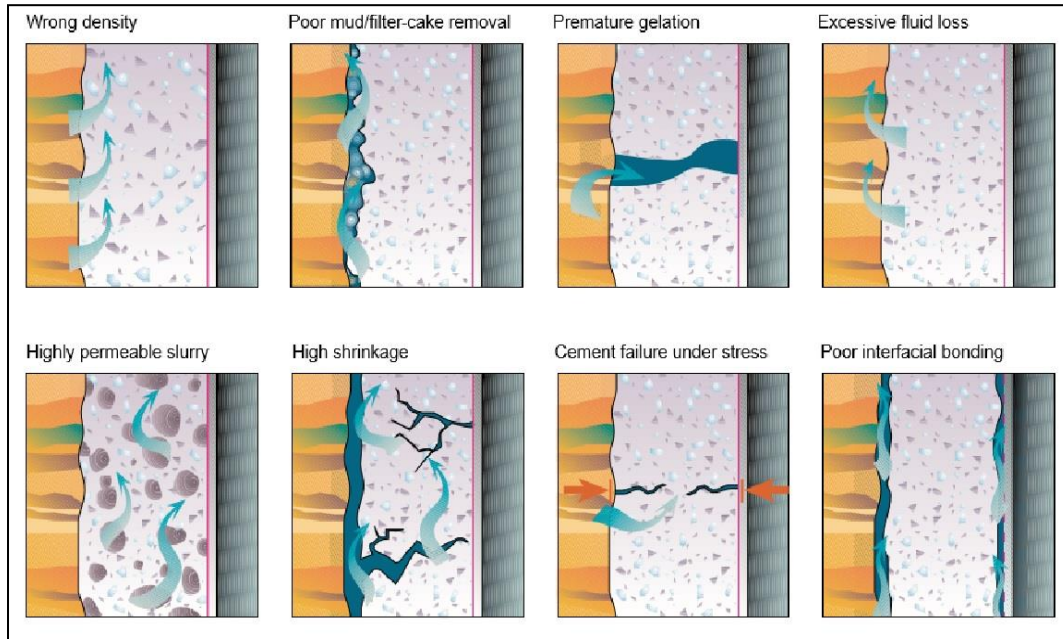


Figure 2-1: Major contributing parameters during the cementing process, after (Bonett and Pafitis 1996)

2.2 Overview of Well Integrity and Potential Wellbore Leakage Pathways

Well integrity has more than one definition that is widely used in the industry. The first definition is “*Application of technical, operational, and organizational solutions to reduce the risk of uncontrolled release of formation fluids throughout the life cycle of the well*” (NORSOK D-010 2013). In another definition (ISO 16530-1 2017), well integrity is defined as “*Containment and prevention of the escape fluids to subterranean formations or surface.*” Both of the definitions above focus on mitigation and prevention of fluids trapped in formations, fractures, and cavities into the wellbore or through the cement. These standards focus on improving oil and gas wells’ safety to prevent health, safety, and environmental impacts. Well integrity must be maintained across all the phases of the well life cycle: drilling, completion, production, and plug and

abandonment (P&A) phases (Davies et al. 2014; Nygaard et al. 2014; Kiran et al. 2017; Kristiansen et al. 2018; Phi et al. 2019). Well integrity concept has been a hot subject in recent years. Many researchers are trying to enhance well integrity due to the reported failure to maintain the integrity of a well, resulting in catastrophes such as blowouts. Therefore, well integrity is being studied to ensure the crew's safety, environment, well, and rig. To ensure a well's integrity, well barriers must be used.

Before diving into well integrity and potential leakage pathways, it is crucial to define some terms used heavily in standards, regulatory guidelines, and literature. The first term is well barrier. "Well barrier" has no common definition in regulatory guidelines or standards. However, well barrier can be defined as an object or practice that redounds to the overall system reliability by inhibiting formation fluids from flowing if installed/appropriately used (API RP 96 2013). According to PSA (2013), another definition of well barrier is any technical, operational, and organizational elements that aim to mitigate/prevent any disaster or accident from occurrence or reduce its destruction.

"Barrier system" is defined as "*one or more barriers that act in series to prevent fluid flow*" (API 65-2 2010). As per API RP 96 (2013), barrier system is defined as a combination of multiple barriers in one system that perform collectively to prevent the flow of unintended fluids. NORSOK D-010 (2013) represents a barrier system as an envelope of one or multiple barriers that prevent/mitigate the movement of formation fluids into the wellbore, adjacent formation, or the surface. For a barrier system, the well barriers must act in series to prevent fluid movement (API 65-2 2010). "Well barrier element" is defined as "*one or several components that are combined to form a well barrier*" (ISO 16530-1 2017).

According to Torbergsen et al. (2012), the main objectives of a well barrier are: i) prevention of formation fluid movement to the external environment during drilling and production phases; ii) shut-in the well immediately in case of an emergency to inhibit the movement of fluid to the surface. To achieve the aforementioned objectives, ISO 16530-1 (2017) and PSA (2013) stated that well barriers must meet several specific performance criteria to ensure the effectiveness of a well barrier. The performance criteria include reliability, functionality, robustness, availability, capacity, accessibility, integrity, ability to withstand loads, effectiveness, expertise, survivability, and mobilization time.

To ensure the integrity of a well, a minimum of two independent well barriers have to be used against the unintended flow of formation fluids (API RP 96 2013; NORSOK D-010 2013; PSA 2013; ISO 16530-1 2017; API 65-1 2018). The independent barriers are categorized into primary and secondary barriers. A primary barrier is defined as the first protective barrier element(s) that interact with the pressure source. The secondary barrier is usually not in communication with fluid or pressure; however, it interacts with the unintended fluid flow whenever the primary barrier fails to contain it. According to ISO 16530-1 (2017), a well barrier can be classified into a primary or a secondary barrier based on the life cycle phase. Here is a list of well barrier elements that can be considered as primary barriers, depending on the operational phase of the well (ISO 16530-1 2017):

- Cap rock
- Drilling fluid
- Casing cement
- Production casing
- Completion string

- Subsurface safety valve

The secondary barrier, as stated earlier, works as a backup when the primary barrier is breached to contain the unintended fluid flow to the surface. Here is a list of well barrier elements that can be used as secondary barriers, depending on the operational phase of the well (ISO 16530-1 2017):

- Impermeable formation
- Blowout preventer (BOP)
- Completion fluids
- Casing cement
- Liner, liner-hanger, and seal assembly
- Tubing hanger with seals

In 2006, a survey was conducted by the Petroleum Safety Authority (PSA) in Norway on 406 offshore wells (Vignes and Aadnoy 2008). A total of 75 wells, 18 %, had well integrity failures, issues, or uncertainties, as shown in Figure 2-2. Out of these 75 wells, 27 wells (36%) were injection wells, while others were production wells. Another survey conducted between 2008 and 2009 for the same area showed that 26 % of the wells, 452 out of 1741 wells surveyed, had integrity issues and failures (Vignes 2011).

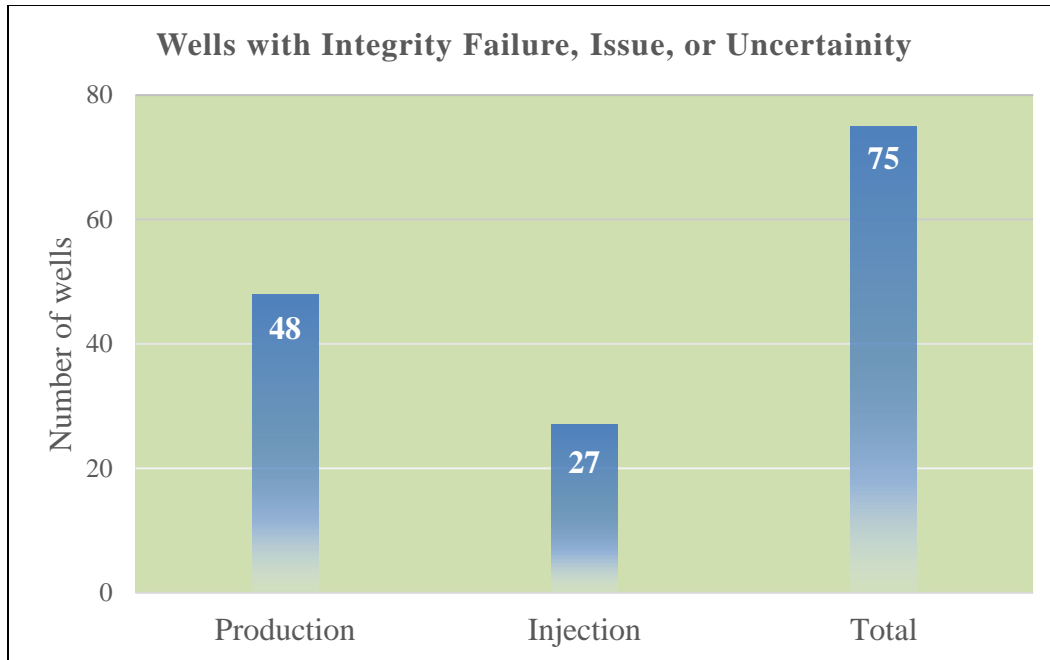


Figure 2-2: Number of wells reported to have had integrity issues (reproduced after Vignes and Aadnoy 2008)

According to a survey conducted in 2009, 760,000 wells worldwide were reported to be suffering from well integrity issues (Jafarzade 2014). Around 20% (142,400) of the reported wells were shut-in; half of them were permanently shut-in, while the other half were shut-in temporarily. Also, around 45% of these wells exhibited sustained casing pressure (SCP).

A recent report published in 2019 by Carlsen (2019) surveyed the oil & gas wells in Norway. The author reported the number of well integrity failures per 100 wells drilled between 2000 to 2018 as shown in Figure 2-3. For exploratory drilling in 2018, 15 failures due to well integrity per 100 drilled wells were reported, while four production drilling failures were reported. These numbers were normalized per 100 wells, representing the percentage of wells at this point.

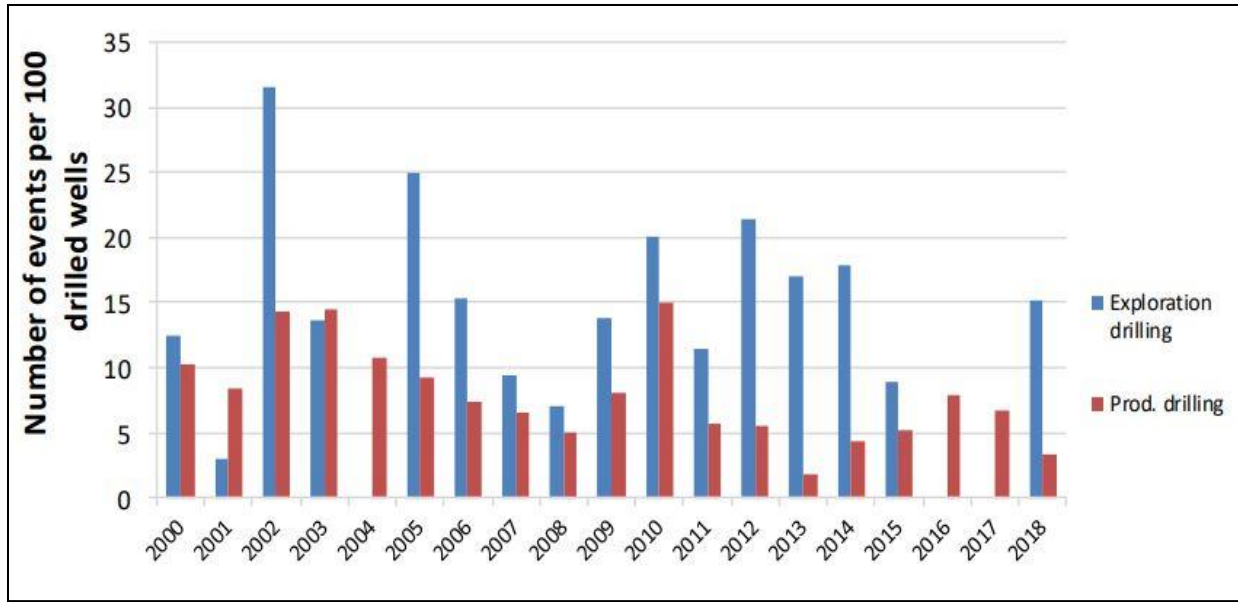


Figure 2-3: Number of well integrity failures per 100 drilled wells (Carlsen 2019)

Well integrity failures are strongly related to the leakage of wellbore. Leakage of the wellbore is usually associated with potential pathways that allow fluids to migrate to surface or adjacent formations. Therefore, identifying and detecting the possible wellbore leakage pathways is vitally important since it can provide information on how the wellbore is leaking and how they can be treated or controlled (Ahmed et al. 2019b; Ahmed 2020). Some of the potential wellbore leakage pathways are related to cement sheath's mechanical failure. In contrast, others are related to cement properties, chemical reactions, and wellbore environment. Potential leakage pathways can be developed due to defective completion operation or changes in the well over a long period. According to Ajayi and Gupta (2019) and Crow et al. (2010), completion flaws usually occur due to a poor well design, poor bonding between cement and casing, poor bonding between cement and rock surface, and cement deterioration and degradation. According to Kiran et al. (2017), there are three mechanisms of well integrity failures, including chemical, mechanical, and physical. All of these mechanisms are dependent on wellbore leakage (Nelson and Guillot 2006).

2.3 Review of Well Integrity and Potential Wellbore Leakage Pathways According to Current Regulations and Standards

In this section, various standards have been reviewed to discuss well integrity and potential wellbore leakage pathways. Table 2-1 shows the standard codes and titles that are used in this section.

Table 2-1: Standards that have been reviewed in this section

Standard Code	Standard Title
NORSOK D-010 (2013)	Well Integrity in Drilling and Well Operations
ISO 16530-1 (2017)	Petroleum and Natural Gas Industries—Well Integrity. Part 1: Life Cycle Governance.
API RP 96 (2013)	Deepwater Well Design and Construction
API 65-1 (2018)	Cementing Shallow-Water Flow Zones in Deepwater Wells
API 65-2 (2010)	Isolating Potential Flow Zones During Well Construction
ANSI/API RP 100-1 (2015)	Hydraulic Fracturing-Well Integrity and Fracture Confinement

2.3.1 *NORSOK D-010 (2013): Well Integrity in Drilling and Well Operations*

NORSOK D-010 (2013) discusses well integrity in depth during all the phases of a well lifespan. Also, it describes the bare minimum functionality and performance the well barrier elements need to ensure the well's integrity. Also, it provides well barrier schematics, well barrier acceptance criteria, and action procedures for well control during drilling, well testing, completion, production, and abandonment activities. It states that well and rig equipment specifications are not provided or discussed in this standard. This document does not discuss in regard to potential wellbore leakage pathways.

2.3.2 *International Organization for Standardization ISO 16530-1 (2017): Petroleum and Natural Gas Industries—Well Integrity. Part 1: Life Cycle Governance.*

ISO 16530-1 (2017) provides a thorough discussion on well integrity for each phase in the well life cycle. This standard is applicable for the onshore and offshore well(s) despite age, type, or location. This standard categorized the phases of life cycle into six phases, unlike the other standards, and they are given as i) basis of design phase; ii) design phase; iii) construction phase; iv) operational phase; v) intervention phase, and vi) abandonment phase.

This standard briefly indicated some potential leakage pathways; however, no specific details are provided. Potential leakage pathways include subsurface safety valve (SSSV), side pocket mandrel, conductor casing, surface casing, liner hanger (seal assembly), liner cement, and pathways in cement due to poor bonding between cement and casing/rock surface. This standard state that well integrity can be affected by the following aspects of cementing: hole cleaning, casing centralization, cement slurry density, lost circulation, presence of corrosive/high salt content environment, post-cementing practices, and temperature. Also, this standard briefly discusses when barrier elements are permitted or not permitted to leak. Also, it provides an insight of acceptable leak rates for some barrier elements.

2.3.3 *API Standards*

2.3.3.1 *API RP 96 (2013): Deepwater Well Design and Construction*

API RP 96 (2013) focuses on well integrity in the design and construction stages of deepwater wells. It has many well design considerations that should be reviewed carefully when an offshore well is to be constructed. This standard is written to ensure the well integrity in deepwater wells due to the complexity of drilling operations and the harsh environment that might jeopardize the wells. It also discusses the well design criteria and equipment associated with drilling deepwater wells. This standard addresses the following points:

- Pinpoints the proper barrier to maintain well control throughout the well's life cycle (drilling, completion, production, and abandonment).
- Load and resistance assumptions are commonly applied techniques to attain high reliable well design.
- Discusses the risk assessment and describes the implementation of mitigation procedures during casing operations.

2.3.3.2 *API 65-1 (2018): Cementing Shallow-Water Flow Zones in Deepwater Wells*

API 65-1 (2018) addresses well integrity from the cementing point of view. It extensively discusses methods intended to prevent and mitigate shallow flows during cementing and post-cementing operations for deepwater wells. Casing cement is considered one of the potential wellbore leakage pathways that can endanger the well's integrity. This standard aims to maintain the well integrity by preventing shallow gas/water migration through and around the cement sheath by improving cement properties. This standard is only applicable to the following well conditions:

- The tophole section(s) of the well.
- Assessment of potential shallow flows.

According to this standard, shallow flows are associated with the following failure modes:

i) insufficient zonal isolation by cement sheath, causing the casing to buckle/shear; ii) communication between shallow formation, resulting to overpressurized formation; and iii) invasion of shallow flows to mudline, causing a disturbance on the seafloor.

This standard discussed one of the potential wellbore leakage pathways: flow channels through and around the casing cement. They attributed the development of flow channels within and around the casing cement to the following causes:

- Poor design of cement slurry or execution of primary cementing.
- Flow occurring due to dilution during cement placement.
- Poor hole cleaning and condition.
- Lack of using centralizers, which results in poor displacement of mud and poor cement placement in the narrow side of the annulus.
- Cement transition phase from a slurry to a solid, where it has low ability to prevent the flow from formation fluid.

2.3.3.3 *API 65-2 (2010): Isolating Potential Flow Zones During Well Construction*

API 65-2 (2010) addresses methods and practices for preventing the flow of formation fluids and isolating potential flow zones, a crucial component for ensuring a well's integrity. This standard also discusses appropriate barrier elements (including casing cement) and systems during well construction. This standard is only applicable when a potential flow zone needs to be isolated. This standard's first objective is to mitigate and/or control fluid influxes before, during, and post-cementing operation to install casing and liners in wells. The second one is to help in preventing sustained casing pressure (SCP). For SCP, API RP 90 (2006) provides extensive guidelines for managing wells that exhibit this phenomenon.

Some potential leakage pathways in cement, such as microannulus and voids, are described in this standard. The development of such cement flaw can jeopardize the well integrity as the fluid can migrate through this feature. It can also lead to SCP. Microannulus can develop due to dimensional cement shrinkage. Shrinkage of cement occurs due to the hydration of cement. The volume of final products of the reaction between water and cement, is less than the initial volume, hence, cement might shrink. Also, microannulus can be created due to pressure cycles (also pressure testing) as the casing expands and contracts. Microannulus can also be developed due to

the pipe movement at the time of hanging the casing to activate the seal assembly in liner-hangers. This movement can only cause such a flaw in the cement once the cement gel strength has developed. Therefore, cement properties must be enhanced, and recommended practices should be followed to decrease the likelihood of microannulus creation. Microannulus development scenarios in casing and liners have also been discussed in this standard as follows:

1. Holding pressure inside casing/liner as cement slurry cures.
2. Hole fluid level is not kept full.
3. Casing movement during the WOC.
4. A lighter fluid replaces the cement displacement fluid.
5. If the replacement fluid is much cooler than the displacement fluid.
6. Casing pressure tests are performed:
 - a) After the cement starts to gain static gel strength (SGS) during WOC.
 - b) After the cement sets at a test pressure above the cement's tensile strength.
 - c) Repeatedly during the life of the well that exceeds the cement's fatigue limit,
7. Mechanical seals are activated before the cement has gained enough structural integrity to resist pipe expansion from loss of hydrostatic head pressure in the annulus.

2.3.3.4 ANSI/API RP 100-1 (2015): Hydraulic Fracturing-Well Integrity and Fracture

Confinement

ANSI/API RP 100-1 (2015) discusses well integrity during the construction phase of onshore wells. Also, it provides recommended practices for fracture stimulation design to ensure fracture containment and maintain the well integrity. This standard is crucial especially for wells that undergo hydraulic fracturing. The hydraulic fracturing job design might fail during the operation where the fracture can grow uncontrollably and go beyond the designed interval. Hence, this

fracture might hit the cap rock, resulting in a potential leakage pathway for hydrocarbons to escape from reservoir rock. This standard also provides cementing consideration for wells that will undergo hydraulic fracturing due to the damage that might occur to cement during this operation. Potential leakage pathways can be developed during hydraulic fracturing, which might jeopardize the integrity of the well.

2.4 Development of Potential Wellbore Leakage Pathways on the Short and Long Terms

Leakage pathways can develop early during cement hydration reactions. Cement does not thoroughly hydrate in hours or days; it takes a long time for the cement to hydrate fully. Figure 2-4 shows the degree of hydration for cement and all the major crystalline compounds as they hydrate with time. As the cement slurry hydrates, the slurry volume starts to reduce due to the reaction between water and the chemical compounds. This reduction in the cement volume is known as cement shrinkage. According to Yodsudjai and Wang (2013), cement shrinkage occurs due to several reasons, such as hydration, thermal contraction, and phase transition. Volume reduction of cement can vary between 1% and 6% depending on the cement slurry design (Chenevert and Shrestha 1991; Yodsudjai and Wang 2013).

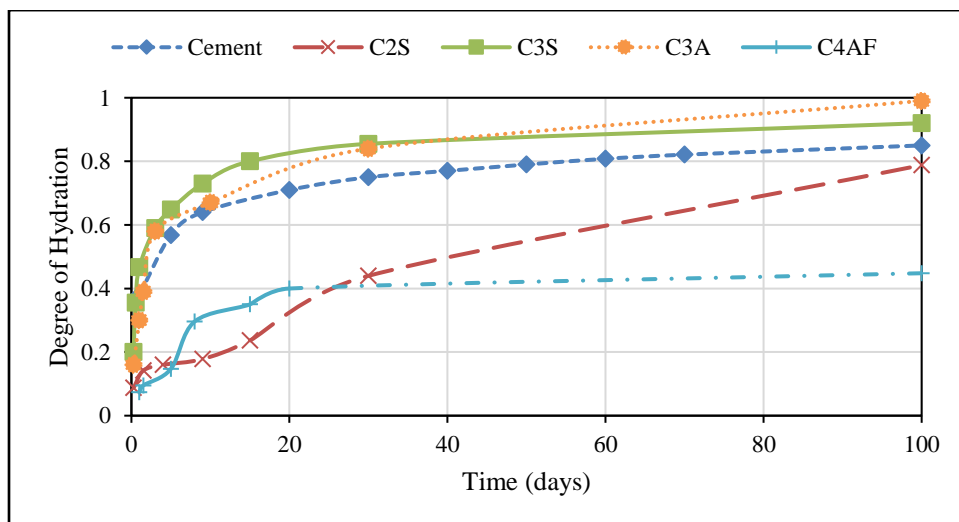


Figure 2-4: Degree of hydration with time (reproduced after Icheim 2017)

For gas migration to occur, two conditions must occur that will allow gas to flow through and around the cement sheath (Stiles 2006). These conditions are i) Underbalanced condition; and ii) A potential leakage pathway along the cement column. Four forms of wellbore leakage pathways can be developed. These forms are channels within the cement sheath, pathways at the casing-cement interface, pathways at the cement-rock interface, and fractures in a damaged formation. According to Bois et al. (2017), there are three mechanisms associated with leakage pathway development through cement and at the casing-cement interface: i) Cement placement; ii) Liquid-state hydration, and iii) Solid-state hydration and short term.

Several factors influence the development of leakage pathways during cement placement (Carter and Evans 1964; Carter and Slagle 1972; Bois et al. 2017). Mud channels can form a potential pathway once they dehydrate, resulting in cracks. Another factor is poor casing cleaning, which might lower the hydraulic bond between the cement and casing, resulting in microannulus development. Also, cement injection pressure might exceed the formation fracture pressure, hence damaging the formation and creating a leakage pathway.

Several researchers addressed voids' development during liquid-state hydration of cement slurry (Stewart and Schouten 1988; Dubash and Frigaard 2004; Pinto et al. 2012). High fluid loss of cement slurries can result in void spaces within the cement matrix itself, resulting in the development of channels within the cement sheath. The fluid loss of cement slurry influences the development of leakage pathways and free fluid (Webster and Eikerts 1979). Both contributes to the development of voids within the cement sheath and voids at the interface of cement-rock surface.

Hydration reactions will continue even after the cement is wholly solidified (solid-state hydration). The development of leakage pathways during the solid-state hydration has been

discussed in the literature (Bybee 2005; Ladva et al. 2005; Bois et al. 2011; Bois et al. 2012). Shrinkage of cement and reduction in slurry pore pressure can lead to the development of cracks and/microannulus. Also, changes of wellbore fluid density and temperature can damage the cement sheath and create flaws such as cracks within the cement or microannulus. Pressure and thermal cycling can also result in debonding at the casing-cement interface, which can serve as a potential leakage pathway. Leakage pathways can also generate during late life due to mechanical failure of hardened cement.

Mechanical failure of hardened cement can be classified into three modes: i) radial cracking; ii) radial debonding; and iii) shear cracking (Teodoriu et al. 2013; Lavrov and Torsæter 2016; Patel and Salehi 2019; Ahmed et al. 2021). Figure 2-5 shows mechanical failure modes in annular cement and cement plugs. The mechanical failures of cement sheath result in developing potential leakage pathways for fluids to flow through these features. Each one of the failure modes as mentioned above have to meet particular criterion to occur:

- Radial cracking occurs when hoop stress is greater than or equal to the tensile strength.
- Radial debonding takes place when radial stress is greater than or equal to tensile strength.
- Debonding occurs when shear stress is greater than or equal to the cohesion strength.

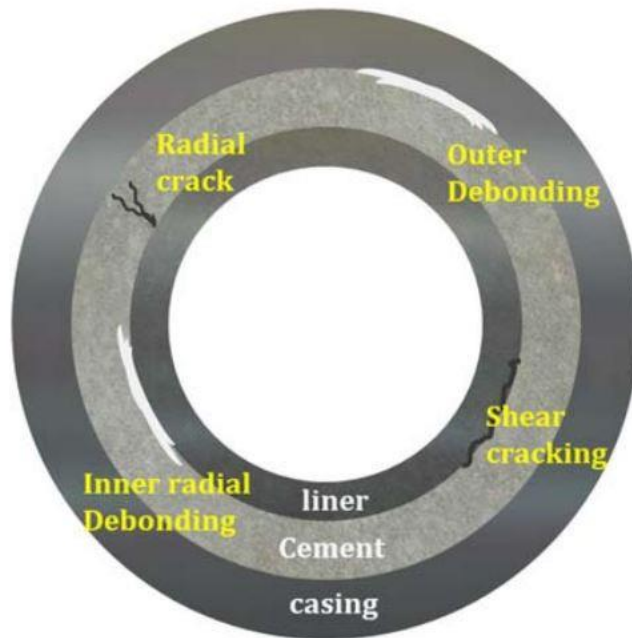


Figure 2-5: Mechanical failure modes of cement (Patel and Salehi 2019)

2.5 Review of Experimental Studies of Gas Leakage through Cement Column

Gas leakage through and around cement sheath has been an issue for oil & gas wells since 1960's. Failure to prevent and mitigate gas migration can lead to well control incidents, contamination of freshwater formation, and catastrophes like blowouts. Researchers have been working to understand the causes of gas leakage and find a solution to this problem. Also, field case studies on gas migration were reported in the literature. (Watters and Sabins 1980; Grinrod et al. 1988; Al-Buraik et al. 1998). Over the years, especially in the last four years, experimental investigation of gas leakage in cemented annulus has gained recognition as an applied approach to evaluate the cement sealability. In this section, an extensive review of experimental studies that have been conducted for gas leakage in cement column is presented.

Bannister et al. (1984) built an apparatus to mimic gas leakage through annular cement. This experiment's objective was to examine the ability of cement to prevent gas migration at the

transition time where the slurry turns to a solid structure. Two methods were applied to reduce gas propagation through the cement column. The first method was using an impermeable cement filter cake against the gas inlet (where the gas inlet mimics a gas bearing zone). The authors stated that this approach could prevent gas incursion; however, once the filter cake is broken, gas can easily migrate inside the cement column. The other method was to modify the cement slurry by adding an agent to inhibit the gas flow by interacting with the migrated gas inside the cement and forming an impermeable barrier. Several experiments were conducted using a different formulation of cement slurry. They used neat Class H cement and Class H cement with different concentration of the inhibiting agent. The results of this approach showed that the gas flow rate decreased by almost 99% when they used the inhibiting agent, as shown in Table 2-2.

Table 2-2: Cement systems (Bannister et al. 1984)

Cement Slurry	Thickening Time (hr:min)	Flow Rate (cc/min)	
		Before Set	After Set
Class H, 16.27 ppg, 66 °C	2:10	+400	+400
Class H, 16.27 ppg, 0.3% dispersant, 50 L/ton GFPA, 66 °C	2:20	110	-
Class H, 16.27 ppg, 0.37% dispersant, 900 L/ton GFPA, 66 °C	4:03	10	6
Class H, 16.27 ppg, 0.2% dispersant, 140 L/ton GFPA, 66 °C	5:00	1.7	0.2

Teodoriu et al. (2010) fabricated a wellbore model to investigate oil well cements' sealability. The authors used neat Class G cement, and they cured the cement for 21 days under atmospheric conditions. The cement was pressurized and leaked immediately. The authors stated that the injection pressure resulted in a leakage pathway between the cement and the inner pipe. They ran a longer experiment where they applied 28900 pressure cycles on that specimen. The authors reported that the gas leaked through the cemented annulus almost after 500 cycles.

Stormont et al. (2015) built a wellbore model to investigate gas migration through annular cement. In this study, neat Class G cement was used to prepare the cement samples. The cement samples were cured at 55 °C for 14 days. A release film was used to create a 75 μm microannulus on the cement sheath, while they used liquid nitrogen to generate smaller microannulus. The authors reported that the size of the interpreted hydraulic aperture formed by the release film was at least 100 μm, while the aperture size reduces to 40 μm under a confining pressure of 680 psi. The microannulus created by liquid nitrogen had a hydraulic aperture of 10 μm. The authors concluded that the microannulus are affected by the confining pressure more than the casing pressure. Also, they ended that the microannulus acts as fractures in rocks.

Gomez et al. (2017) used a lab scale setup to mimic gas leakage through cement and microannulus experimentally. They used neat Class G cement in their study. The cement specimens were cured at 55 °C for 14 days. They created microannulus intentionally to investigate the behavior of gas flow under different casing and confining pressures. They claimed that as determining pressure increases, the hydraulic aperture of the microannulus decreases. Also, the hydraulic aperture reduction when applying confining pressure depends on the initial hydraulic aperture. The authors stated that the way the microannulus responds to pressure changes might impact the estimate of wellbore leakage.

Opedal et al. (2018) performed a series of experiments to assess cement sealability for P&A applications. They used a neat Class G cement for all the experiments, where they cured the cement samples for 5 days at 290 psi and 66 °C. They used nitrogen gas to pressurize the cement system. The first experiment was conducted with no water on top of the 40 cm cement column. They called this experiment a dry experiment since there was no water on top of the cement. Results from this experiment showed that cement leaked after applying only 15.28 psi. They performed another

experiment similar to the previous one, but this time with 4 cm of water on top of the 40 cm cement column. This experiment was called a wet experiment. They found that the cement plug leaked only after applying 145 psi (10 bars) and more, as it is shown in Figure 2-6. The authors attributed the delay of gas leakage to the capillary effect of water.

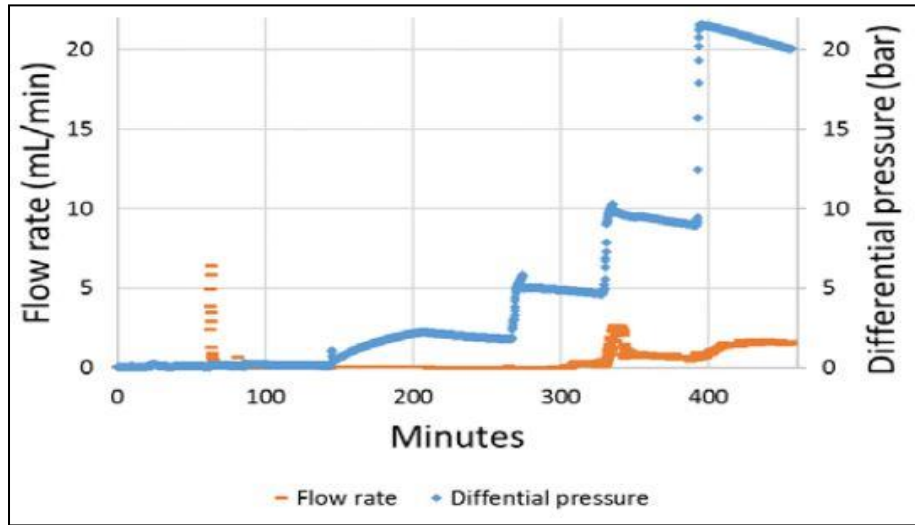


Figure 2-6: Flow rate and applied differential pressure with time (Opedal et al. 2018)

Stormont et al. (2018) published experimental results of gas migration in cement column. This study's objective was to investigate the effect pore, confining, and casing pressures on one of the potential leakage pathways (microannulus). The authors conducted all of the experiments using Class G cement cured at 55 °C for 7 days. A microannulus was purposely created inside 10 of the cement samples, while two other samples were intact. Table 2-3 shows a summary of the experimental data conducted in this study. The hydraulic apertures of microannulus varied from 5 to 118 μm which resulted in permeabilities between 0.6 and 5877 mD.

Table 2-3: Summary of test results (Stormont et al. 2018)

Specimen label	Method to create microannulus	Confining pressure (MPa)	Casing pressure (MPa)	Range of permeabilities (m²)	Range of hydraulic apertures (μm)
I1	N/A	0.7–34.5	0	$< 1 \times 10^{-18}$	< 0.6
I2	N/A	0.7–34.5	0	$< 1 \times 10^{-18}$	< 0.6
R1	Release film	0.7–34.5	0	6.9×10^{-13} – 3.1×10^{-12}	58–95
R2	Release film	4.1–17.9	0	1.1×10^{-13} – 5.2×10^{-13}	32–53
R3	Release film	5.5–13.8	0–13.8	3.0×10^{-13} – 8.4×10^{-13}	44–62
R4	Release film	6.9	0	4.6×10^{-12} – 5.8×10^{-12}	109–118
R5	Release film	0.7–34.5	0	7.5×10^{-14} – 4.9×10^{-13}	28–52
R6	Release film	0.1	0	1.9×10^{-11}	175
T1	Thermally de-bond	4.1–29.0	0	5.9×10^{-16} – 6.7×10^{-15}	5–12
T2	Thermally de-bond	4.1–12.4	0–21.0	6.5×10^{-16} – 9.6×10^{-15}	5–14
C1	Corroded casing	2.1–9.7	0	3.2×10^{-15} – 6.0×10^{-15}	10–12
C2	Corroded casing	0.7–20.7	0	1.6×10^{-16} – 4.3×10^{-15}	4–11

Ahmed et al. (2019a) designed a novel experimental setup to mimic gas leakage through cement and seal assembly by replicating the liner hangers' dual barrier system. This study's objective was to investigate the ability of cement to act as a secondary barrier to combat gas leakage in case of failure of the seal assembly. The authors used neat Class H cement, Class H cement with an anti-gas migration additive, and EPDM elastomer for this study. They intentionally damaged the seal assembly to leak and let the gas propagate through it to the cemented section. They injected nitrogen gas at 10 psig to pressurize the setup and expose the gas's elastomeric seal. The gas penetrated the elastomeric seal and faced the cement sheath. It did not take long for the gas to migrate through the cement sheath and leaked from the other side. However, when Class H cement was mixed with the anti-gas migration additive, the cement did not leak. The authors concluded that neat class H cement cannot be considered a secondary barrier if mixed with an anti-gas migration additive.

Corina et al. (2019) published experimental results of gas leakage in cement. The objective of this study was to evaluate the sealability of cement plug under varying downhole temperatures. They had three slurry designs composed of Class G cement and additives. The additives used in this study were silica-flour in all slurry designs and an expanding agent for one of the designs. The cement specimens were cured for 4 days at 290 psi and 66 °C and 120 °C. The authors claimed that curing cement specimen at elevated temperatures can reduce cement's sealability due to the shrinkage of cement. Results of this study showed an improvement of the cement sealability at elevated temperature when the expanding agent was mixed with cement and silica flour.

Kwatia et al. (2019) performed a series of experiment on gas leakage through cement sheath. This study was also a part of a Bureau of Safety and Environmental Enforcement (BSEE) project conducted at the University of Oklahoma. This study's objective was to find a cement

formulation that can help prevent gas migration through cement column. The authors used Class H cement for all slurry formulations. Also, they used several additives with different concentrations including latex, microsilica, bentonite, fly ash, nanomaterials, and a commercial additive (anti-gas migration additive). Table 2-4 shows a summary of the results for all the experiment conducted in this study. Based on the experiments conducted, the authors concluded the following:

- Cement slurries formulated without anti-gas migration additives cannot prevent gas leakage.
- Microsilica failed to prevent gas migration due to slurry densification and temperature.
- Nanomaterials improved the sealability of the cement.
- The commercial additive used to prepare the cement slurry helped in completely preventing gas leakage through the cement column.

Table 2-4: Results summary of experiments (Kwatia et al. 2019)

Exp #	Density (ppg)	Composition	Leak time (min:sec)	Bubble description
1	16.65	Neat Class H	1 min	3
2	16.65	Neat Class H	5 min	3
3	16.65	1 gal/sack latex, 0.5 % Bentonite	21 min	1
4	14	1 gal/sack latex, 30 % fly ash	21 min 26 sec	2
5	16.05	5.5% microsilica	15 sec	4
6	N/A	12% microsilica	7 sec	1
7	16.55	0.5 % nanomaterials	9 min 54 sec	1
8	14.5	1 gal/sack latex, 30% fly ash, 0.5 % nanomaterial	1 min 14 sec	5
9	16.4	1.5 Liters/100 kg commercial additive from a service company	N/A	0
1 - Tiny inconsistent bubbling, 2 - Tiny consistent bubbling, 3 - Regular bubbling, 4 - Intense bubbling, 5 - Intense bubbling with multiple locations.				

Corina et al. (2020) experimentally studied the effect of pipe roughness on cement plugs' sealing capability. The authors used neat Class G cement and silica-cement. All cement specimens were cured at 290 psi for 4 days. Specimens prepared with Class G cement were cured at 66 °C, while specimens formulated with silica-cement were cured at 120 °C. They used three pipes with different roughness (smooth, moderate, and high). Nitrogen gas was used to pressurize the cement column. This study showed that all the cement plugs leaked in all the three pipes at the time of gas injection regardless of the pipe roughness. Figure 2-7 shows the gas flow rate against the pressure gradient. The authors stated that high surface rough pipes could reduce the gas leak rate by 80-90%.

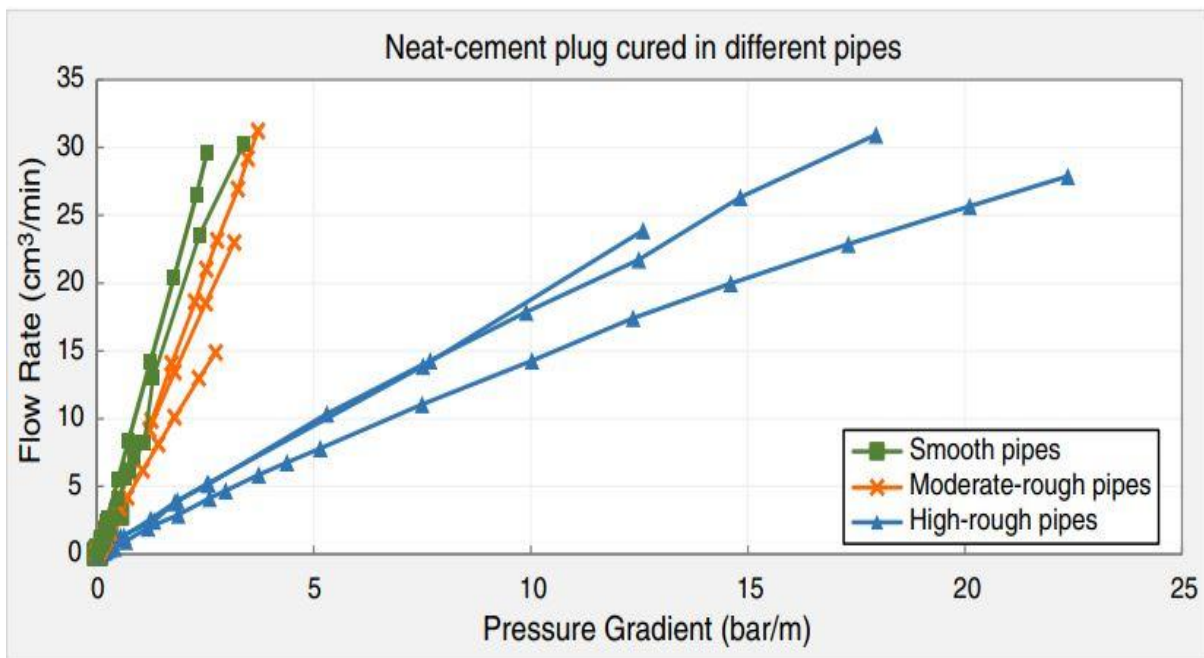


Figure 2-7: Flow rate against pressure gradient for different casing pipe roughness (Corina et al. 2020)

2.6 Review of Wellbore Leakage Models (Analytical, Numerical, and Empirical)

Cement integrity plays a crucial role in maintaining well integrity. As cement slurry starts to solidify and because of the hydration process, pores start to develop inside the cement sheath.

Cement is believed to act as a porous medium that has ultra-low permeability. However, cement flaws such as microannulus, channels, and fractures, can develop and act as a potential leakage pathway that might allow fluids, particularly gas, to migrate through and around the cement. Researchers started to model gas flow through annular cement and cement plugs to better recognize the mechanisms of gas migration in cement. While others tried to empirically predict gas migration (Sutton et al. 1984; Wilkins and Free 1989), various gas flow models through cement have been published in the literature. Some researchers modeled (analytically and numerically) the pressure buildup related to SCP, while others attempted to model gas leakage through cement flaws, and in CO₂ sequestration.

Sustained casing pressure (SCP) can be defined as “ any measurable casing pressure that rebuilds after being bled down, which can be attributed to causing (s) other than artificially applied pressures or temperature fluctuations in the well” (Rocha-Valadez et al. 2014). Poor cementing is considered the main reason for SCP during the early life of the well (Xu 2002; Xu and Wojtanowicz 2017). Poor cementing allow gas to migrate from a gas-bearing zone through and around the cement sheath, which can jeopardize the well integrity. On the other hand, mechanical and thermal stresses can result in cement flaws responsible for the SCP (Goodwin and Crook 1992; Jackson and Murphey 1993). According to a survey conducted on 26 offshore wells in GoM, 22 wells had SCP problems (Xu and Wojtanowicz 2017). Figure 2-8 shows SCP incidents by casing type. This survey showed that 45% of intermediate casings suffer from SCP, followed by surface casing with 24 %.

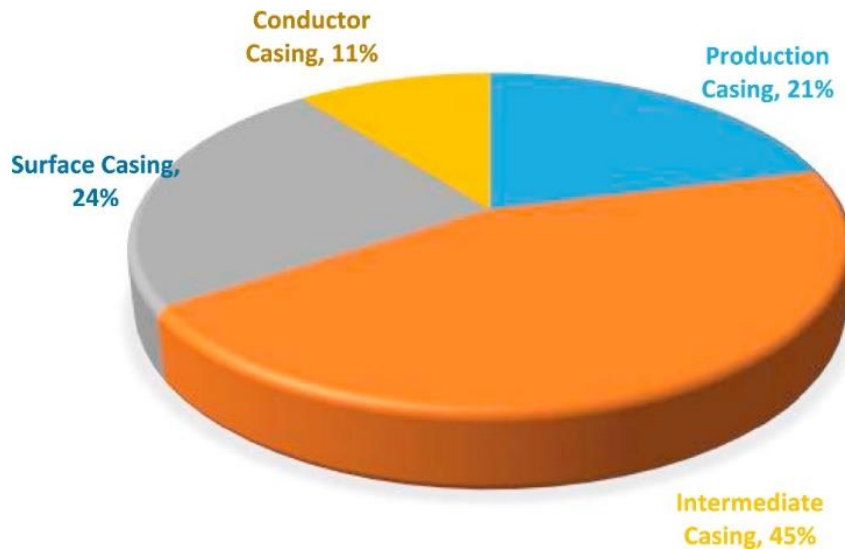


Figure 2-8: SCP incidents by casing type (Xu and Wojtanowicz 2017)

Nishikawa (1999) developed a numerical model for SCP. The author modeled single phase gas flow through annular cement to the surface. Cement was considered as a permeable porous medium in this model. The author studied the effect of cement porosity, gas specific gravity, and temperature on SCP. The author concluded that having lower cement porosity values, gas specific gravity, and temperature will result in higher SCP. This model was never implemented on a field case.

Xu and Wojtanowicz (2001) modeled gas flow through a cemented annulus by developing a mathematical model for diagnosing SCP. This model's objective was to recognize the gas flow mechanisms resulting in SCP and identify the key critical parameters related to gas flow; hence, it can be used in selecting some corrective steps. Figure 2-9 shows a schematic of gas flow through cemented annulus where the gas accumulates at the top of the cement column. According to this study, some parameters controls SCP buildup including cement permeability, compressibility of mud, and gas invasion zone. Based on the results, the authors stated that the early stage of SCP is greatly impacted by cement permeability and mud compressibility. They

also concluded that gas formation pressure has a great influence at the late stages, especially on the stabilized SCP's maximum value. The mathematical model developed in this study was applied in two field cases, and the results were within an acceptable range of the actual results. Xu and Wojtanowicz (2003) extended their mathematical model by accounting for gas flow in the mud column previously ignored. The authors stated that gas flow in the mud column could influence the early pressure buildup, and pressure bleed down.

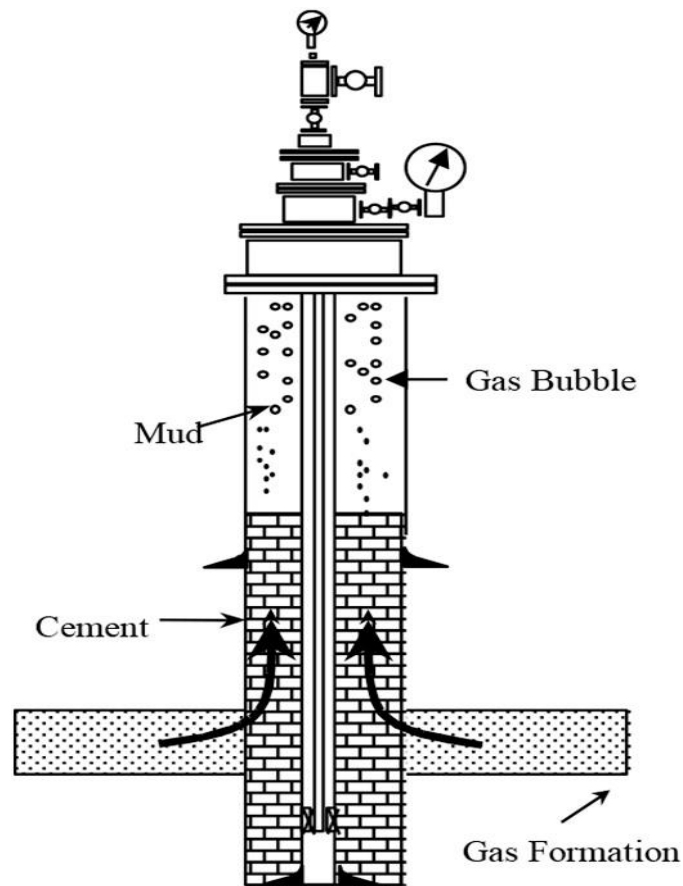


Figure 2-9: Schematic of gas migrating through cemented annulus causing SCP (Xu and Wojtanowicz 2017)

Huerta et al. (2009) simplified the Xu and Wojtanowicz (2003) model and utilized it to quantify the potential leakage of CO₂ wells. They matched their model with field data, which helped them to get crucial information (leakage depth and effective cement permeability). The cement's

effective permeability was converted to geometries of potential wellbore leakage pathways (fractures, gas channel, and microannulus). This model was then used by Tao et al. (2010a); Tao et al. (2010b). The authors modified the CO₂ leakage model to obtain the effective permeability of the potential leakage pathways. They obtained the effective permeability and the gas leakage source depth by matching the SCP data with the model.

Salehi (2013) conducted experimental and numerical investigations of potential leakage pathways in shale gas wells. The objective of this study was to investigate different leakage scenarios in which well integrity can be compromised. The author built a 3D finite element model to achieve this objective. He described the actions involved in the well's phases to examine preceding deformation that arose by extreme loads throughout drilling and stimulation. The model and approach were employed in a field case in the Haynesville shale play.

Rocha-Valadez et al. (2014) developed an analytical solution for an SCP numerical model developed by (Xu 2002). The authors applied some assumptions to develop their model, including gas inflow pressure, which was assumed to be constant. The gas leaked through the cement column would propagate directly to the gas cap without interacting with the mud column. To reduce the number of unknowns, they assumed a value of gas source formation pressure and were left with only cement permeability as an unknown. The authors matched the field data with their analytical solution, which helped them get a cement permeability value in agreement with the value gained from the previous model developed by (Xu 2002).

Aas et al. (2016) performed full-scale tests on cement sheath inside a long casing string. The objective of this study was to assess the ability of cement to prevent water leakage. The authors used conventional and expandable cements. They examined these cement's sealing ability by forcing water to flow through the set cement. The authors stated that the developed microannuli

were reasonably small to a point where they only delivered small flow rates. The authors developed a leakage model based on the tests conducted in this study. The model developed was only based on the flow through the generated microannuli.

Ford et al. (2017) built a leakage calculator based on three existing models to evaluate the leakage rate through and around cement plugs. The authors categorized the flow based on the leakage pathways: i) Leakage through the set-cement; ii) Leakage through cracks and fractures; and (iii) Leakage through microannuli. They treated each one of the pathways individually. For leakage rate calculation within the set cement, they used Darcy's equation. An analytical model developed by Sarkar et al. (2004) was used to calculate the leakage rate through the fractures and cracks. They calculated the flow rate through microannuli using the analytical model developed by Aas et al. (2016).

Stormont et al. (2018) designed a wellbore setup to simulate gas invasion through cement sheath and cement flaws. The experimental objectives and results were discussed thoroughly in the previous section. Besides the empirical study, the authors developed an analytical leakage model for gas leakage through microannuli based on the experiments conducted. Their leakage model was based on the Navier–Stokes equation coupled with the cubic law. The authors stated that the microannuli act like fractures. This model's power is that it considers the gas flow within the mathematical law, unlike the aforementioned models.

Al Ramadan et al. (2019c) developed an analytical gas leakage model for P&A applications. They considered cement as a porous medium with ultra-low permeability and assumed that the gas will only flow through potential leakage pathways (microannulus). Based on the developed model, they built leakage scenarios to assess the current minimum required cement plug length according to NORSOK D-010 (2013) and Oil & Gas UK (2015) standards. The leakage

scenarios were developed by varying the microannulus permeability, differential pressure exerted on the cement plug, and the cement plug's length. The authors conclude the following:

- The leakage scenarios show that increasing the cement plug length will allow a longer time for the gas to leak to the top of the plug.
- It was stated that an increase in the microannulus permeability would yield to a shorter time for the gas to leak.
- The leakage time was lowest for the minimum required plug length (30 m) by Oil & Gas UK standard.
- The leakage scenarios associated with a microannulus permeability of 0.1 mD indicate that 54% of leakage time is less than 50 hours.
- The minimum required cement plug lengths are severely affected by the differential pressures.

Chapter 3: Experimental Investigation

3.1 Scope of Work

Since no study available in the literature has addressed the cement sealability within the casing-liner overlap, the scope of the conducted experiments is to evaluate the cement sealability within the casing-liner overlap, and to investigate the effect of WOC and anti-gas migration additives on cement ability to seal the annular space. Four major experiments were conducted using Class H and Class G cements. Two different WOC times (12 and 24 hours) were used to study WOC's impact on the cement sealability. Anti-gas migration additives (Latex and Bentonite) were used to assess their effect on cement sealability. In all experiments, nitrogen gas (N₂) was used to pressurize the system at 60 psig to evaluate the cement sealability. In each experiment (slurry design), two to three primary pressure cycles were performed and each of these cycles contained at least two to three tests. The pressure decline curves were used to generate the combined permeability. Three methods were used to measure the combined permeability of the system for each test. These were used to evaluate cement sealability and in developing a model for the critical liner-casing overlap.

3.2 Experimental Setup

The wellbore setup designed for the experimental investigation replicates the annular space within the casing and the liner. The wellbore setup is composed of two concentric pipes to create an artificial annulus in between. The top of the wellbore setup is uncovered to expose the cement to atmospheric pressure. Flanges, flange caps, high strength bolts, and gaskets were used to fabricate the wellbore setup and prevent any leaks. Table 3-1 shows the pipe dimensions used to construct the experimental setup. The experiments in this study were performed at ambient temperature and pressure to mimic shallow formations that typically have low pressure and temperature.

Table 3-1: Pipe dimensions used to fabricate the wellbore setup

Length (ft.)	Inner diameter (in)	Outer diameter (in)	Wall thickness (in)
3	6.025	6.625	0.28
4	4.026	4.5	0.237

The outer pipe has four holes drilled and threaded to mount the pressure transmitters and the injection port. The gas injection port is located at the very bottom of the setup. The other holes are utilized to install pressure transmitters to monitor the cement column's pressure at different heights. The data acquisition system (DAQS) is connected to the pressure transmitters to record the pressure readings and display it on a computer screen. Also, three cameras were mounted on top of the experimental system and focused on the top of the annulus to detect gas bubbles appearing on top of the cement column. The video cameras were connected to a network video recorder (NVR) to save all the recordings. Figure 3-1 illustrates the schematic of the experimental setup used to perform the experiments in this study, while Figure 3-2 shows the real wellbore setup used in this study.

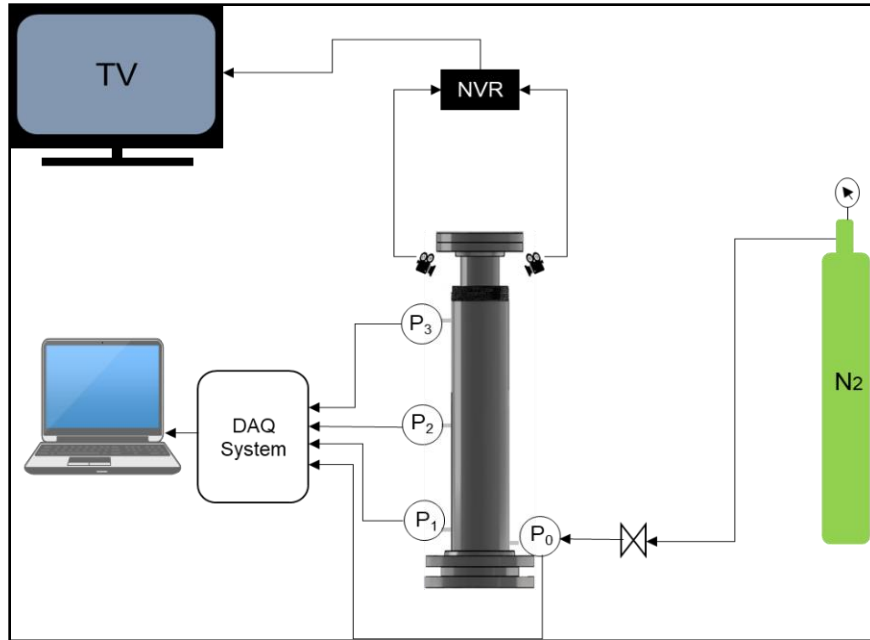


Figure 3-1: The schematic of the wellbore setup used in this study



Figure 3-2: The real experimental system

3.3 Test Matrix & Procedure

3.3.1 Test Matrix

This study's test matrix is shown in Table 3-2. Class H cement was used to formulate the cement slurries for the first three specimens, while Class G cement was used in the fourth experiment. No additives were mixed with the cement for specimens 1 and 2. The difference between them was the WOC time. Cement slurry in third specimen was formulated with Latex and Bentonite with a WOC of 24 hours similar to the first specimen. Cement slurry in the fourth specimen was formulated with neat Class G cement and had WOC time of 24 hours.

Table 3-2: Test matrix for the experimental investigation

Specimen No.	Cement Grade	Additives		WOC (hrs)	Cement Density (ppg)
		Latex (gal/sack)	Bentonite (%)		
1	Class H	N/A	N/A	24	16.65
2	Class H	N/A	N/A	12	16.65
3	Class H	3	1	24	12
4	Class G	N/A	N/A	24	16.65

3.3.2 Test Procedure

Before describing the test protocols, it is essential to describe some terms that would be used frequently in this chapter. First, the term “Specimen” is used to describe different cement slurry formulations. The term “test” is used to describe the nitrogen gas injection through the cemented annulus. A “cycle” is used to describe two to three consecutive tests. For instance, cycle 2 test 2 would mean the second cycle of the second day for a given cement slurry formulation (specimen). In this study, four cement slurries were used. For each specimen, at least two to three cycles were conducted.

The cement slurry was mixed following the API procedures described in API RP 10B-2 (2013). The cement slurry is mixed and poured into the setup. After pouring the slurry in the annulus, the specified WOC time is allowed before the next steps. Before the end of WOC time, the next step was connecting the video cameras and the pressure sensors to the setup and keep them activated for at least 12 hours. After the WOC is completed, a test begins by flowing nitrogen gas through the annulus at the proposed pressure. The nitrogen gas is only injected for 30 minutes. After this time, the inlet gas valve is closed, and the remaining pressure left in the cement annulus is allowed to decline with time. The time for the first bubble appearance is recorded and the area around the annulus where the bubble is observed is marked.

3.3.3 Data Preparation and Calculation

Leakage time can be defined as the time it takes for the Nitrogen gas to travel from the bottom of the experimental setup through the cement sheath column and reach the top. In other words, the time it takes for the first bubble to appear at the top of cement, bearing in mind the time at which the Nitrogen gas was injected.

In each test, one or more positions were bubbling at the same and at different times. Positions were marked and monitored during all tests. The first bubble detected in each position is noted. Also, the time at which the last bubble in each of these positions is noted too. Some of these positions might disappear in the subsequent tests where no gas bubble is coming out anymore from those positions. On the other hand, new positions appeared in some of the subsequent tests.

Two different methods were used to calculate the gas flow rate: the bubble counting method and the quasi-steady method (Jannot and Lasseux 2012). In the bubble counting method, gas flow rate was calculated based on the number of bubbles and bubble's volume using the following equation:

$$q_g = \sum_{j=1}^m \frac{n_j V_j}{t} \quad (3.1)$$

where q_g is the gas flow rate in cc/min, n_j is the number of bubbles at position j , V_j is the volume of bubbles at position j in cm^3 , and t is the time in min.

The recorded videos for all experiments conducted were analyzed to estimate the gas flow rate roughly. Gas flow rate was calculated by counting the number of bubbles coming out from all the bubbling positions. Bubble diameters were measured to get the bubble volume. Each bubbling position was treated separately since the bubbling intensity and volume of bubbles changed from one position to another. To proceed with the permeability calculation, gas flow rate was assumed to be constant after 29 minutes from when the gas was injected. Therefore, the gas flow rate was estimated from the last minute before stopping the gas injection. In the quasi-steady method, equation 3.2 below was used. The flow rate can be calculated at different upstream pressures with equation 3.2 since there is a fixed volume and a constant downstream pressure, which is the atmospheric pressure.

$$q_g = \frac{V}{P_1} \frac{dP}{dt} \quad (3.2)$$

where q_g is the gas flow rate in cc/sec, V is the upstream volume in cc, P_1 is the upstream pressure in psi, and dP/dt is the change in pressure with respect to time in psi/sec.

Three different methods were utilized to calculate the wellbore permeability using the estimated gas flow rates. The methods are the Darcy's method, Forchheimer's (Forchheimer 1901) method, and pulse-decay method (Brace et al. 1968). In Darcy's method, the wellbore permeability is calculated following Darcy's law using equation 3.3. The gas flow rate used in equation 3.3 is the one estimated from the bubble counting method. It should be noted that Darcy's method was

not implemented for some of the tests due to the complexity of counting and/or detecting the bubbles.

$$K = \frac{2000 \times \mu \times q_g \times P_b \times L}{A(P_i^2 - P_o^2)} \quad (3.3)$$

where K is the permeability in mD, μ is the gas viscosity in cP, q_g is the gas flow rate in cc/sec, P_b is the base pressure in atm, L is the length of cement column in cm, A is the annular area in cm^2 , P_u is the upstream pressure in atm, and P_d is the downstream pressure in atm.

The second method used is Forchheimer's method, where the wellbore permeability of the system was calculated based on Forchheimer equation 3.4. This equation accounts for the inertial flow and is written as (Feng et al. 2017):

$$\frac{MA (P_u^2 - P_d^2)}{2zRT\mu L\rho q} = \frac{1}{k} + \left(\frac{\rho q}{\mu A}\right)\beta \quad (3.4)$$

where M is the molecular weight in kg/mol, A is the annular area in m^2 , P_u is the upstream pressure in Pa, P_d is the downstream pressure in Pa, Z is the gas compressibility factor, R is the universal gas constant in J/mol.°K, T is the temperature in °K, μ is the viscosity in Pa-sec, L is the length of the cement column in m, ρ is the gas density in kg/m^3 , q is the gas flow rate in m^3/sec , K is the permeability in m^2 , and β is the inertial coefficient in m.

This equation assumes a steady state condition and can be rewritten as $Y=1/k + \beta X$, where Y is $\frac{MA (P_u^2 - P_d^2)}{2zRT\mu L\rho q}$ and X is $\frac{\rho q}{\mu A}$. Gas flow rate is calculated based on the quasi-steady method and will result in multiple sets of x and y. Plotting the multiple sets will generate a straight line, and the line intercept is equal to the reciprocal of permeability. Figure 3-3 shows the results from specimen 1 using Forchheimer's equation where multiple sets of X and Y are plotted, and they result in a straight line whose intercept is the inverse of the wellbore permeability.

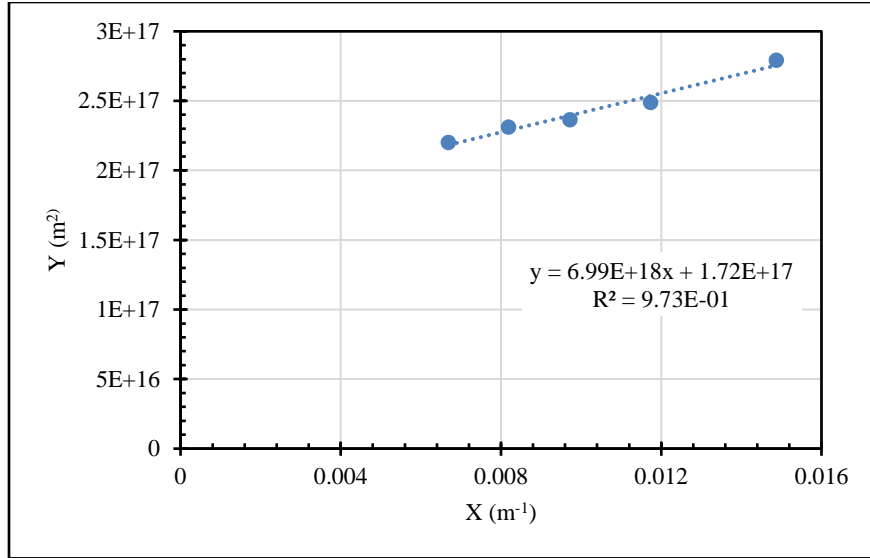


Figure 3-3: Specimen 1 results using Forchheimer's equation

Pressure pulse-decay measurements have been commonly used to measure the permeability of low and ultra-low permeable rocks. This method was developed by Brace et al. (1968) to evaluate the permeability of granite under high pressure. This method does not require steady state condition and as a result, the time it takes to measure the permeability of tight porous media is short. Oil well cement is known to have low permeability values; thus, this method can be applied to measure the cement sheath's wellbore permeability in a shorter time. The wellbore permeability was calculated based on the pressure decline curves using the following equations:

$$P_{u(t)}^2 = P_d^2 + (P_{u(i)}^2 - P_d^2)e^{-\beta t} \quad (3.5)$$

$$\beta = \frac{KA}{\mu V L C_g} \quad (3.6)$$

where P_u is upstream pressure in psi, $P_{u(i)}$ is the initial upstream pressure in psi, $P_{u(t)}$ is the upstream pressure at time t in psi, P_d is the downstream pressure in psi, t is time in sec, K is permeability in

cm², A is area in cm², μ is gas viscosity in dyne-sec/cm², V is volume in cc, L is cement length in cm, and C_g is gas compressibility in cm²/dyne. Equation 3.5 can be rewritten as

$$(P_{u(t)}^2 - P_d^2) = (P_{u(i)}^2 - P_d^2)e^{-\beta t} \quad (3.7)$$

where the left-hand side of the equation can be plotted against time, resulting in an exponential equation with a β exponent. The wellbore permeability can then be calculated from equation 3.6. Figure 3-4 shows the pressure decline curve for specimen 1 using the pulse-decay method, where the exponent of the generated equation is then used to calculate the wellbore permeability. The gas flow rate is not included in calculating the pressure decay method, which is considered an advantage. Using this method allows for comparing the wellbore permeability obtained from the two previous methods, where the flow rates were used in their calculations.

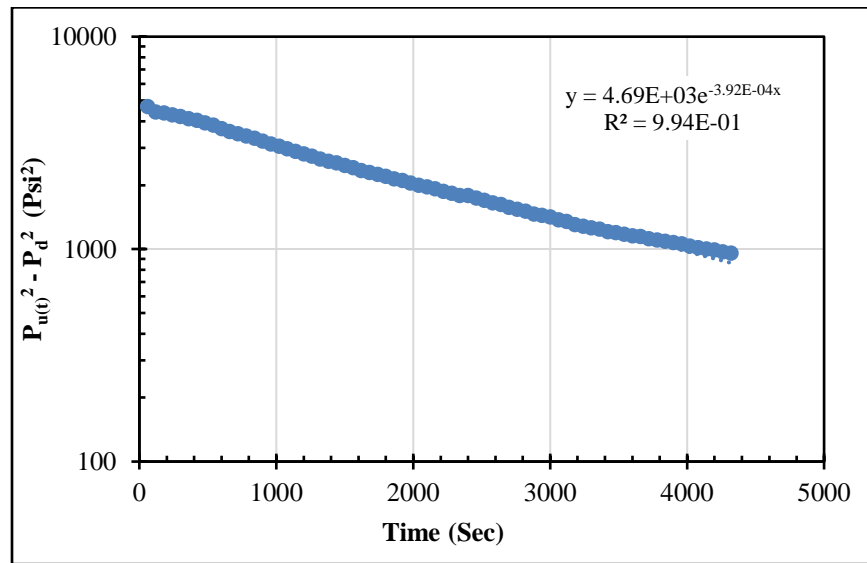


Figure 3-4: Specimen 1 results using the pulse-decay approach

3.4 Results and Discussions

3.4.1 Specimen 1: Class H Cement Without Additives (24hrs of WOC)

Class H cement without additive was used to formulate the cement slurry in specimen 1. This slurry had a 38 % water/cement (W/C) ratio. After 24 hours of WOC time, the first test was

conducted on this specimen. Figure 3-5 illustrates the leakage time for different cement age. The plot composed of three cycles with three tests in cycles 2 and 3, and two preliminary tests in cycle 1. The first bubble was detected in the first test within the first cycle after 11 minutes of gas injection. The second test was conducted when the cement age was 2 days, and the cement sheath leaked 5 minutes after the commencement of the test.

The first test in cycle 2 was conducted after 11 days. The cement leaked after 11 minutes of gas injection, and then leakage time declined for the following tests within the second cycle. This behavior was also observed in the third cycle. The increase in the leakage time between the last test in a cycle and the first test in the following cycle can be attributed to the fallow period between cycles. Another contributor to this behavior can be the fading of some bubbling positions. The phenomenon of fading positions is known as “self-healing” and has been discussed in the literature (Carey 2013; Huerta et al. 2013; Carroll et al. 2016). Self-healing was attributed to the mobilization and precipitation of minerals along the pathways within the cement sheath.

Three methods were utilized to calculate the wellbore permeability for each test. However, the permeability of the first cycle was only estimated using Darcy’s method and that is attributed to the lack of pressure measurements that are necessary for the other methods. In the third cycle, the permeability estimation did not consider Darcy’s method due to the difficulty in counting and detecting the bubbles. The wellbore permeability estimated from the aforementioned methods for all cycles are shown in Figure 3-6. A general trend that was observed is that as the cement age increases, the wellbore permeability increases. Parrott (1995) reported such a trend when measuring the air permeability for different cement specimens for almost 800 days. The estimated permeability values fall under the range of neat Class H cement permeability reported in the literature (Crow et al. 2010; Checkai et al. 2013; Gasda et al. 2013; Kang et al. 2015; Omosebi

2016; Stormont et al. 2018). Neat Class H and G cement permeability value range from 0.001mD to 0.045 mD; they are shown with the red rectangle in Figure 3-6. Figure 3-7 shows a microannulus that is bubbling from specimen 1. It can also be observed that the bubbling is not intense.

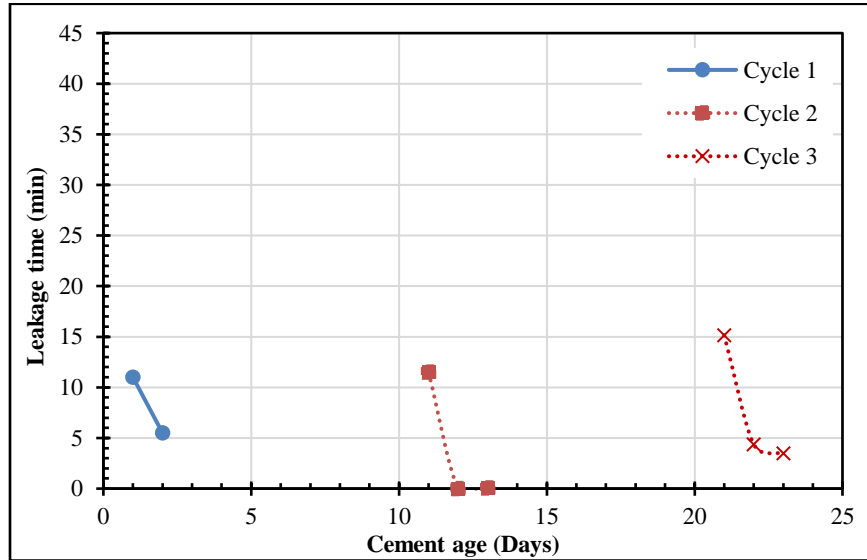


Figure 3-5: Specimen 1 results of leakage time at different cement age (Class H w/o additives, WOC: 24 hours)

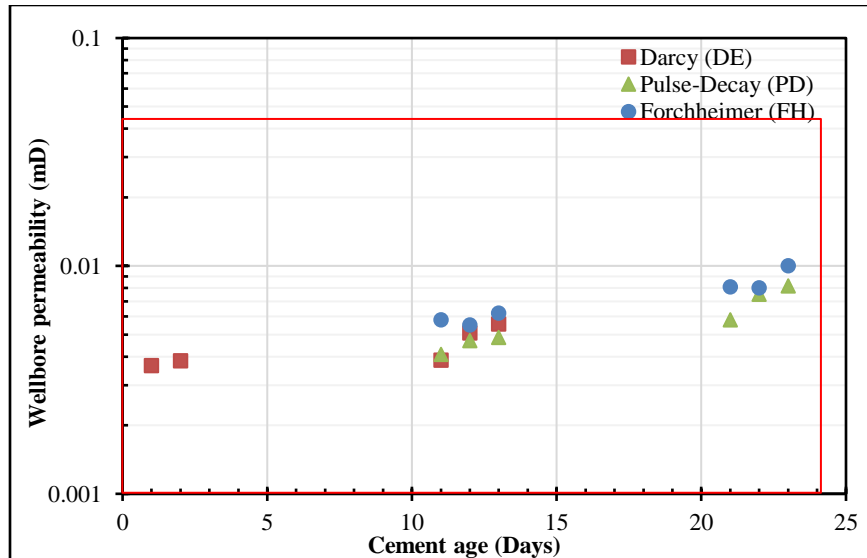


Figure 3-6: Specimen 1 results of wellbore permeability using three methods at different cement age (Class H w/o additives, WOC: 24 hours)

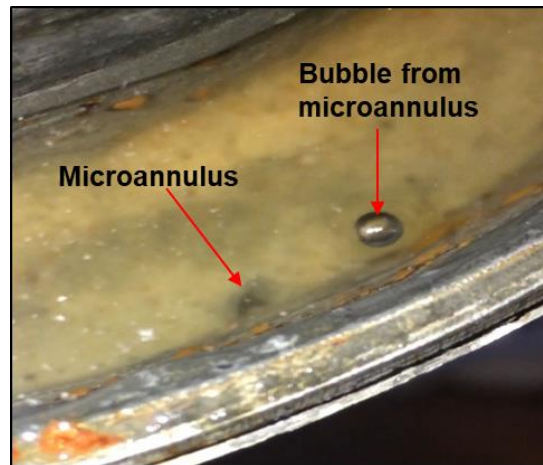


Figure 3-7: A microannulus bubbling from the cemented annulus in specimen 1

3.4.2 Specimen 2: Class H Cement Without Additives (12hrs of WOC)

The purpose of the second specimen was to examine the impact of WOC time on the wellbore permeability. Specimens 1 and 2 were formulated with neat Class H cement; however, the WOC time differed. The first test was performed after 12 hours of WOC. The cement leaked 5 minutes after the commencing the test. Only one cycle was with this specimen since the objective was to determine WOC time's effect on the permeability. The leakage time for different cement age is shown in Figure 3-8. The leakage time increased to almost 14 minutes for the second test performed after eight days of WOC. The “self-healing” phenomenon was also noticed in this test. The wellbore permeability for different cement age is shown in Figure 3-9. The wellbore permeability values were estimated using the three methods, and they fall under the reported values in literature, except the value calculated from Darcy’s method in test 1. A cautious conclusion can be drawn that WOC of 12 hours might not be adequate for the cement to develop an impermeable barrier to seal the annular space and prevent the gas migration.

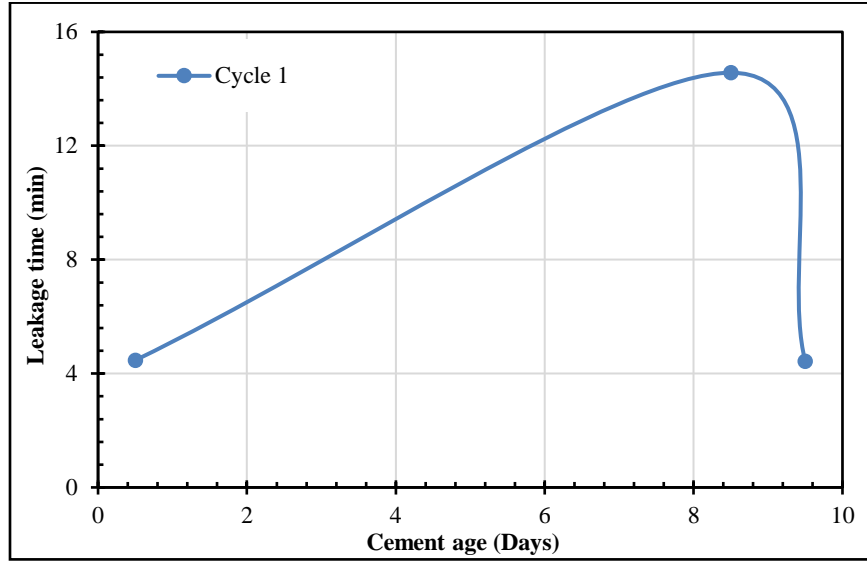


Figure 3-8: Specimen 2 results of leakage time at different cement age (Class H w/o additives, WOC: 12 hours)

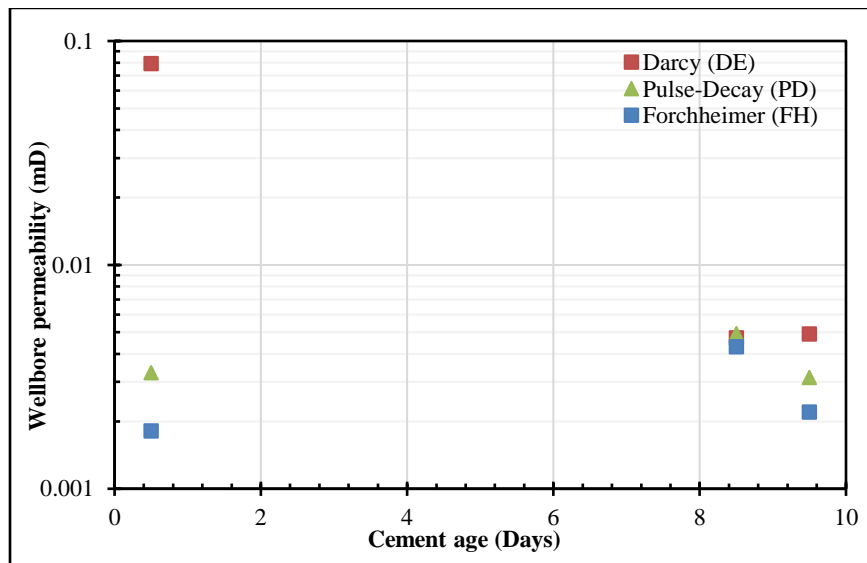


Figure 3-9: Specimen 2 results of wellbore permeability using three methods at different cement age (Class H w/o additives, WOC: 12 hours)

3.4.3 Specimen 3: Class H Cement, Latex, and Bentonite (24hrs of WOC)

Class H cement, 3 gallons/sack Thin Mortar Latex, and 1% of Bentonite were used to formulate the cement slurry for specimen 3. The purpose of the additives mixed with the cement in this specimen was to prevent gas invasion and lower the cement's fluid loss. The first test in the first cycle was conducted after 24 hours of WOC. The cement sheath leaked after 16 minutes from the beginning of the test as shown in Figure 3-10. The leakage time declined in the subsequent tests. The phenomenon of self-healing was not observed in this specimen and that can be attributed to the additives. Latex is a gas migration control additive. Latex develops an impermeable polymer structure within the cement pore spaces, which lowers the cement sheath's permeability. Although, specimen 3 had the highest first bubble appearance time (leakage time) compared to specimens 1 and 2, this slurry was expected to have superior performance by preventing gas migration. Visual observations also suggested that specimen 3 had a higher bubbling intensity than specimens 1 and 2, and that the bubble diameters appeared to be larger as shown in Figure 3-11.

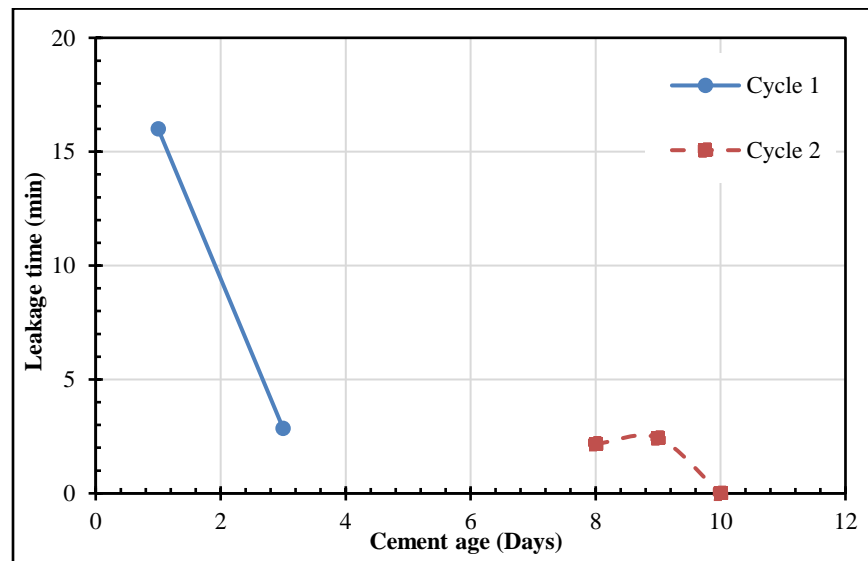


Figure 3-10: Specimen 3 results of leakage time at different cement age (Class H cement with Latex and Bentonite, WOC: 24 hours)

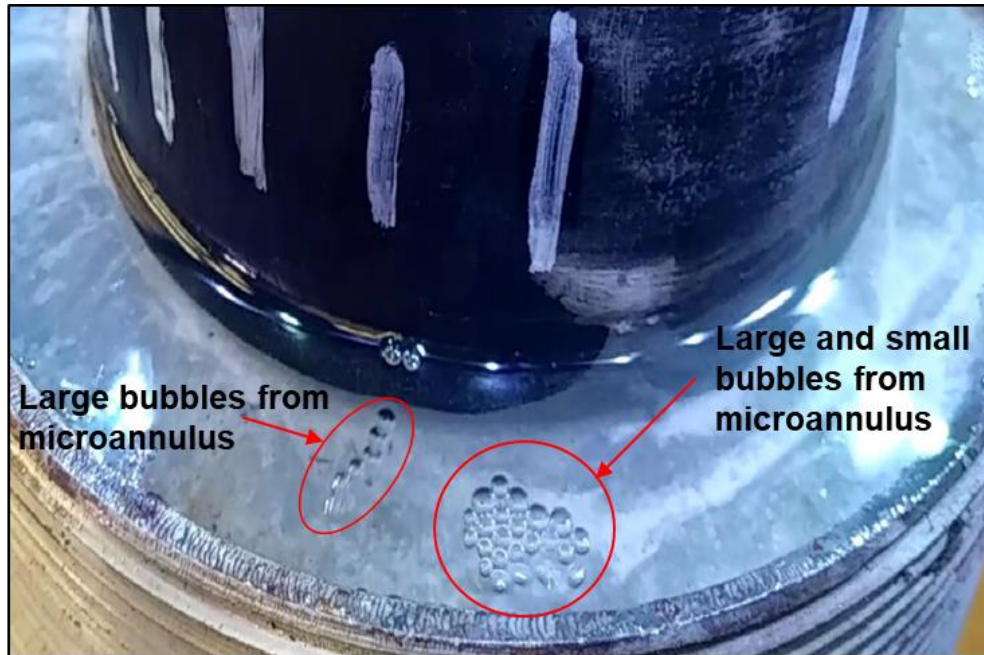


Figure 3-11: Different bubble sizes from microannuli within the cement sheath in specimen 3

The reason behind the reduced performance of specimen 3 is that Latex requires some degree of elevated temperature to activate the polymer chain (Jones and Carpenter 1991; Al-Buraik et al. 1998). This temperature-activated process allows the cross linking of latex polymer chains to form impermeable structures within the cement pores; thus, reducing the pore spaces and impeding the development of potential microannuli. All the tests were conducted at a temperature condition that is not entirely ambient (80°F, temperature of the workshop where the experiments were conducted). Considering the wellbore setup fabricated for this study, it was challenging to simulate elevated temperature conditions.

While this setup was only able to mimic pressure tests at conditions that aren't high, another setup was utilized to characterize one important cement property (gas transit time) used to assess cement sealability and short-term well integrity. Gas transit time is when it takes for the cement slurry to change from a true fluid that can provide hydrostatic pressure to a highly viscous material showing solid characteristics (Sabins et al. 1982). Once the cement slurry starts to develop

adequate static gel strength (SGS) to limit full hydrostatic pressure transmission, the gas transit time begins, and it ends when the cement is solid enough to prevent gas flow. Cement consistometer is used to measure the SGS. Typically, gas transit time is the time it takes the cement's SGS to rise from 100 lbf/100ft² to 500 lbf/100ft².

Figure 3-12 shows the cement slurry's gas transit time formulated with Class H, 3 gals/sack latex, and 1% of Bentonite. The gas transit time was measured at 2300 psi and two different temperatures, 82 °F (to simulate the experimental temperature), and 200 °F (to affect an elevated temperature). It can be observed from this plot that the gas transit time at 82 °F was 90 minutes while it was approximately 34 minutes at 200 °F. In other words, the gas transit time was decreased by 62% with an increase in temperature. This decrease in transit time can be attributed to the temperature effect on cement and the cross linking of latex polymer chains at elevated temperature to form impermeable structures within the cement pores.

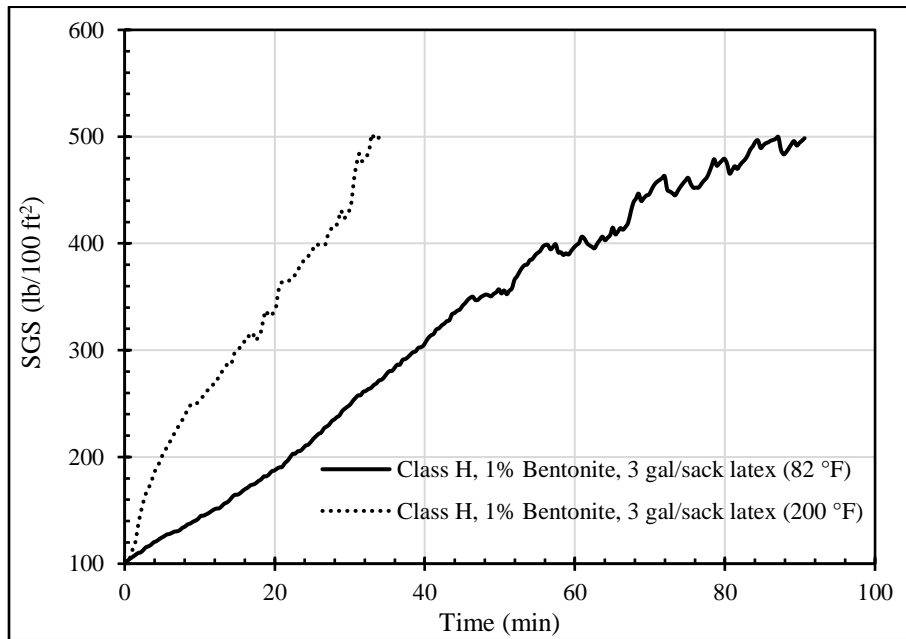


Figure 3-12: Gas transit time for cement slurries formulated with Latex and Bentonite at different temperatures

This slurry's wellbore permeability was higher than values obtained in specimen 1 and 2, as illustrated in Figure 3-13. This can be attributed to the poor formation of the polymer structure within the cement por spaces. Moreover, the wellbore permeability values were not within the range reported in the literature for neat Class H and Class G. Given that this slurry had additives, its permeability values were expected to be lower than those of neat cement, or at least fall within their range. This specimen had severe and big microannuli that resulted in larger bubbles and high bubble intensity than the previous specimens, as shown in Figure 3-14. It can be noticed that specimens 1 and 2 had smaller bubbles compared to those of specimen 3.

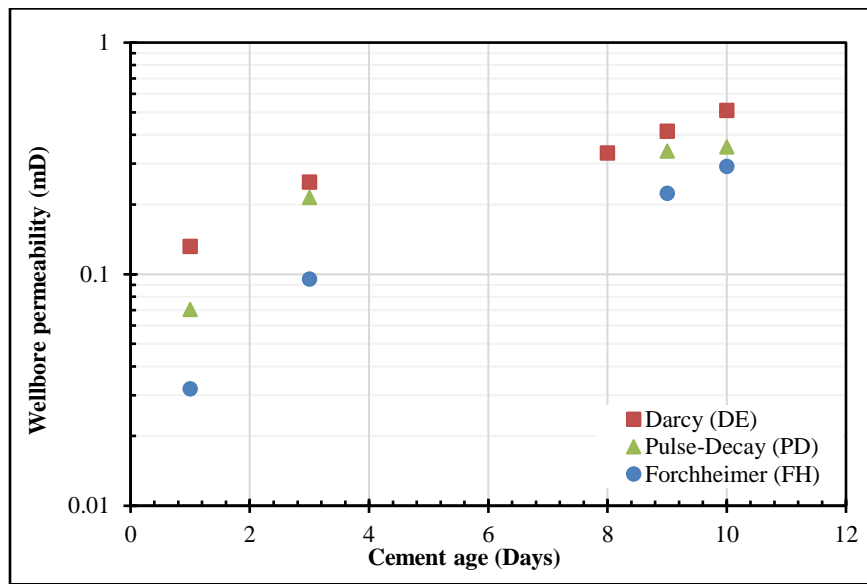


Figure 3-13: Specimen 3 results of wellbore permeability using three methods at different cement age (Class H cement with Latex and Bentonite, WOC: 24 hours)

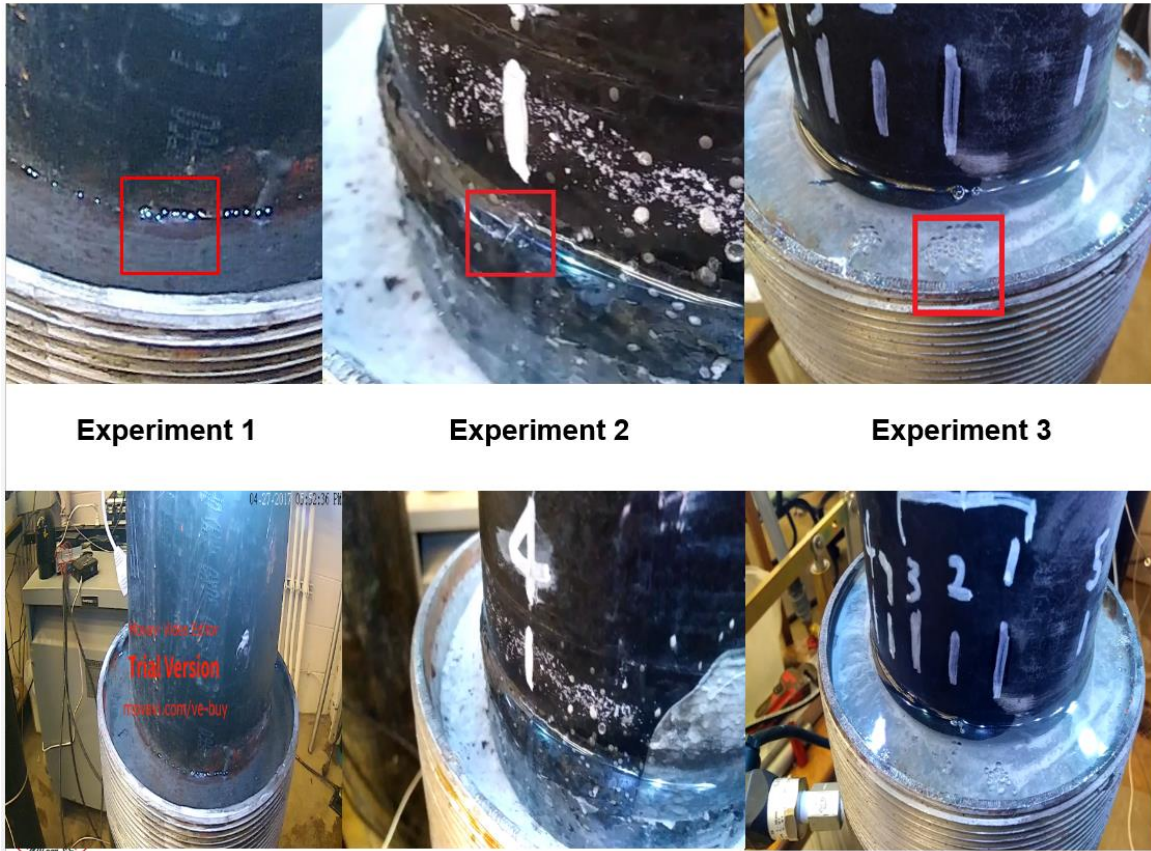


Figure 3-14: Bubble size and intensity in specimens 1, 2, and 3

3.4.4 Specimen 4: Class G Cement Without Additives (24hrs of WOC)

Neat Class G cement was used to prepare the fourth specimen with 44% W/C. The first test was performed after WOC of 24 hours. Specimen 4 had the lowest leakage value compared to all the previous specimens. The leakage time for cement at different cement age is shown in Figure 3-15. The first bubble was detected 13 seconds after the beginning of the test. It can be observed that all the tests conducted on this specimen had a leakage time less than one minute. Only two methods were used to estimate the wellbore cement permeability: pulse-decay and Forchheimer's methods. The naked eye detected bubbles in all the tests, and they were not detected successfully by the video cameras because they were tiny and inconsistent. Therefore, Darcy's method was not used to estimate the wellbore permeability for this specimen. The wellbore cement permeability for all

the tests is shown in Figure 3-16. This specimen's results also show the generic trend of increasing wellbore cement permeability as the cement age increases. This trend was noticed in all the specimens. One possible reason for the increase in wellbore permeability is that the flow path has been created earlier, and as more tests are conducted, the injection of gas will cause the flow path to be eroded; hence, the permeability will increase. The wellbore permeability values of the tests conducted on this specimen are within the range of reported permeability values and the values from both methods were very close.

Table 3-3 summarizes the results of the first test in the first cycle performed on each specimen. Specimen 3 had the highest leakage time which was 16 minutes, and it is believed that the latex was the reason for this increase. On the other hand, specimen 4 had the lowest leakage time, which was less than a minute after the test's commencement. Based on all the methods used to calculate the wellbore permeability, specimen 3 had the highest permeability value compared to the other specimens while specimen 4 had the lowest wellbore permeability value. It is to be noted that the gas flow was laminar in all the tests. The highest Reynold's number in all the tests was 0.35. Further information about flow rate, gas velocity, microannulus gap sizes are shown in Appendix A.

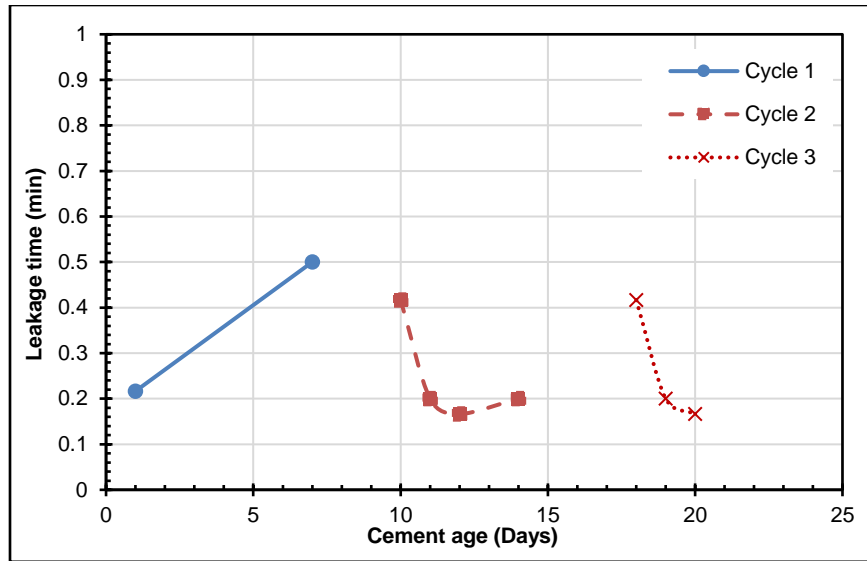


Figure 3-15: Specimen 4 results of leakage time at different cement age (Class G, WOC: 24 hours)

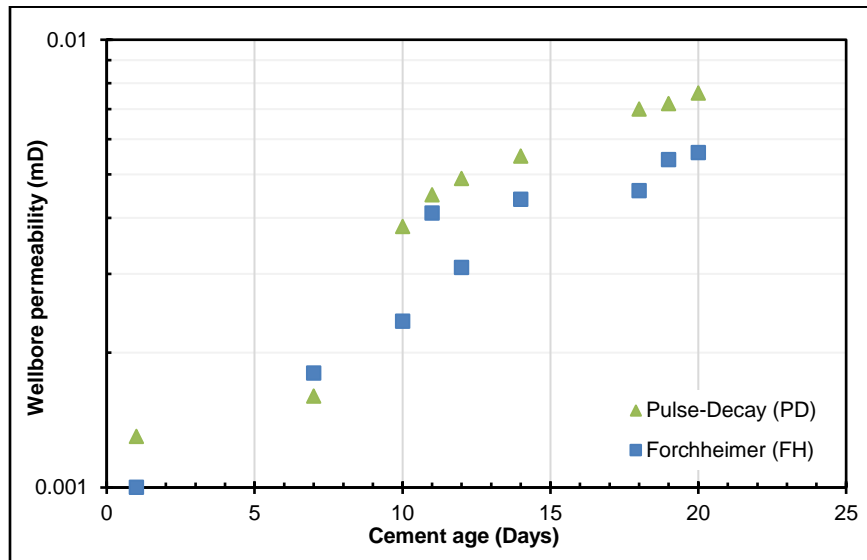


Figure 3-16: Specimen results of wellbore permeability using two methods at different cement age (Class G, WOC: 24 hours)

Table 3-3: Summary of findings from the first tests performed on each specimen

Specimen No.	Cement Grade	WOC (hrs)	Leakage Time (min)	Wellbore Permeability (mD)		
				Darcy's Method	Pulse-Decay Method	Forchheimer's Method
1	H	24	11	0.004	N/A	N/A
2	H	12	5	0.079	0.003	0.002
3	H	24	16	0.132	0.070	0.032
4	G	24	0.22	N/A	0.001	0.001

For in-depth evaluation of the cement sealability and to overcome the limitations of the experimental investigation, analytical investigation is discussed in the next chapter. The data from the conducted experiments are used to upscale the experimental investigation by utilizing them in the analytical investigation. The analytical investigation was carried out by developing leakage scenarios to investigate the critical length of casing-liner overlap.

Chapter 4: Analytical Investigation of the Critical Length of Casing-Liner Overlap

4.1 Overview

This chapter discusses and investigates the critical length of casing-liner overlap. The investigation carried out in this chapter uses an analytical model. The analytical model was used to develop gas leakage scenarios through the cement within the casing-liner overlap. Three parameters were varied to establish the leakage scenarios: cement permeability, casing-liner overlap, and pressure differential exerted across the casing liner overlap. The governing equations are discussed in section 4.2. Then, the results and discussions of the developed leakage scenarios are discussed in section 4.3.

4.2 Methodology

The model used in this study is the one developed by Stormont et al. (2018):

$$Q = -\frac{\nabla P}{6\mu} \pi R_i (R_m - R_i)^3 \quad (4.1)$$

This model was developed based on the microannulus gap generated intentionally between the inner casing and cement, and it depends on the hydraulic aperture. More details about this model can be found in section 2.6. Estimation of the hydraulic aperture depends on the permeability assumed, and it can be approximated as follows (Witherspoon et al. 1980):

$$h^3 = \frac{12 kA}{\omega} \quad (4.2)$$

where ω is the circumference of the inner casing ($2\pi R_i$), and h is the hydraulic aperture (microannulus gap size) which can be estimated as $(R_m - R_i)$, where R_m is the microannulus radius and R_i is the radius of the inner casing.

After that, the flow rate is determined based upon the following equation:

$$Q = \frac{M (P_u^2 - P_d^2) \omega h^3}{24zRTL\rho\mu} \quad (4.3)$$

where M is the gas molecular weight in kg/mole, P_u is the upstream pressure in Pa, P_d is the downstream pressure in Pa, z is the compressibility factor, R is the universal gas constant in m³.Pa/mole.K, and T is the temperature in °K.

The hydraulic aperture was calculated first by feeding equation 4.2 with the assumed permeability value. After that, the flow rate of nitrogen gas was estimated using equation 4.3 with substituting the hydraulic aperture value calculated from the previous step. Then, leakage time was calculated by substituting the gas flow rate in the following equation:

$$t = \frac{A_m L}{Q} \quad (4.4)$$

where t is the leakage time in seconds and A_m is the microannulus area in m². The leakage time is the time it takes the gas to migrate from the top to the bottom of the cement that is placed within the casing-liner overlap. The leakage time was deemed the key parameter for finding out the optimum length of casing-liner overlap. According to API Bulletin E3 (2018) the casing-liner overlap length can vary from 50 to 500 ft. Therefore, the overlap lengths in all the cases were varied from 50 to 500 ft with 50 ft increment.

To investigate the critical length of casing-liner overlap, leakage scenarios were generated to mimic gas migration through the liner lap's cement. Four major cases were developed, where each case is composed of 40 leakage scenarios. The difference between the developed cases is the differential pressure applied across the cement placed within the casing-liner overlap. Four differential pressures were used in this investigation: 250, 500, 1000, and 1500 psi. In each case, permeability was varied from 0.01 to 0.5 mD to evaluate the impact of each value on the leakage time. The assumption of the permeability values in this section was made based on the values of the microannulus gap sizes obtained from the experimental investigation. Also, the length of

casing-liner overlap was varied to examine its impact on the leakage time, and how it is going to help ensure good well integrity. Another case was developed; however, the permeability was fixed, and the pressure differential was varied. Figure 4-1 illustrates schematics of gas invasion through liners and liner hangers, considering different lengths of casing-liner overlap.

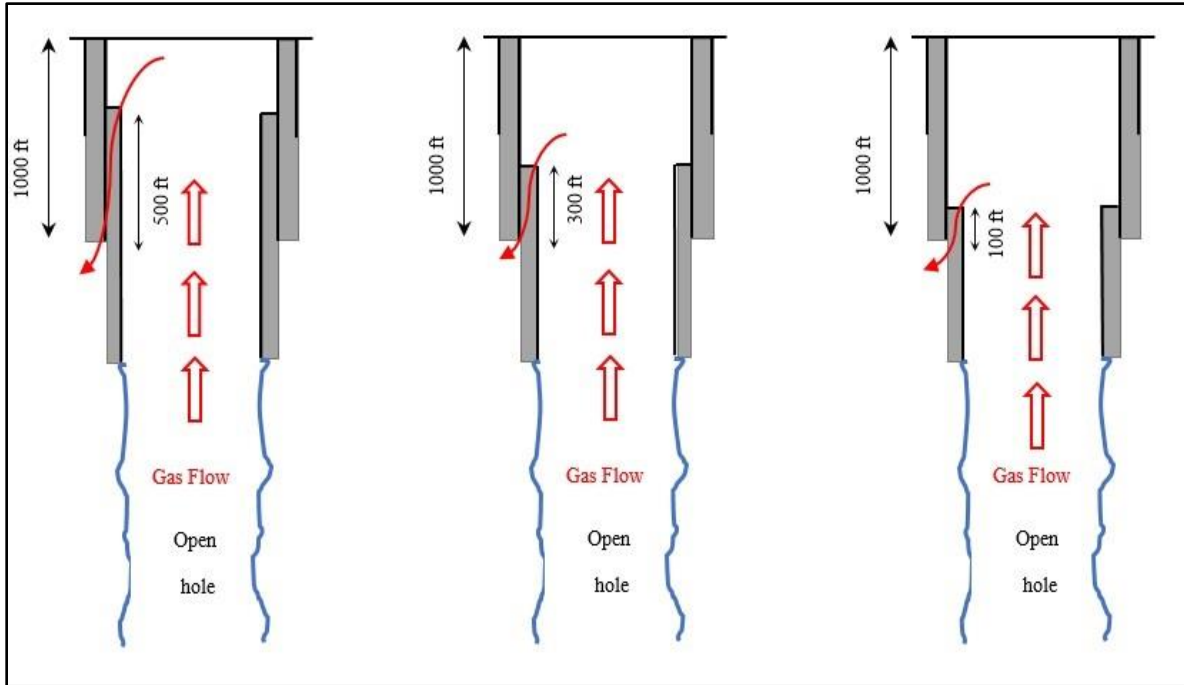


Figure 4-1: Schematic of gas migration through liners and liner hangers with different lengths of casing-liner overlap

4.2.1 Model and Leakage Scenarios Assumptions

To simplify and use the analytical gas leakage model discussed in this chapter, select assumptions were applied. Equation 4.3 assumes steady state isothermal gas flow and the gas flows through completely gas-filled microannulus. This model is only valid for laminar flow condition. Also, constant outlet and inlet pressures were considered.

To develop the gas leakage scenarios and investigate the critical length of casing-liner overlap, the following assumptions were made:

- The last casing shoe is set at 1000 ft.
- Faulty elastomers are installed in the liner hanger.

The input data used for the analytical model to develop different leakage scenarios and build the four cases are shown in Table 4-1.

Table 4-1: Input data for studying the effect of cement matrix permeability

Input Data	Field Unit
Casing-liner overlap length	50, 100, 150, 200, 250, 300, 350, 400, 450, and 500 ft
Casing diameter	22 in
Liner diameter	18 in
Permeability	0.01, 0.1, 0.3 and 0.5 mD
Inlet pressure	750, 1000, 1250, 1500, 2000 psi
Outlet pressure	500 psi
Temperature	100 °F

4.3 Results and Discussions

In the following cases, the findings depict the impact of differential pressure, microannulus permeability, and overlap length on the leakage time. From the experimental investigation conducted in this study, the cement permeability can vary between 0.001 mD to 0.5 mD. This influenced the selection of the permeability values used to develop the leakage scenarios.

4.3.1 First Case (Differential Pressure of 250 psi)

The first case was developed with an assumption of 250 psi differential pressure applied across the cement behind the casing-liner overlap. Figure 4-2 portrays the results of the leakage scenarios.

The leakage time was plotted against the casing-liner overlap at different permeability values. The leakage time was roughly 3 hours for a permeability value of 0.01 mD, while the leakage time was less than 18 minutes for the other permeability values, all concerning 50 ft casing-liner overlap. A general trend observed is that as the length of casing-liner overlap increased, the leakage time increased. For 0.5 mD, the gas takes almost 24 minutes to migrate to the bottom side of the overlap when the overlap length is 100 ft, while it takes 60 minutes for 200 ft overlap length.

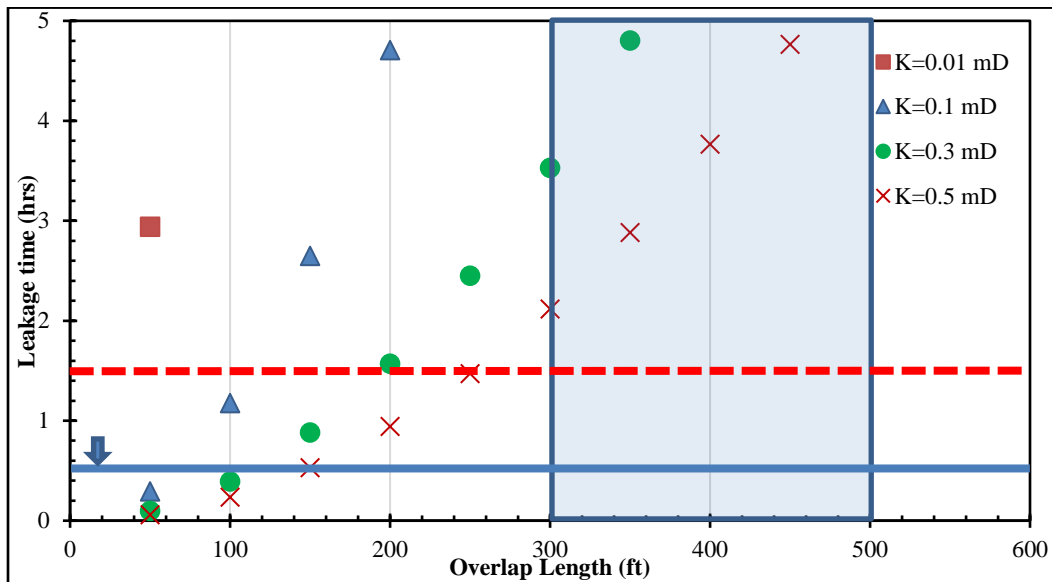


Figure 4-2: First case results of leakage time for different lengths of casing-liner overlap for various permeability values at 250 psi pressure differential.

4.3.2 Second Case (Differential Pressure of 500 psi)

In the second case, a differential pressure of 500 psi across the cement applied on the cement within the liner lap was assumed. The results of the leakage scenarios, in this case, are shown in Figure 4-3. For a 50 ft overlap, the time it took the gas to reach the bottom of the overlap was almost 90 minutes (with a permeability of 0.01 mD), while it was less than 15 minutes for the other permeability values. For a permeability of 0.5 mD, the leakage time was 8 minutes for 100 ft of casing-liner overlap, while it increased to 32 minutes for 200 ft of overlap. It can be noticed that

as the differential pressure across the cement (within the overlap) increased, the leakage time decreased nonlinearly. The leakage scenarios depict that longer casing-liner overlap can affect the gas propagation time to the bottom of the overlap into the nearest formation or aquifer.

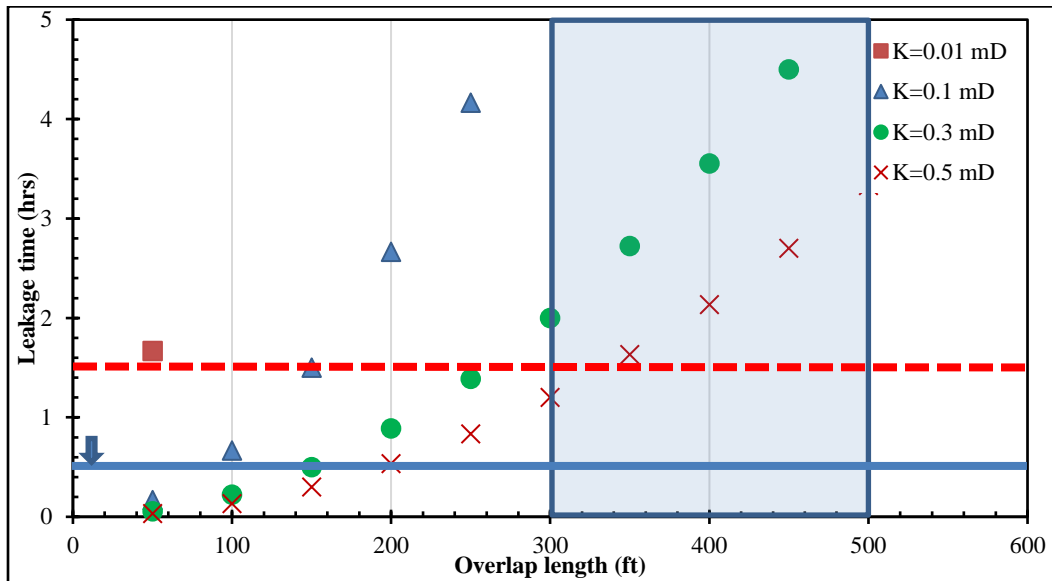


Figure 4-3: Second case results of leakage time for different lengths of casing-liner overlap for various permeability values at 500 psi pressure differential.

4.3.3 Third and Fourth Case (Differential Pressures of 1000 and 1500 psi)

Differential pressures of 1000 and 1500 psi across the cement within the liner lap were assumed for the third and fourth cases, respectively. Figure 4-4 and Figure 4-5 show the results of the third and fourth cases, respectively. It can be noticed that the 50 ft of casing-liner overlap had the lowest leakage time compared to the other lengths. The leakage time drops significantly for permeability value of 0.1 mD and higher. Longer leakage time can help the drilling operators deal with a kick once it is detected. Also, it helps in maintaining freshwater formations not be contaminated by any kick encountered.

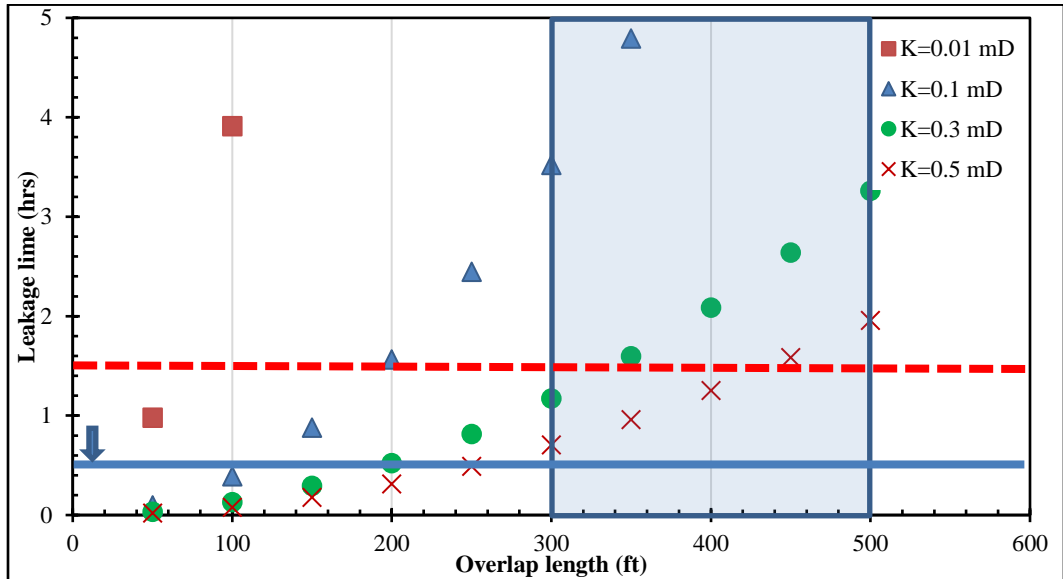


Figure 4-4: Third case results of leakage time for different lengths of casing-liner overlap for various permeability values at 1000 psi pressure differential.

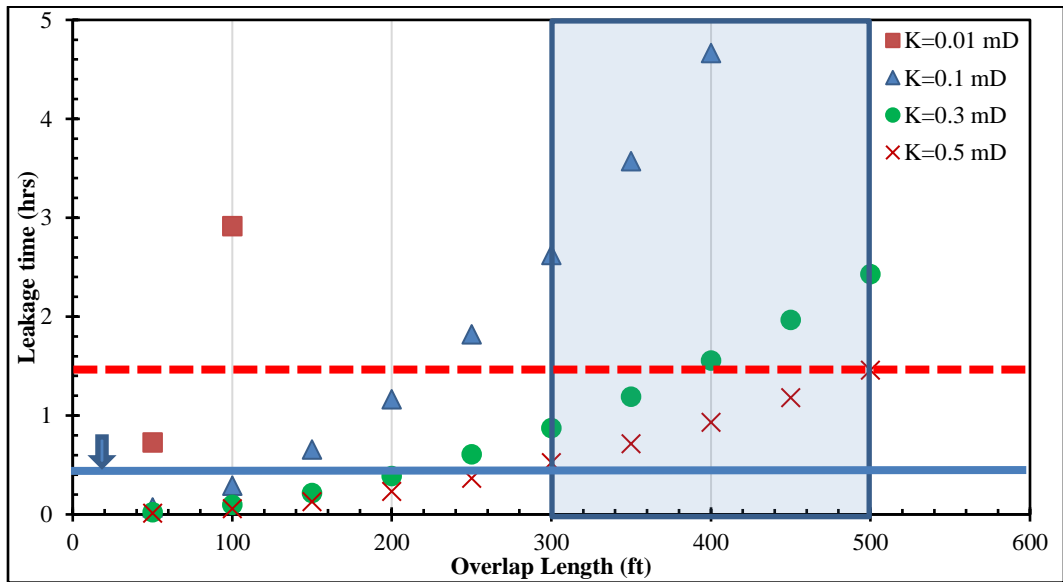


Figure 4-5: Fourth case results of leakage time for different lengths of casing-liner overlap for various permeability values at 1500 psi pressure differential.

4.3.4 Fifth Case (Fixed Permeability and Varying Differential Pressures)

The permeability value was fixed at 0.5 mD while the differential pressure was varied between 250 psi and 1500 psi. Figure 4-6 shows the impact of differential pressure on the leakage time for various casing-liner overlap lengths. It can be observed that as the differential pressure across the overlap increased, the leakage time decreased. For 150 ft overlap and 250 psi differential, the leakage time was 30 minutes, while for 1000 psi it was 10 minutes. However, as the overlap length increased, the difference in leakage time increased as well. For 300 ft overlap and 250 psi differential, the leakage time was approximately 2 hours 7 minutes. While for 1000 psi differential, it was 42 minutes. Obviously, as the differential pressure across the cement within the overlap increased, the leakage time decreased. It can also be observed that shorter casing-liner overlaps (50 ft to 200 ft) have leakage times less than one hour.

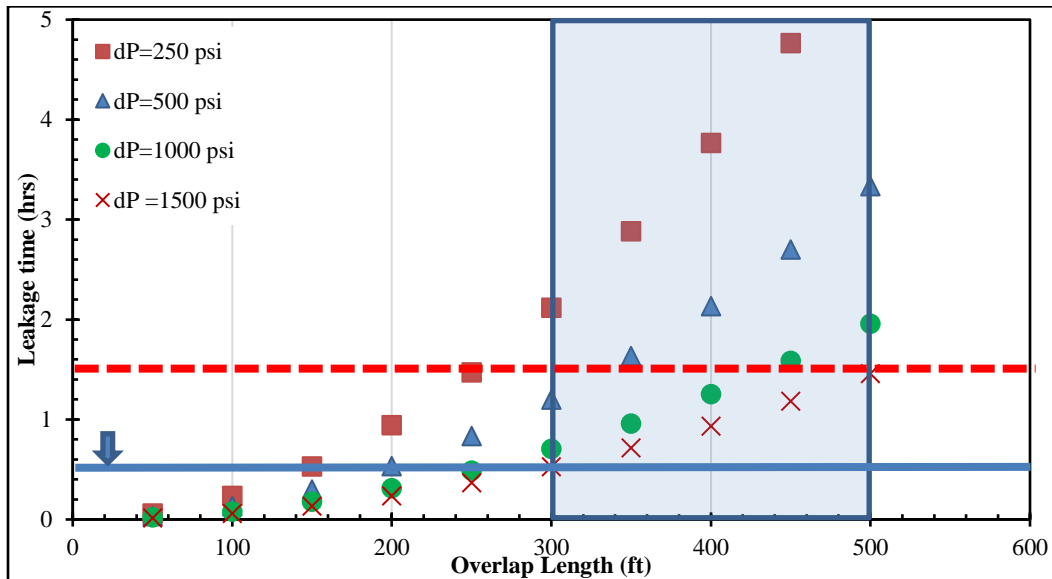


Figure 4-6: Fifth case results of leakage time for different lengths of casing-liner overlap for a permeability value of 0.5 mD at various differential pressures.

The analytical investigation considers the gas flow through the microannulus only. The gas flow through cement matrix is not considered. Also, laminar flow of gas and steady state gas flow were assumed to develop the leakage scenarios in this chapter. These assumptions can impact the results significantly. The Reynold's number was calculated for all the leakage scenarios, and it was very small. The highest Reynold's number of the presented leakage scenarios was 13.61, which is less than 2000. This implies that the gas flow in the leakage scenarios was laminar. The data used to develop the leakage scenarios in this chapter are presented in Appendix B.

To overcome these limitations and create leakage scenarios with higher accuracy, a numerical gas leakage model is needed. There is no numerical gas leakage model in literature to predict the gas flow through cement matrix and microannulus. The next chapter discusses a numerical gas leakage model that was developed in this study to overcome the aforementioned limitations.

Chapter 5: Development of Numerical Gas Leakage Model

5.1 Overview

In this study, a numerical gas leakage model was developed in MATLAB. The model was developed to overcome the limitation of the analytical model used in the previous chapter. This leakage model does not only consider the flow through the cement sheath, but also through microannulus. The novelty in this work is that the gas flow is considered in both cement and microannulus. There is no numerical model that considered the flow of gas through cement and microannulus. Some researchers only considered the flow through cement matrix, while others considered the flow through microannulus only. In this chapter, the methodology and the main equations used to develop this model are discussed in section 5.2. The governing equations and discretization methodology are discussed in Appendix A. Section 5.3 discusses the model validation and verification against analytical solution and experimental data. The results from the modeling study are discussed in section 5.4. The impact of various parameters on leakage time are discussed in section 5.4.1. Finally, a field case study based on the developed numerical model is presented and discussed in section 5.4.2.

5.2 Methodology

The model was derived based on the diffusivity equation for the linear flow. To model the gas flow through cement, the pressure squared method was used to overcome the limitation of the basic form of the diffusivity equation. The finite volume approach was implemented to solve the partial differential equation (PDE) with the appendix's discretization details. Below are the mathematical derivations, domain descriptions, boundary conditions, and model limitations. Fluids flow in porous media is usually described through Darcy's law which is written as:

$$\mathbf{u} = -\frac{\mathbf{k}}{\mu} \cdot \nabla P \quad (5.1)$$

where \mathbf{u} is the velocity vector, μ is the fluid viscosity, P is the pressure, and \mathbf{k} is the permeability tensor. Gas flow in cement is laminar, and no adsorption takes place; hence, the non-Darcy and Knudsen effects were neglected. Transportation of fluids in a porous medium can be described through mass conservation (i.e., continuity equation), which is described mathematically as:

$$\nabla \cdot (\rho \mathbf{u}) = -\frac{\partial(\phi \rho)}{\partial t} \quad (5.2)$$

where ρ is fluid density, ϕ is the cement porosity, and t is time. The equation simply states that the mass entering a control volume minus the mass exiting is equal to mass accumulation. Notice that both fluids and cement compressibility can be written as:

$$c_r = \frac{1}{\phi} \frac{d\phi}{dP} \quad (5.3)$$

$$c_f = \frac{1}{\rho} \frac{d\rho}{dP} \quad (5.4)$$

$$c_t = c_f + c_r \quad (5.5)$$

where c_r is cement compressibility, c_f is fluid compressibility, and c_t is the total compressibility.

The density of gas also can be written as:

$$\rho = \frac{PM}{zRT} \quad (5.6)$$

where M is the gas molecular weight, z is the gas compressibility factor, T is the temperature, and R is the universal gas constant. Substituting the definitions of velocity and density into equation 5.2, manipulating, and rearranging it results in the following partial differential equation (PDE):

$$\nabla \cdot \left(\frac{p}{\mu z} \mathbf{k} \cdot \nabla P \right) = -\frac{\partial \left(\frac{\phi P}{z} \right)}{\partial t} \quad (5.7)$$

If the product of μz is assumed to be constant, which is valid up to 2000 psi according to Lee and Wattenbarger (1996), and substituting the definitions of compressibility, the following equation can be obtained:

$$\nabla \cdot (\mathbf{k} \cdot \nabla P^2) = -\phi \mu c_t \frac{\partial(P^2)}{\partial t} \quad (5.8)$$

Figure 5-1a shows a schematic diagram of a 3-D casing annulus consisting of cement and a microannulus. The gas flows from the bottom to the top through the cement and microannulus gap which is highlighted in red. The microannulus gap is assumed to surround the cement and inner casing area as shown in Figure 5-1c. Since the system is axisymmetric and no angular flow was assumed, the solution is similar in the theta direction. Hence, only a stripe perpendicular to the theta direction was considered (see Figure 5-1b) which simplifies the problem and saves computational time. The 2-D domain considers only the cement and microannulus gap which was gridded logarithmically. The logarithmic grids were used because the microannulus gap can vary between a couple of micrometers to 100 micrometers. With these small gaps, it is unreasonable to use a uniform gridding system since it will lead to high mesh density, resulting in high computational time and sometimes lead to solution instability. Based on the simplified 2-D domain (see Figure 5-1b), equation 5.8 can be written as:

$$\frac{\partial}{\partial x} \left(k_x \frac{\partial P^2}{\partial x} \right) + \frac{\partial}{\partial y} \left(k_y \frac{\partial P^2}{\partial y} \right) = \phi c_t \mu \frac{\partial P^2}{\partial t} \quad (5.9)$$

where x is the cement length direction and y is the cement width direction. To solve the PDE, the following initial and boundary conditions were implemented based on the 2-D stripe:

- 1- The initial pressure in the cement column is equal to the system pressure before gas leakage (i.e., gas injection):

$$P(x, y, t = 0) = P_i \quad (5.10)$$

2- Injection pressure at the inlet is assumed to be constant:

$$P(x = 0, y, t) = P_{in} \quad (5.11)$$

3- Pressure at the outlet is assumed to be constant:

$$P(x = L, y, t) = P_{out} \quad (5.12)$$

4- No flow condition was assumed in the other boundaries:

$$\mathbf{n} \cdot \nabla P = 0 \quad (5.13)$$

where L is the cement column length and \mathbf{n} is the normal vector. Notice that the permeability of microannulus gap, k_{ma} , is related to the gap width, w , through the following:

$$k_{ma} = \frac{w^2}{12} \quad (5.14)$$

The leakage model presented in this study was derived based on the following assumptions:

1. The microannulus and cement pore spaces are not filled with any fluid.
2. Transient flow.
3. It is only valid for single phase flow.
4. Inlet & outlet pressures are constant.
5. Axisymmetric flow.
6. Isothermal

The pressure squared method is limited to a system pressure of 2000 psi. After 2000 psi, the solution will start to deviate from the real solution. This is one of the limitations of the developed model. This model assumes isothermal transient flow of gas. This assumption is valid in the experimental set up where the temperature is usually kept constant. Also, in field simulations of relatively small column height where temperature variation is negligible. In addition, the cement

sheath is assumed to have no liquid within its pore spaces due to the hydration process that took place earlier (Koenders and van Breugel 1997). It is only valid for single phase flow. In addition, only a small stripe of the annulus is considered to simulate the gas leakage in the cement column; that is why axisymmetric flow is assumed. The flow rate of the full annular space is then calculated based on the outer and the inner diameters of the casing and liner strings, respectively.

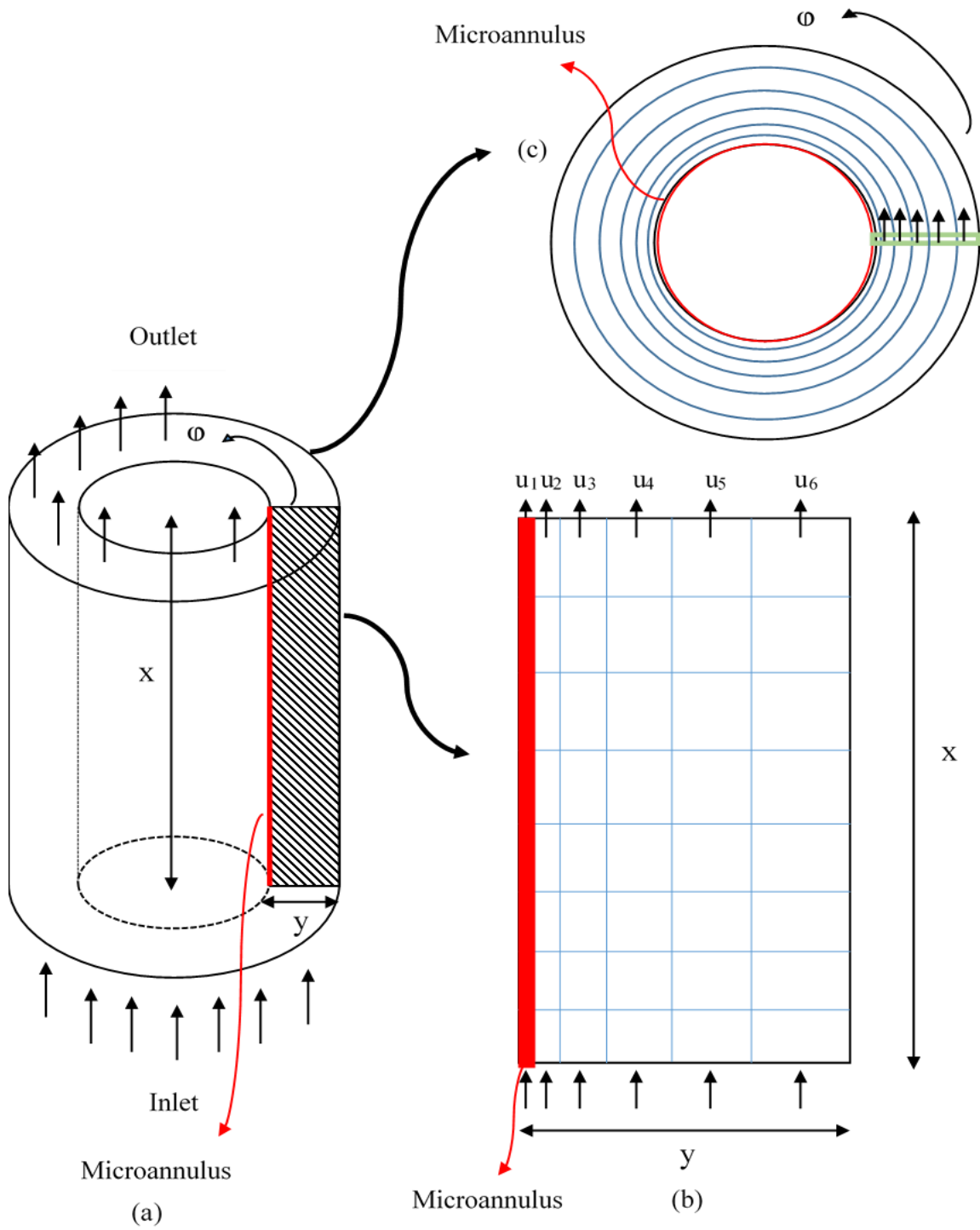


Figure 5-1: Leakage model (a) 3D annular casing cement; (b) side view of the simulated stripe with logarithmic grid system; and (c) top view of the system

5.3 Model Validation & Verification

Prior to model validation, mesh size was investigated by refining its size and comparing it with a very fine mesh to examine its convergence. The model was then validated by using an analytical solution of the diffusivity equation. The analytical solution used to compare the results from the model developed is pressure squared analytical equation. Assuming a steady state condition and no microannulus gap. The analytical equation used is:

$$q = \frac{kA}{\mu L P_o} \frac{(P_{in}^2 - P_{out}^2)}{2} \quad (5.15)$$

where q is the gas flow rate, A is the cross-sectional area, L is the cement column length, P_{in} is the inlet pressure, P_{out} is the outlet pressure, and P_o is the ambient pressure. The input data used in this model are shown in Table 5-1.

Table 5-1: Input data used for model validation

Input Data	Field Unit
Cement column length	50 ft
Casing inner diameter	22 in
Liner outer diameter	18 in
Cement thickness	2 in
Cement porosity	0.2
Cement permeability	0.0001 mD
Inlet pressure	1000, 1250, 1500, 1750, and 2000 psi
Outlet pressure	500 psi
Initial pressure	500 psi
Temperature	110 °F
Nitrogen viscosity	0.01946 cP
Number of grids in x-direction	1524
Number of grids in y-direction	50

Figure 5-2 shows a comparison between the analytical and numerical solutions, where the normalized flow rates against different inlet pressures of 1000, 1250, 1500, 1750, and 2000 psi,

were examined. The pressure squared method is valid up to 2000 psi with an error of less than 0.2%.

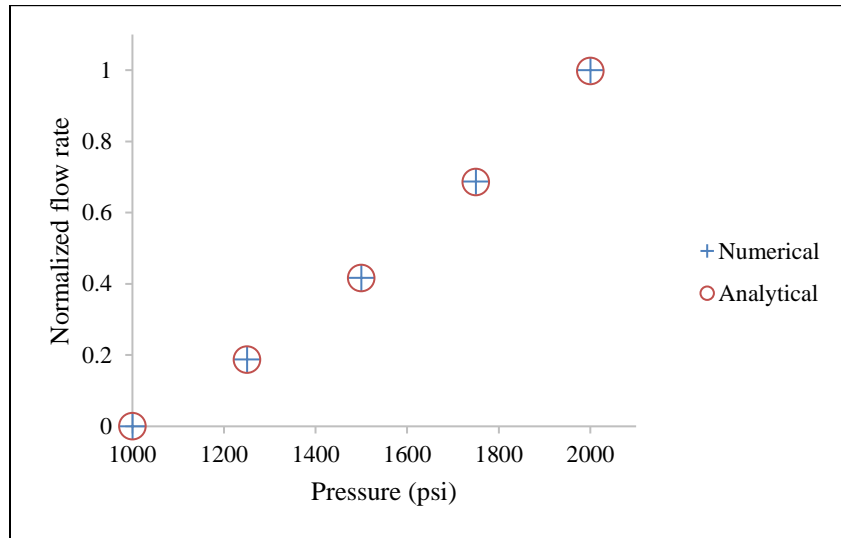


Figure 5-2: Normalized flow rate for analytical and numerical solutions versus pressure

The developed numerical model was also verified with the experimental work that was presented in chapter 3. The pressure decline curves were used to estimate the cement permeability for the experiments conducted. For model verification, the pressure decline curve was used. The model was fed with the input data shown in Table 5-2.

Table 5-2: Input data used for model verification

Input Data	Field Unit
Cement column length	3 ft
Casing inner diameter	6 in
Liner outer diameter	4.5 in
Cement Permeability	0.07 mD
Inlet pressure	74.7 psi
Outlet pressure	14.7 psi
Initial pressure	14.7 psi
Temperature	80 °F
Nitrogen viscosity	0.01796 cP

Two unknown parameters were varied to match the pressure decline curve: cement porosity and microannulus gap size. Figure 5-3 shows the pressure decline curves for the experimental data and the model. The cement porosity and microannulus gap size that were used to get this match was 17% and 10 μm , respectively. The model agrees with the experimental data with a root mean square error (RMSE) of 2.63.

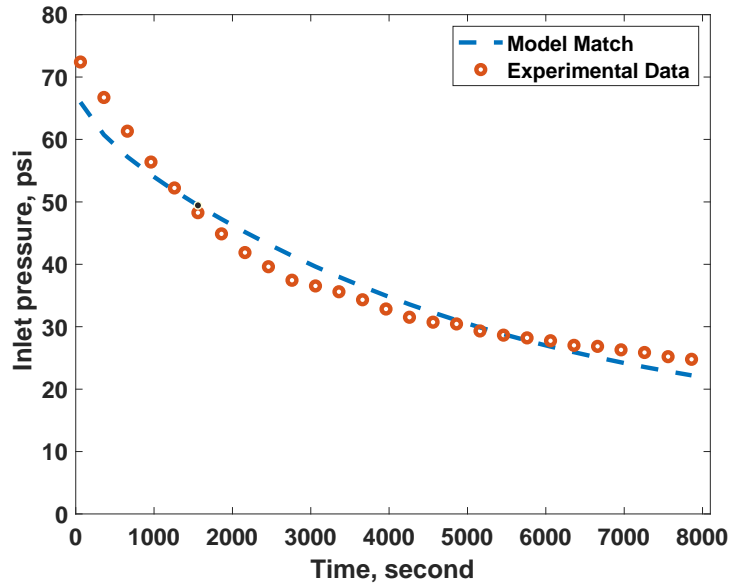


Figure 5-3: Pressure decline match of the experimental data

5.4 Results and Discussions

This section is focused on discussing some parameters that impact the leakage time of gas within the cement sheath considering the microannulus gap. Also, a field case scenario is developed and discussed. The microannulus gap importance arises from the fact that the fluids flow in the gap before it propagates through the rest of the cement sheath. Figure 5-4 shows the simulation of gas flow, considering a previous experimental study. This figure shows the cement column's pressure distribution at different time frames: 1 minute, 30 minutes, and 60 minutes. In these figures, the inlet is at the bottom, and the outlet is at the top. Also, the casing string is on the right, and the

liner string is on the left (no flow boundary conditions). One might notice that the gas is injected from the bottom and the microannulus gap exists in the left (adjacent to the liner string). Since the microannulus is considered a high permeable streak, the gas will favor flowing through this path, and then the gas will propagate through the cement matrix. This is why the pressure propagates first at the left side and then pressure waves moves inside the cement sheath. The length orthogonal to the microannulus represents the cement thickness (the clearance between the casing and the liner). These figures can be observed that the gas propagates and leaked during the first 10 minutes of gas injection. As the pressure starts to propagate more inside the cement sheath, and the flow rate starts to increase. This behavior might impact the width of microannulus from a geomechanical perspective.

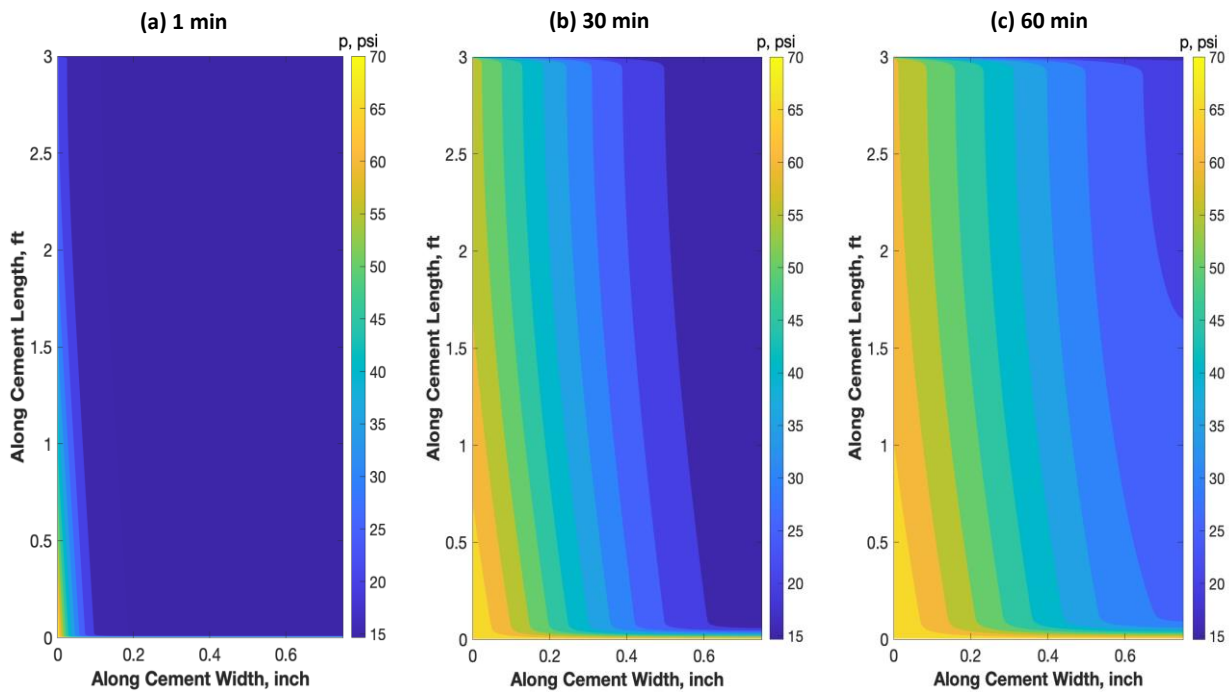


Figure 5-4: Pressure profile within the cement sheath at different gas injection times

5.4.1 Parametric Study

This section includes parametric study of cement matrix permeability, cement porosity, microannulus gap size, and casing-liner overlap length with regards to how they impact the leakage time. The leakage time is defined as “*the time it takes the gas to travel from the top to bottom of the cemented annulus*”(Al Ramadan et al. 2019a).

5.4.1.1 Cement Matrix Permeability

Cement sheath is considered a porous media with porosity and permeability properties. The cement's permeability is usually low; however, the permeability can increase due to cement degradation, nearby well activities, and carbonation. In this section, the impact of cement matrix permeability on the leakage time is examined.

The effect of cement matrix permeability on leakage time is studied by varying the cement matrix permeability from 10^{-5} mD to 10^{-1} mD with an increment of one magnitude. A cement column length of 50 ft is used to construct the leakage scenarios. The differential pressure across the cement column is 500 psi. Nitrogen gas was used as the migrating fluid. Also, microannulus gap size of 50 μm is assumed, where this is a typical value reported in the literature (Boukhelifa et al. 2004; Aas et al. 2016; Stormont et al. 2018). The input data used in the leakage scenarios is given in Table 5-3.

Table 5-3: Input data for studying the effect of cement matrix permeability

Input Data	Field Unit
Cement column length	50 ft
Casing diameter	22 in
Liner diameter	18 in
Cement thickness	2 in
Cement porosity	0.2
Cement permeability	0.00001, 0.0001, 0.001, 0.01, and 0.1 mD
Microannulus gap size	50 μ m
Inlet pressure	1000 psi
Outlet pressure	500 psi
Initial pressure	500 psi
Temperature	110 °F
Nitrogen viscosity	0.01946 cP
Number of grids in x-direction	1524
Number of grids in y-direction	50

Figure 5-5, Figure 5-6, Figure 5-7, Figure 5-8, and Figure 5-9 show the impact of the cement matrix permeability on the leakage time for different permeability values. It is evident that the cement matrix permeability plays a crucial role in zonal isolation. The leakage time decreases as the cement matrix permeability increases. The leakage time for cement matrix permeability of 0.00001 mD is almost 45 minutes, and it dropped to 20 minutes for 0.0001 mD. The leakage time for 0.001, 0.01, and 0.1 mD is less than 5 minutes. It can be observed that the flow becomes steady state after almost 30 minutes for cement matrix permeability of 0.01 and 0.1 mD. Therefore, additives should be added to reduce the permeability of the cement matrix such as latex, nanoparticles, and microsilica. This will help in mitigating and preventing gas migration through the cement sheath and maintaining well integrity.

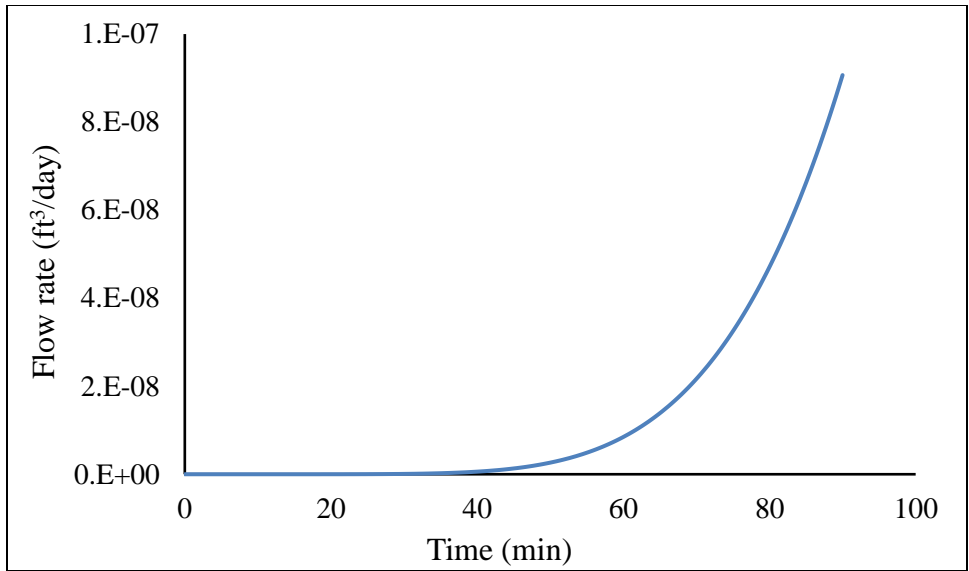


Figure 5-5: Impact of cement matrix permeability on leakage time for $K_c=0.00001$ mD (flow rate at 1000 psi and 110 °F)

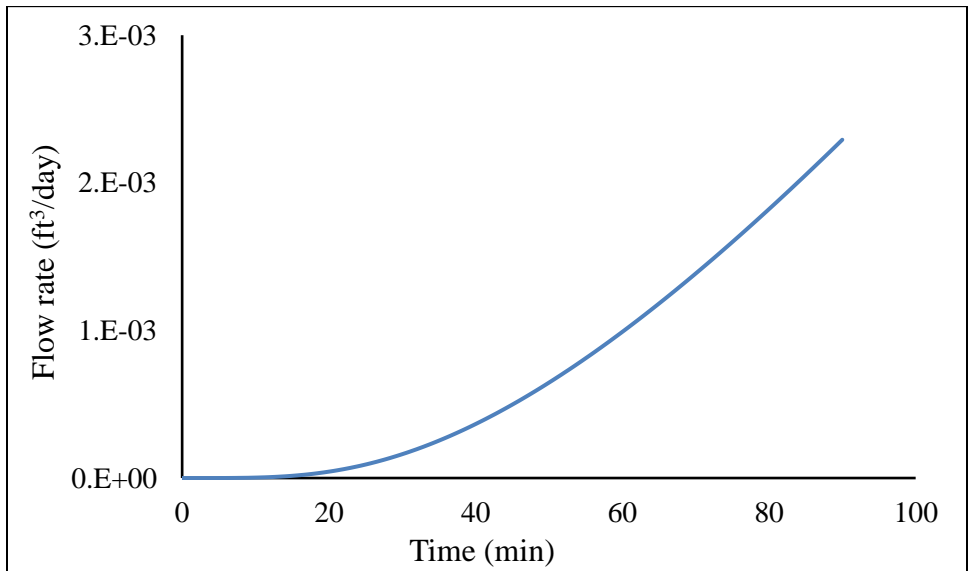


Figure 5-6: Impact of cement matrix permeability on leakage time for $K_c=0.0001$ mD (flow rate at 1000 psi and 110 °F)

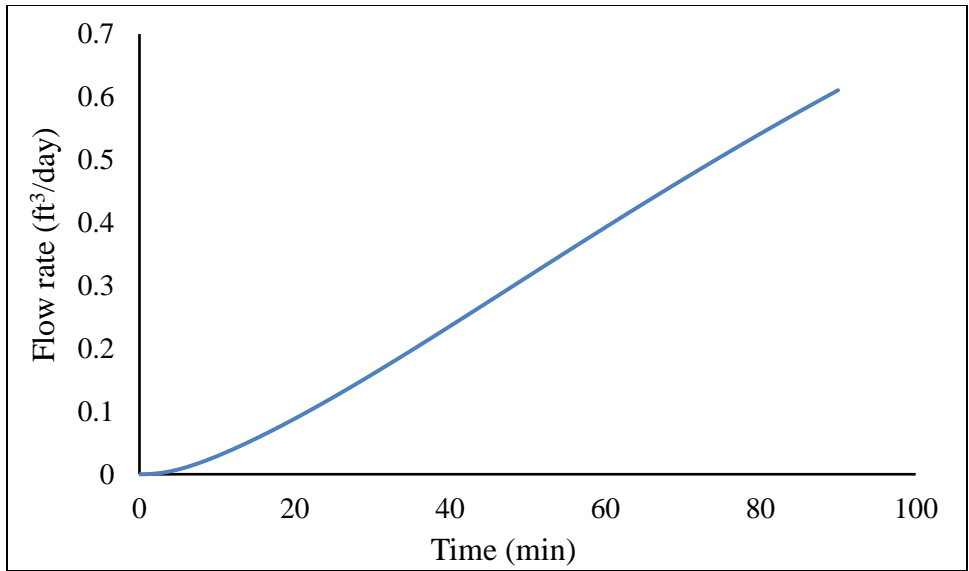


Figure 5-7: Impact of cement matrix permeability on leakage time for $K_c=0.001$ mD (flow rate at 1000 psi and 110 °F)

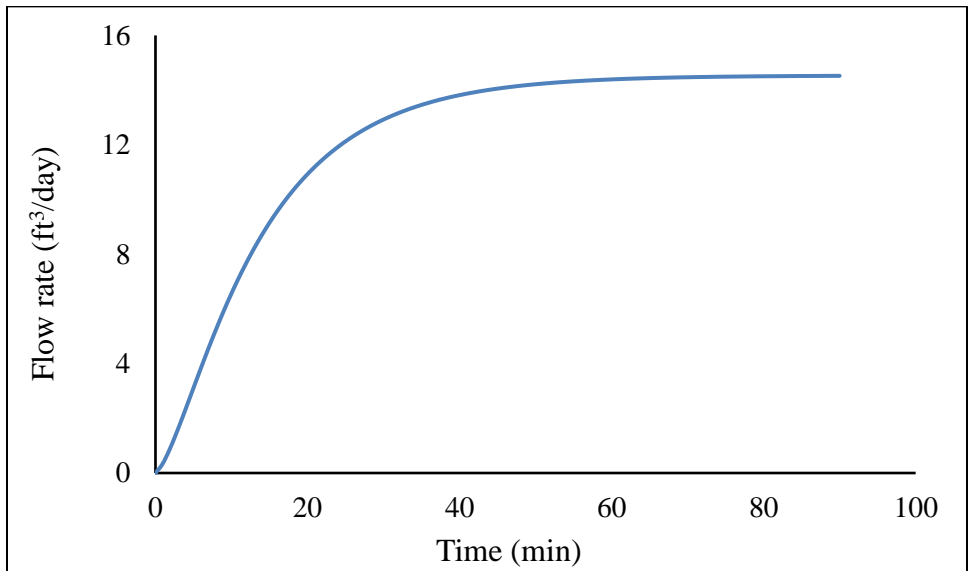


Figure 5-8: Impact of cement matrix permeability on leakage time for $K_c=0.01$ mD (flow rate at 1000 psi and 110 °F)

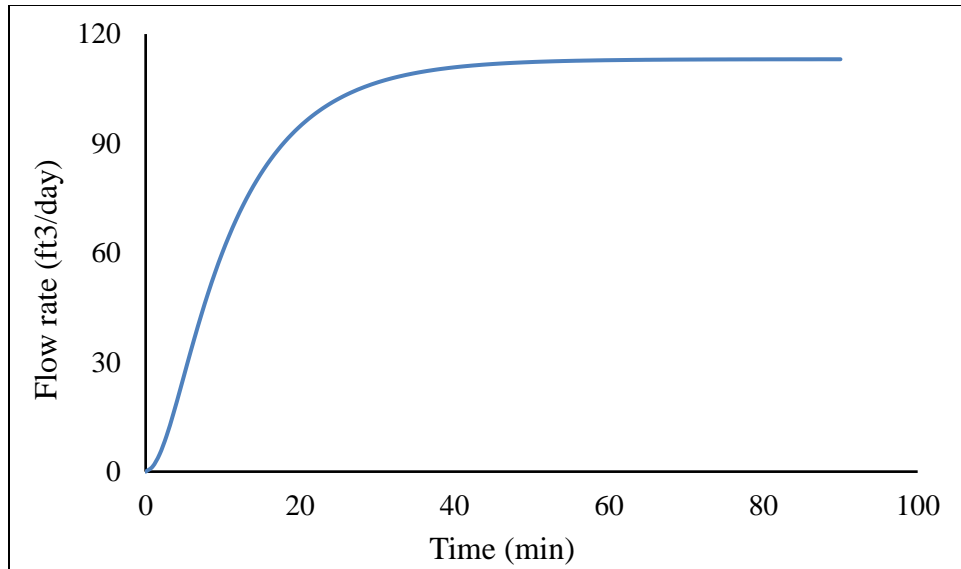


Figure 5-9: Impact of cement matrix permeability on leakage time for $K_c=0.1$ mD (flow rate at 1000 psi and 110 °F)

5.4.1.2 Cement Porosity

Cement porosity effect on leakage time is examined by varying the porosity from 7% to 35%, while keeping the other parameters fixed and assuming constant permeability. These values were reported by Ichim (2017), where cement porosity was measured as a function of time. The input data used to construct the leakage scenarios are shown in Table 5-4.

Table 5-4: Input data for studying the impact of cement porosity on leakage time

Input Data	Field Unit
Cement column length	50 ft
Casing diameter	22 in
Liner diameter	18 in
Cement thickness	2 in
Cement porosity	7, 10, 15, 20, 25, 30, and 35 %
Cement permeability	0.001 mD
Microannulus gap size	50 μ m
Inlet pressure	1000 psi
Outlet pressure	500 psi
Initial pressure	500 psi
Temperature	110 °F
Nitrogen viscosity	0.01946 cP
Number of grids in x-direction	1524
Number of grids in y-direction	50

Cement porosity changes with time as the cement hydrates. Once the cement slurry starts to solidify, large pore spaces begin to develop, resulting in high cement porosity. As the hydration reaction continues, the cement matrix expands and reduces the cement sheath's pore spaces (Ichim 2017). Figure 5-10 shows the impact of cement porosity on leakage time. The leakage time decreased from 10 minutes for cement porosity of 35% to 3 minutes for 5% porosity. It can be inferred that cement porosity has minimal effect on the leakage time. The best way to investigate the effect of cement porosity on the leakage time, is by using a correlation between porosity and permeability of cement.

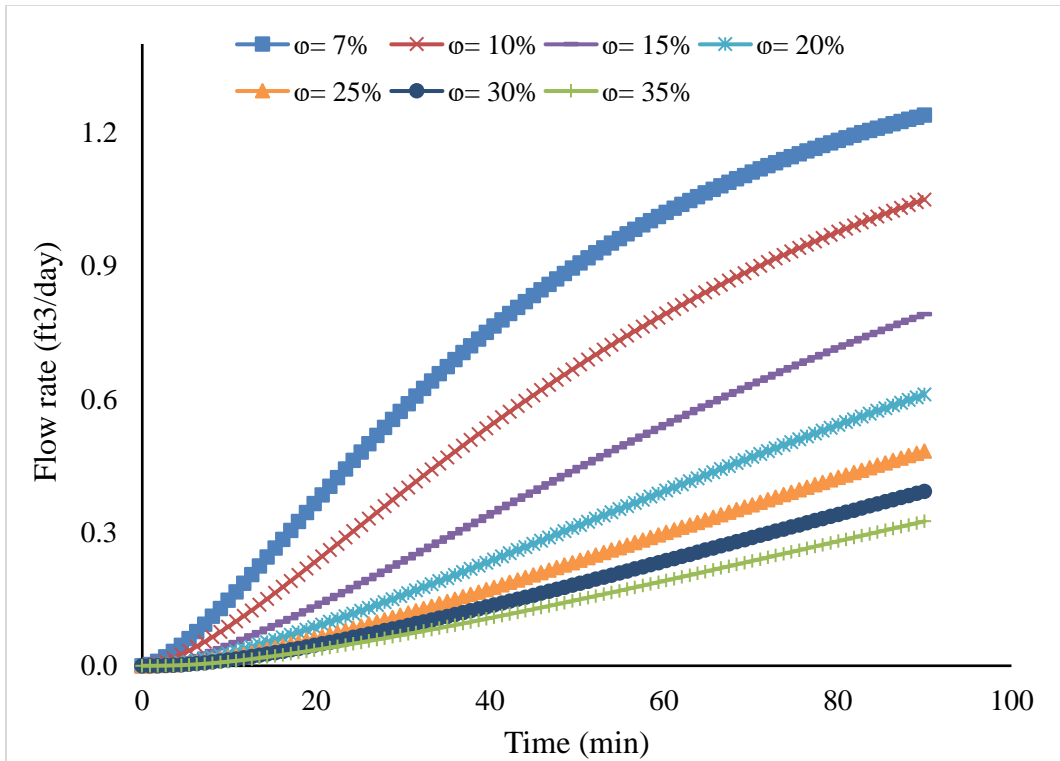


Figure 5-10: Impact of cement porosity on leakage time (flow rate at 1000 psi and 110 °F)

5.4.1.3 Microannulus Gap Size

The microannulus gap size is also known as microannulus hydraulic aperture. The impact of microannulus gap size on the leakage time was also studied and analyzed. The impact on the leakage time was studied by varying the microannulus gap size. Table 5-5 shows the input data used to build the leakage scenarios to investigate the effect of microannulus gap size on the leakage time.

Table 5-5: Input data for studying the impact of microannulus gap size

Input Data	Field Unit
Cement column length	50 ft
Casing diameter	22 in
Liner diameter	18 in
Cement thickness	2 in
Cement porosity	20%
Cement permeability	0.001 mD
Microannulus gap size	10, 25, 50, 75, and 100 μm
Inlet pressure	1000 psi
Outlet pressure	500 psi
Initial pressure	500 psi
Temperature	110 °F
Nitrogen viscosity	0.01946 cP
Number of grids in x-direction	1524
Number of grids in y-direction	50

Microannulus gap size was varied as follows: 10, 25, 50, 75, and 100 μm . Differential pressure across the cement sheath is 500 psi. Figure 5-15, Figure 5-11, Figure 5-12, Figure 5-13, Figure 5-14, and Figure 5-15 illustrate the impact of microannulus gap size on leakage time for various sizes. It can be observed that as the microannulus gap gets bigger, the leakage time decreases. It takes less than 7 minutes for the gas to leak past the cement sheath for microannulus gap size that is higher than 50 μm . Therefore, casing-liner overlap length should not be 50 ft.

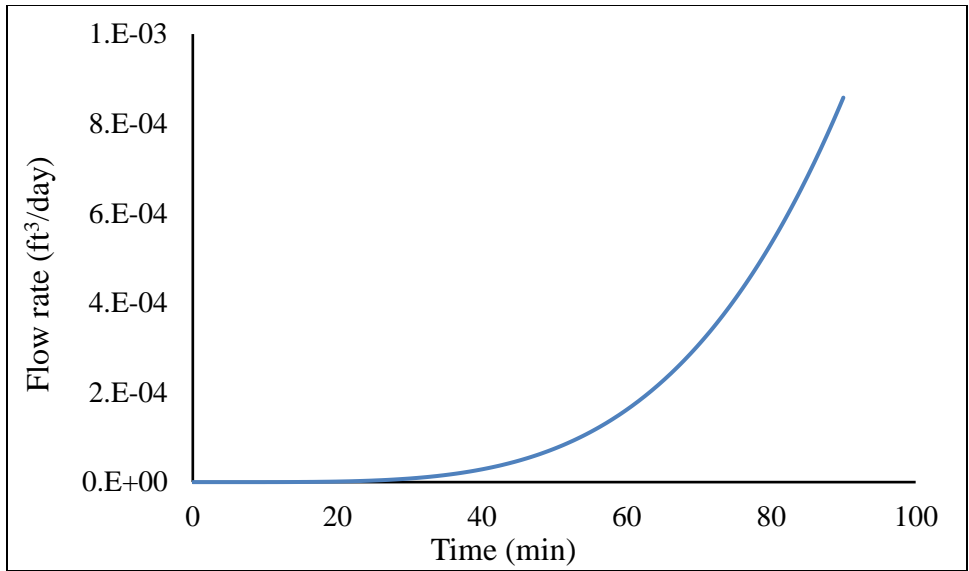


Figure 5-11: Impact of microannulus gap size on leakage time for $\omega=10 \mu\text{m}$ (flow rate at 1000 psi and 110 °F)

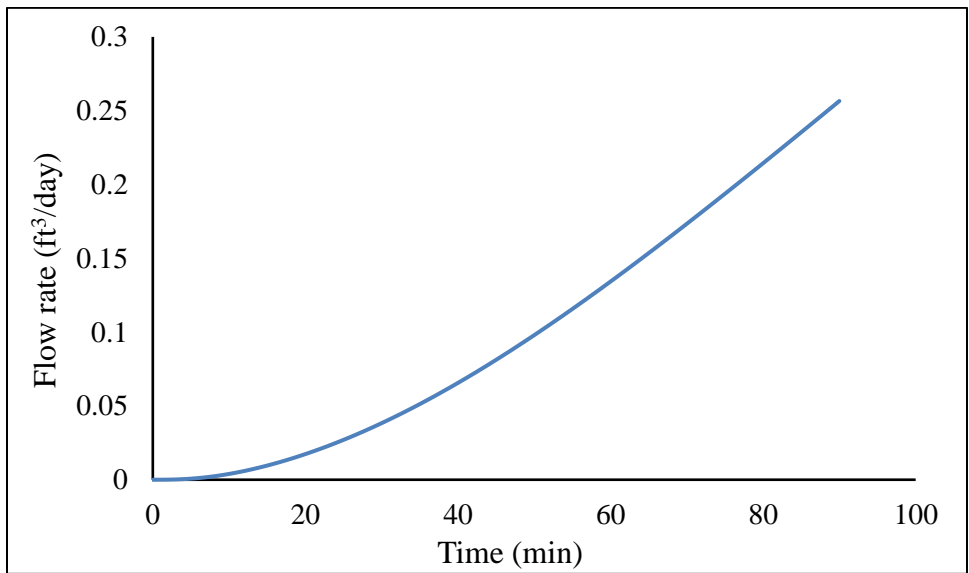


Figure 5-12: Impact of microannulus gap size on leakage time for $\omega=25 \mu\text{m}$ (flow rate at 1000 psi and 110 °F)

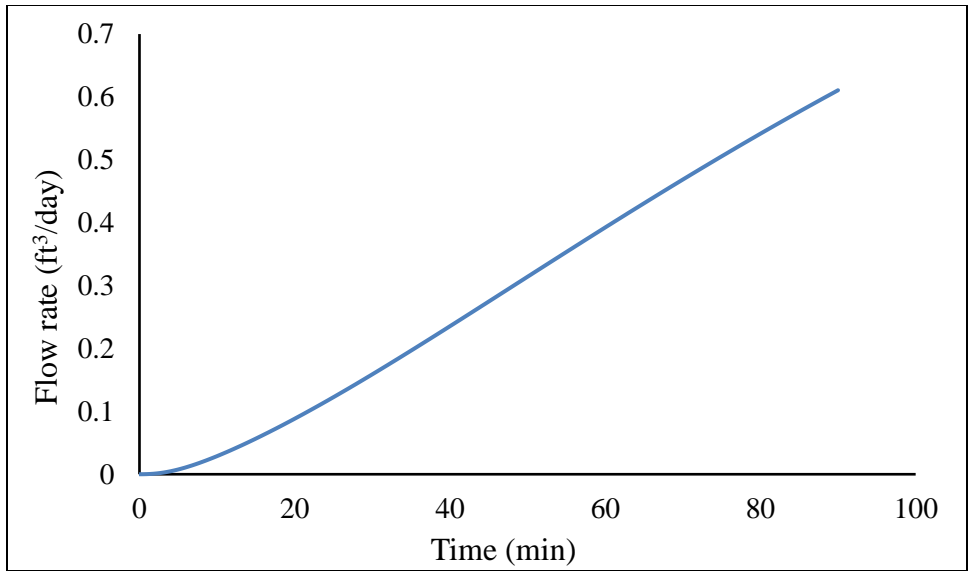


Figure 5-13: Impact of microannulus gap size on leakage time for $\omega=50 \mu\text{m}$ (flow rate at 1000 psi and 110 °F)

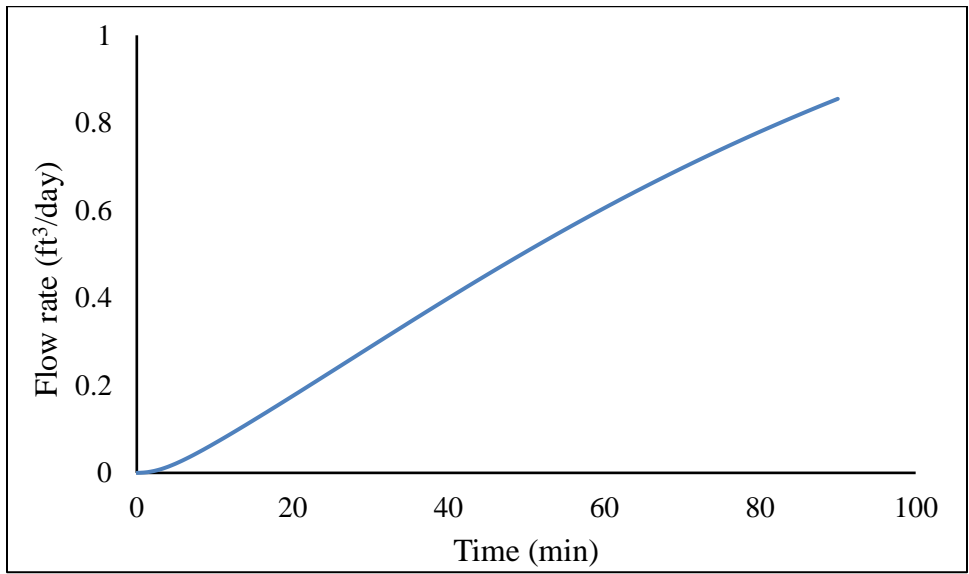


Figure 5-14: Impact of microannulus gap size on leakage time for $\omega=75 \mu\text{m}$ (flow rate at 1000 psi and 110 °F)

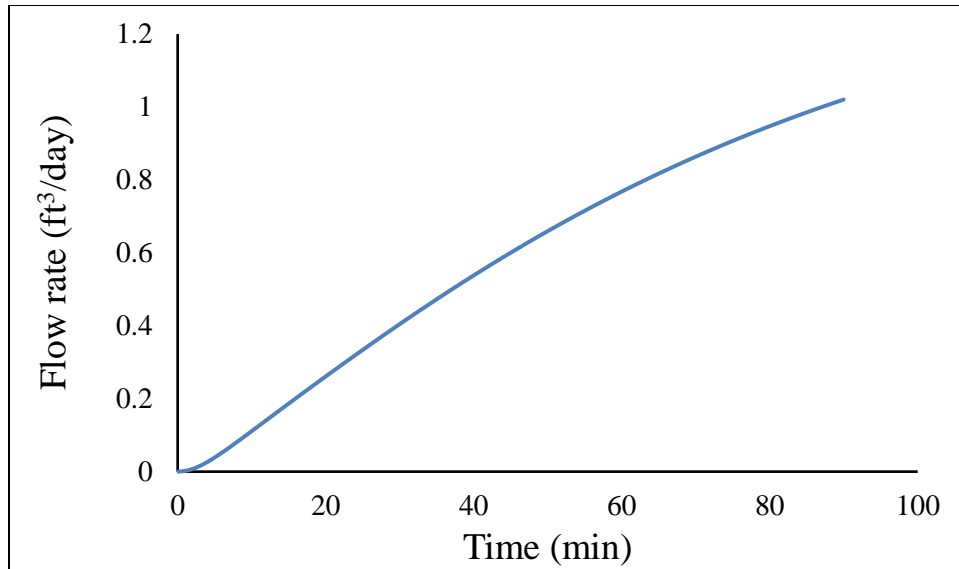


Figure 5-15: Impact of microannulus gap size on leakage time for $\omega=100 \mu\text{m}$ (flow rate at 1000 psi and 110 °F)

5.4.1.4 Casing-Liner Overlap Length

The effect casing-liner overlap length on leakage time was also investigated. The casing-liner overlap length can be between 50 and 500 ft (API BULLETIN E3 1993). To build the leakage scenarios, overlap length was varied between 50 and 500 ft with a 50 ft increment at different microannulus gap sizes (50, 75, and 100 μm). The cement column was exposed to 500 psi differential pressure. Table 5-6 shows the input data used to study the effect of casing-liner overlap length on the leakage time.

Table 5-6: Input data for investigating the impact of cement length on the leakage time

Input Data	Field Unit
Cement column length	50, 100, 150, 200, 250, 300, 350, 400, 450, 500 ft
Casing diameter	22 in
Liner diameter	18 in
Cement thickness	2 in
Cement porosity	20%
Cement permeability	0.001 mD
Microannulus gap size	50, 75, and 100 μm
Inlet pressure	1000 psi
Outlet pressure	500 psi
Initial pressure	500 psi
Temperature	110 °F
Nitrogen viscosity	0.01946 cP

Figure 5-16 comprises 30 leakage scenarios for different casing-liner overlap lengths at 3 different microannulus gap sizes. It can be observed that the leakage time for 50 ft with different microannulus gap sizes is less than 5 minutes. It can also be noted that the leakage time is less than 40 minutes for 50 to 150 ft. It is evident that as the casing-liner overlap length gets shorter, the leakage time decreases. Therefore, this can jeopardize the well integrity in taking a kick, where the kick moves from the wellbore and then through the cement placed within the casing-liner overlap. This scenario occurred in an actual drilling operation. This can lead to an underground blowout and contaminating freshwater zones. This is why casing-liner overlap length is so important to stop such disasters.

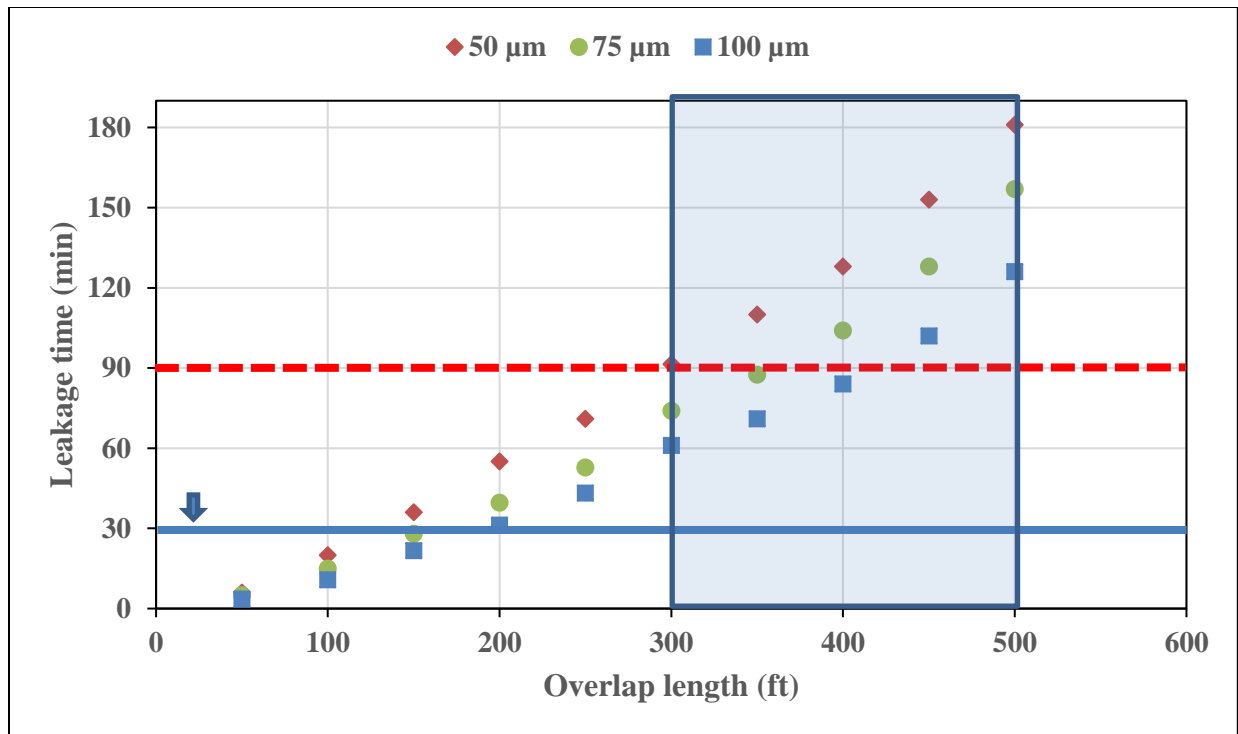


Figure 5-16: Leakage scenarios for different overlap lengths and microannulus gap sizes

5.4.2 Field Case Study

The incident presented here took place in the Main Pass Block 295 (MP295) in the Gulf of Mexico in 2013. Loss of well control occurred during a drilling operation. This field case is reported in QC-FIT report#2014-02 (BSEE 2014). This event's major cause was due to gas migration through the casing hanger seal and cement sheath into a shallow sand formation as shown in Figure 5-17. The sub mudline casing hanger was designed following the first edition of API SPEC 17 D, which only requires hydrostatic pressure testing with water. However, the current (second) edition of API SPEC 17 D (2011) was revised in 2011. It requires gas qualification testing of the equipment, addresses the design methodology, and verifies and validates wellhead production hangers sub mudline casing hangers, and seals.

Referring to the incident documented in the QC-FIT report, the last casing shoe was set at 1000 ft while the liner hanger was set at 700 ft, creating a 300-ft casing–liner overlap. According to CFR 250.425 (2004), the duration of the pressure test of conductor and casing/liner strings is recommended to be 30 minutes. The pressure test was conducted at 900 psi for 30 minutes without any leak indication. Assuming the casing's formation pressure is 450 psi, this will create a 450-psi differential pressure on the cement column behind the casing–liner overlap. Assuming a faulty barrier system (cement with 0.001-mD permeability, microannulus gap of 70 μm, and faulty elastomer) was present at the time of the incident. The casing, which the liner was engaged in, had a diameter of 22 inches, while the liner used had a diameter of 18 inches.

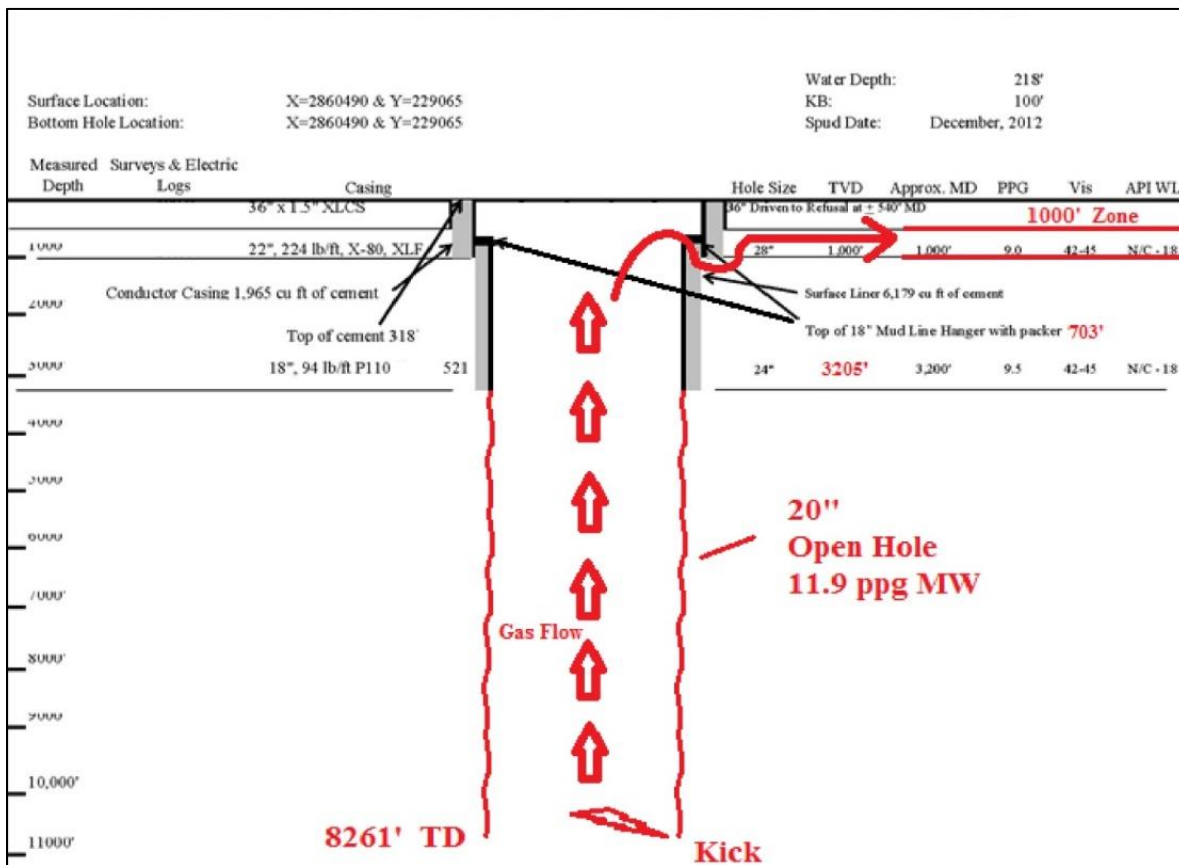


Figure 5-17: Actual wellbore schematic at the time of loss of well control (BSEE 2014)

Prior to simulating the leakage scenario for the field case, the model was validated again. The input data used to validate the field case model are the ones used to simulate this incident, but without a microannulus. The input data are shown in Table 5-7.

Table 5-7: Input data used to simulate the field case scenario

Input Data	Field Unit
Cement column length	300 ft
Casing diameter	22 in
Liner diameter	18 in
Cement thickness	2 in
Cement porosity	20%
Cement permeability	0.001 mD
Microannulus gap size	70 μm
Inlet pressure	900 psi
Outlet pressure	450 psi
Initial pressure	450 psi
Temperature	110 °F
Nitrogen viscosity	0.01946 cP

A leakage scenario was developed for this case during the time of pressure testing of the casing-liner overlap. Some assumptions were made to create this leakage scenario. It was assumed that the cement was tight and had a permeability value of 0.001 mD. Also, the cement sheath had a microannulus gap of 70 μm .

The duration of the pressure test was 30 minutes. The pressure test was conducted at 900 psi for 30 minutes without any leak indication. Figure 5-18 shows the gas flow rate with time for a test duration of 150 minutes. It can be observed that the gas starts flowing after almost 75 minutes. This implies that a 30-minute pressure test may not have been enough to reveal any significant leak for a 300-ft overlap. Therefore, the pressure duration should be at least 90 minutes for a cement column length greater or equal to 300 ft in the casing–liner overlap. This model can assess the risk in well design by feeding the model with the required data.

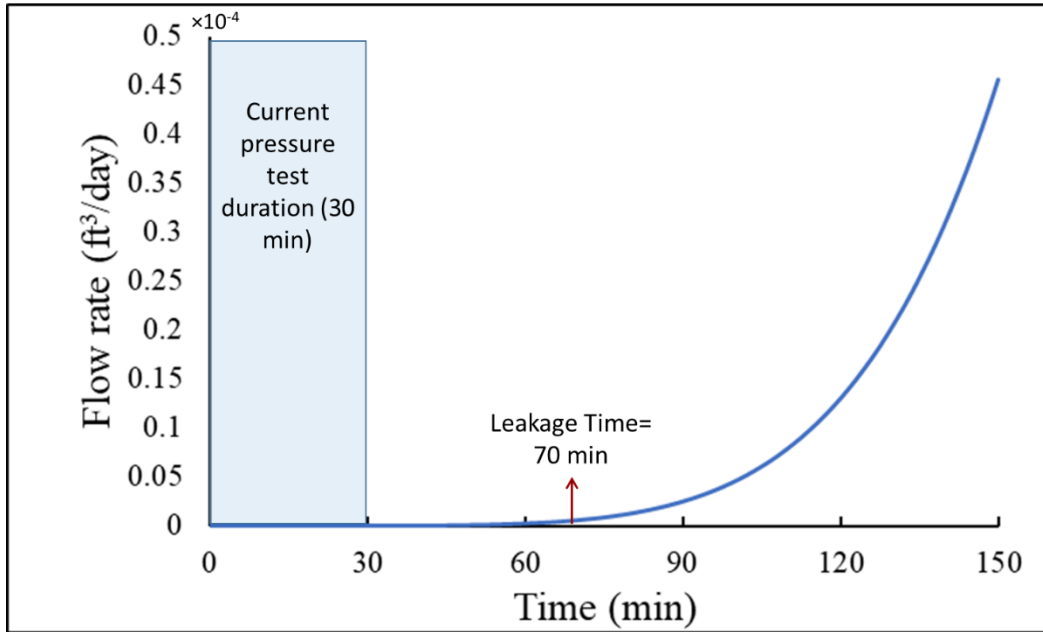


Figure 5-18: Gas flow rate with time during the pressure test conducted on the casing-liner overlap (flow rate at 900 psi and 110 °F)

Another scenario of the field case was developed by using the same input data shown in Table 5-7, while varying only the cement matrix permeability from 0.001 mD to 0.01 mD. Figure 5-19 shows the gas flow rate with time for a test duration of 150 minutes. It can be observed that the gas starts flowing after almost 45 minutes. This implies that a 30-minute pressure test may not have been enough to reveal any significant leak

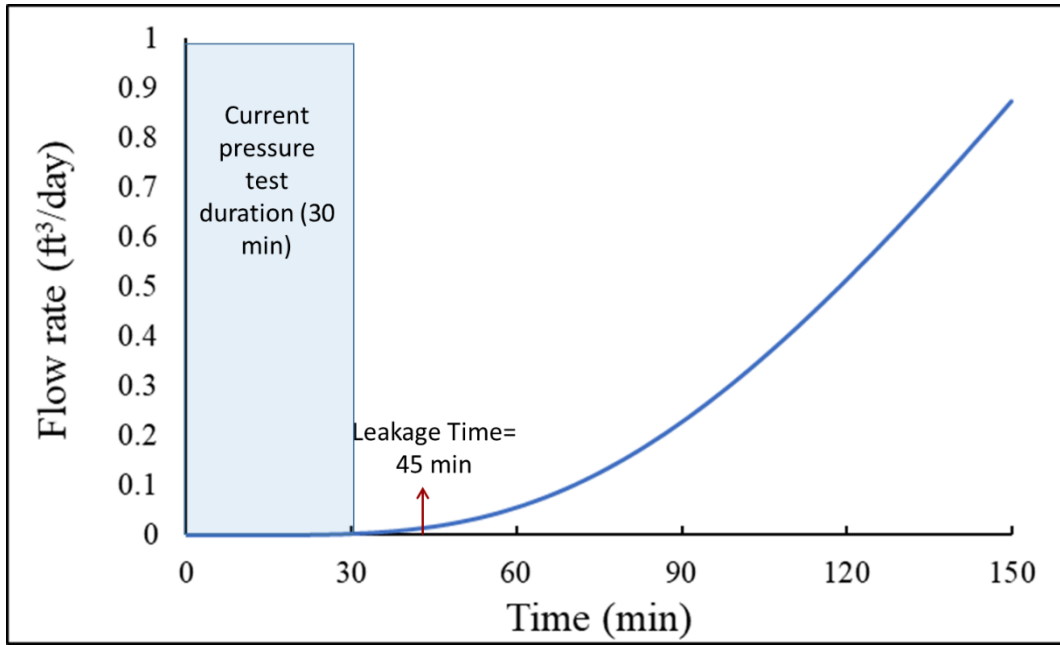


Figure 5-19: Gas flow rate with time during the pressure test conducted on the casing-liner overlap for $K_c=0.01$ mD (flow rate at 900 psi and 110 °F)

Chapter 6: Summary, Conclusions, and Recommendations

6.1 Summary

This dissertation addresses annular gas migration through cement sheath and microannulus. In this study, the cement sealability investigation, the critical length of casing-liner overlap, and pressure test duration were performed. The investigation was carried out using experimental, analytical, and numerical approaches. An experimental investigation was performed in response to the first hypothesis. Two different cements mixtures were considered, and anti-gas migration additives were mixed with cement in one of the mixtures. An analytical approach was used to test the second and third hypotheses. Leakage scenarios were developed to investigate the critical length of casing-liner overlap. Also, a numerical gas leakage model was developed, validated, and verified to examine the second and third hypotheses. This numerical model can predict the leakage time of gas, and it can assess the risk associated with well design.

The outcome of this research can benefit the oil and gas industry. The developed numerical model can be used as a tool for risk assessment in well design. This model can generate leakage scenarios and find the optimum liner overlap length that can be used for specific conditions. This will keep the environment safe and clean by mitigating gas migration to freshwater formations and surfaces. It will also save time and money, and it will ensure the safety of the crew and the integrity of the well.

6.2 Conclusions

Based on the experimental, analytical, and numerical studies performed in this work, the following conclusions have been drawn:

1. Neat Class H, Class G, or other slurry designs with additives (but without gas migration control additive) cannot serve as a primary barrier in the annular space. Thus, implementation of

specific anti-gas migration additive(s) (especially in gas migration prone zones) should be incorporated as standard recommended practices by API.

2. Based on the experiments conducted, the wellbore permeability of annular cement using neat Class H and Class G cement can range between 10^{-3} and 10^{-1} mD.
3. The experiments performed revealed that the wellbore permeability of annular cement increases as cement age increases. One possible reason for this increase is that the flow path has been created earlier, and as more tests were conducted, the injection of gas will cause the flow path to be eroded; hence, the permeability will increase.
4. WOC time can affect gas migration rate and cement permeability. WOC time of 12 hours might not be enough for the cement to completely solidify and form a barrier to seal the annular space.
5. The annular cement should not be considered as a primary barrier, primarily when liner hanger is used. There are several reasons for not considering the annular cement as a primary barrier. Many parameters influence the cement sealability, including but not limited to cement placement, amount of anti-gas migration additives used, quality of water, downhole conditions.
6. Based on the analytical and numerical modeling, the developed leakage scenarios showed that the leakage time increases as the length of the casing–liner overlap increases.
7. Based on the numerical model's parametric study, cement matrix permeability, microannulus gap size, and cement length can greatly impact leakage time. Cement porosity has a minimal effect on the leakage time, assuming other parameters are constant such as permeability.

8. The leakage scenario results revealed that 62% of the total leakage time falls under the casing–liner overlap range between 50 and 250 ft. This overlap range may not permit a longer duration for the detection and control of gas influx, when the cement sheath is faulty.
9. The leakage scenario results suggest that only 35% of the leakage times are between 1 and 30 minutes. The current casing pressure test duration of 30 minutes may not be enough to verify the cement sheath's integrity in the liner hanger overlap.

6.3 Recommendations and Future Work

The recommendation presented in this section are based on the reviews, experimental, and modeling studies:

1. It is recommended to use gas migration additives in formulating a cement recipe for shallow gas formation zones and abnormal pressure intervals. This will prevent the invasion of uncontrolled gas during the transition of cement slurry to the solid phase.
2. It is recommended that the pressure test duration is increased beyond 30 minutes, depending on the cement column length in the casing–liner overlap. As shown from Figure 4-2, Figure 4-3, Figure 4-4, Figure 4-5, Figure 4-6, and Figure 5-16 the dashed-red horizontal line (which represents 90 minutes) is the proposed pressure test duration for a cement column length that is greater or equal to 300 ft in the casing–liner overlap. The proposed test duration is based on the assumptions made to develop the leakage scenarios. This duration can be investigated using the numerical model developed in this study and can be optimized depending on the conditions of the well to be tested.
3. Based on the leakage scenarios and the selected assumptions, it is recommended that the cement column in the casing–liner overlap is not less than 300 ft. The leakage times in Figure 4-6 and Figure 5-16 are less than 1 hour for a 50-ft to 200-ft overlap. Shorter overlaps (50 to

200 ft) can be beneficial because pressure tests may quickly identify leaks if the liner hanger's cement and elastomer are faulty. Cost may also be an incentive for the use of shorter overlaps. However, the leakage scenarios suggest that shorter overlaps have shorter leakage times, which implies a shorter time for gas migration through faulty cement and elastomer in the overlap. To err on the side of caution, particularly in gas zones, the light-blue shaded area in Figure 4-6 represents the proposed cement column length in the casing–liner overlap (300 to 500 ft). This offered range shows longer leakage times for a gas kick to migrate to the end of the overlap. In practice, the increase in leakage time can translate to a longer duration required to detect and control gas influx and migration.

4. It is recommended that the model is used to develop leakage scenarios to investigate the critical length of casing-liner overlap based on the well conditions. The optimum casing-liner overlap length might vary depending on several parameters, such as the depth at which the liner is set, the anticipated pressure of the kick, and the properties of the cement sheath and microannulus.

Here are some future work proposed based on the limitations and assumptions used in this research:

1. An advanced wellbore setup should be fabricated and used to reduce the number of unknown parameters.
2. The experiments performed in this study at temperature of 80°F. It is recommended that future experimental setups should consider the temperatures above 80°F.
3. Future experiments should also consider more anti-gas migration additives such as microsilica, nanoparticles, and fly ash.

4. The developed numerical model uses the pressure squared method, and it is limited to 2000 psi system pressure. It is recommended that the pseudo pressure method enhance the validity of this model and make it more robust.
5. The temperature effect in the numerical model was assumed negligible. It is recommended to consider it for a long cement column in deep wells.

Nomenclature

Acronyms

°F	–	Degree Fahrenheit
°K	–	Degree Kelvin
2D	–	Two dimensional
3D	–	Three dimensional
A	–	Annulus area
A _m	–	Area involved in the flow
API	–	American Petroleum Institute
atm	–	Atmospheric
BOP	–	Blowout Preventer
BSEE	–	Bureau of Safety and Environmental Enforcement
cc	–	Cubic centimetre
C _f	–	Fluid compressibility
CFR	–	Code of Federal Regulations
C _g	–	Gas compressibility
cm	–	Centimetre
CO ₂	–	Carbon dioxide
cP	–	Centi-Poise
C _r	–	Cement compressibility
C _t	–	Total compressibility
DAQ	–	Data Acquisition System
Dx	–	Distance between grids
ft	–	Foot
ft ³	–	Cubic feet
GoM	–	Gulf of Mexico
h	–	Hydraulic aperture
hrs	–	Hours

HPHT	–	High pressure high temperature
in	–	Inches
ID	–	Internal diameter
ISO	–	International Organization for Standardization
K	–	Permeability
k	–	Permeability tensor
k_{ma}	–	Microannulus permeability
L	–	Length of cement column
L_c	–	Liner-casing overlapping length
M	–	Molecular weight
m	–	Meters
m^2	–	Square meters
mD	–	milli-Darcy
Min	–	Minutes
mL	–	milli-Litres
mol	–	Mole
n	–	Normal vector
N_2	–	Nitrogen Gas
n_j	–	Number of bubbles at position j
NVR	–	Network Video Recorder
N_x	–	Number of grids
OCS	–	Outer Continental Shelf
OD	–	Outer diameter
P&A	–	Plug and abandonment
P_1	–	Inlet pressure
P_a	–	Pascal
P_b	–	Base pressure
P_d	–	Downstream pressure

P_i	–	Inlet pressure
P_{in}	–	Inlet Pressure
P_o	–	Initial pressure
P_{out}	–	Outlet Pressure
ppg	–	Pound per gallon
PSA	–	Petroleum Safety Authority
Psi	–	Pound per square inch
Psia	–	Pound per square inch absolute
Psig	–	Pound per square inch gauge
P_u	–	Upstream pressure
$P_{u(i)}$	–	Initial upstream pressure
$P_{u(t)}$	–	Upstream pressure at time t
q	–	Gas flow rate
QC-FIT	–	Quality Control Failure Incident Team
q_g	–	Gas flow rate
R	–	Universal gas constant
R_c	–	Outer casing radius
R_i	–	Inner casing radius
R_m	–	Microannulus radius
scf	–	Standard cubic feet
SCP	–	Sustained casing pressure
Sec	–	Seconds
SGS	–	Static gel strength
SSSV	–	Subsurface safety valve
t	–	Time
T	–	Temperature
u	–	Velocity Vector
UCS	–	Unconfined compressive strength

- V – Upstream volume
- V_j – Volume of bubbles at position j
- W/C – Water to cement ratio
- WOC – Wait on cement
- WT – Wall thickness
- z – Gas compressibility factor

GREEK SYMBOLS

- μ – Gas viscosity/Micro
- β – Inertial coefficient
- ρ – Gas density
- ω – Length of hydraulic aperture
- ϕ – Porosity

References

1. Aas, B., Sørbo, J., Stokka, S. et al. 2016. Cement Placement with Tubing Left in Hole during Plug and Abandonment Operations. Presented at the IADC/SPE Drilling Conference and Exhibition, Fort Worth, Texas, USA. 1-3 March. <https://doi.org/10.2118/178840-MS>.
2. Abbas, G., Irawan, S., Kumar, S. et al. 2014. Experimental Study of Gas Migration Prevention Through Cement Slurry Using Hydroxypropylmethylcellulose. Presented at the IADC/SPE Asia Pacific Drilling Technology Conference, Bangkok, Thailand. 25-27 August. <https://doi.org/10.2118/170538-MS>.
3. Ahmed, S. 2020. *Evaluation of liner hanger seal assembly and cement sheath as a dual barrier system: implications for industry and regulators*. PhD Dissertation, University of Oklahoma, Norman, Oklahoma (May 2020).
4. Ahmed, S., Ezeakacha, C., and Salehi, S. 2018. Improvement in Cement Sealing Properties and Integrity Using Conductive Carbon Nano Materials: From Strength to Thickening Time. Presented at the SPE Annual Technical Conference and Exhibition, Dallas, Texas, USA. 24-26 September. <https://doi.org/10.2118/191709-MS>.
5. Ahmed, S., Patel, H., and Salehi, S. 2021. Effects of wait on cement, setting depth, pipe material, and pressure on performance of liner cement. *Journal of Petroleum Science and Engineering* **196**: 108008. <http://www.sciencedirect.com/science/article/pii/S0920410520310639>.
6. Ahmed, S., Salehi, S., and Ezeakacha, C. 2020. Review of gas migration and wellbore leakage in liner hanger dual barrier system: Challenges and implications for industry. *Journal of Natural Gas Science and Engineering* **78**: 103284. <http://www.sciencedirect.com/science/article/pii/S1875510020301384>.
7. Ahmed, S., Salehi, S., Ezeakacha, C. et al. 2019a. Evaluation of liner hanger seal assembly and cement sheath as a dual barrier system: Implications for industry standards. *Journal of Petroleum Science and Engineering* **178**: 1092-1103. <http://www.sciencedirect.com/science/article/pii/S0920410519303535>.
8. Ahmed, S., Salehi, S., Ezeakacha, C. et al. 2019b. Experimental investigation of elastomers in downhole seal elements: Implications for safety. *Polymer Testing* **76**: 350-364. <http://www.sciencedirect.com/science/article/pii/S0142941819302831>.

9. Ajayi, T. and Gupta, I. 2019. A review of reactive transport modeling in wellbore integrity problems. *Journal of Petroleum Science and Engineering* **175**: 785-803. <http://www.sciencedirect.com/science/article/pii/S0920410518311884>.
10. Al-Buraik, K., Al-Abdulqader, K., and Bsaibes, R. 1998. Prevention of Shallow Gas Migration Through Cement. Presented at the IADC/SPE Asia Pacific Drilling Technology, Jakarta, Indonesia. 7-9 September. <https://doi.org/10.2118/47775-MS>.
11. Al Ramadan, M., Salehi, S., Ezeakacha, C. et al. 2019a. Analytical and Experimental Investigation of the Critical Length in Casing–Liner Overlap. *Sustainability* **11** (23): 6861. <https://www.mdpi.com/2071-1050/11/23/6861>.
12. Al Ramadan, M., Salehi, S., Kwatia, G. O. et al. 2019b. Experimental investigation of well integrity: Annular gas migration in cement column. *Journal of Petroleum Science and Engineering* **179**: 126-135. <http://www.sciencedirect.com/science/article/pii/S0920410519303596>.
13. Al Ramadan, M., Salehi, S., and Teodoriu, C. 2019c. Robust Leakage Modeling for Plug and Abandonment Applications. *Proc.*, ASME 2019 38th International Conference on Ocean, Offshore and Arctic Engineering, Glasgow, Scotland, UK, 9–14 June. <https://doi.org/10.1115/OMAE2019-95612>.
14. ANSI/API-RP-100-1, *Hydraulic Fracturing-Well Integrity and Fracture Confinement* 2015. Washington, DC: American Petroleum Institute
15. API 65-1, *Recommended Practice for Cementing Shallow Water Flow Zones in Deepwater Wells, second edition*, 2018. Washington, DC: American Petroleum Institute.
16. API 65-2, *Standard for Isolating Cementing Shallow-water Flow Zones in Deepwater Wells, Second Edition*, 2010. Washington, DC: American Petroleum Institute.
17. API BULLETIN E3, *Environmental Guidance Document: Well Abandonment and Inactive Well Practices for U.S. Exploration and Production Operations, First Edition*, 1993. Washington, DC: API.
18. API Bulletin E3, *Wellbore Plugging and Abandonment Practices*, 2018. Washington, DC: American Petroleum Institute.
19. API RP 90, *Recommended Practice for Testing Well Cements, second edition*, 2013. Washington, DC: American Petroleum Institute.

20. API RP 90, *Annular Casing Pressure Management for Offshore Wells*, 2006. Washington, DC: American Petroleum Institute.
21. API RP 96, *Recommended Practice for Deepwater Well Design and Construction*, 2013. Washington, DC: American Petroleum Institute.
22. API SPEC 17 D, *Specification for Design and Operation of Subsea Production Systems-Subsea Wellhead and Tree Equipment, 2nd edition*, 2011. Washington, DC: API.
23. Bannister, C. E., Benge, O. G., and Marcinew, R. P. 1984. Critical Design Parameters To Prevent Gas Invasion During Cementing Operations. Presented at the Annual Technical Meeting, Calgary, Alberta. 10-13 June. <https://doi.org/10.2118/84-35-106>.
24. Bois, A.-P., Garnier, A., Rodot, F. et al. 2011. How To Prevent Loss of Zonal Isolation Through a Comprehensive Analysis of Microannulus Formation. *SPE Drilling & Completion* **26** (01): 13-31. <https://doi.org/10.2118/124719-PA>.
25. Bois, A., Garnier, A., Galdiolo, G. et al. 2012. Use of a Mechanistic Model To Forecast Cement-Sheath Integrity. *SPE Drilling & Completion* **27** (02): 303-314. <https://doi.org/10.2118/139668-PA>.
26. Bois, A., Vu, M., Galidiolo G. et al. 2017. Use of Advanced Gas Migration Model to Optimize Zonal Isolation. Presented at the AADE National Technical Conference and Exhibition, Houston, Texas. 11-12 April. <http://www.aade.org/technical-papers/2017-national-technical-conference-papers/>.
27. Bonett, A. and Pafitis, D. 1996. Getting to the root of gas migration. *Oilfield Review* **8** (1): 36-49.
28. Boukhelifa, L., Moroni, N., James, S. G. et al. 2004. Evaluation of Cement Systems for Oil and Gas Well Zonal Isolation in a Full-Scale Annular Geometry. Presented at the IADC/SPE Drilling Conference, Dallas, Texas. 2-4 March. <https://doi.org/10.2118/87195-MS>.
29. Brace, W. F., Walsh, J. B., and Frangos, W. T. 1968. Permeability of granite under high pressure. *Journal of Geophysical Research* **73** (6): 2225-2236. <https://agupubs.onlinelibrary.wiley.com/doi/abs/10.1029/JB073i006p02225>.

30. BSEE. 2014. QC-FIT Evaluation of Seal Assembly & Cement Failures Interim Summary of Findings. Report No. Internal QC-FIT Report #2014-02, Bureau of Safety and Environmental Enforcement.
31. Bybee, K. 2005. The Cement-to-Formation Interface in Zonal Isolation. *Journal of Petroleum Technology* **57** (08): 41-44. <https://doi.org/10.2118/0805-0041-JPT>.
32. Carey, J. 2013. Geochemistry of Wellbore Integrity in CO₂ Sequestration: Portland Cement-Steel-Brine-CO₂ Interactions. *Reviews in Mineralogy and Geochemistry* **77** (1): 505-539. <https://doi.org/10.2138/rmg.2013.77.15>.
33. Carlsen, F. 2019. Trends in Risk Level in the Norwegian Petroleum Activity, The Petroleum Safety Authority, Stavenger, Norway (10 April 2019).
34. Carroll, S., Carey, J., Dzombak, D. et al. 2016. Review: Role of chemistry, mechanics, and transport on well integrity in CO₂ storage environments. *International Journal of Greenhouse Gas Control* **49**: 149-160. <http://www.sciencedirect.com/science/article/pii/S175058361630010X>.
35. Carter, G. and Slagle, K. 1972. A Study of Completion Practices To Minimize Gas Communication. *Journal of Petroleum Technology* **24** (09): 1170-1174. <https://doi.org/10.2118/3164-PA>.
36. Carter, L. G. and Evans, G. W. 1964. A Study of Cement-Pipe Bonding. *Journal of Petroleum Technology* **16** (02): 157-160. <https://doi.org/10.2118/764-PA>.
37. CFR-250.425, *What are the Requirements for Pressure Testing Liners?* , 2004. Dallas, TX: Office of the Federal Register National Archives and Records Administration.
38. Checkai, D., Bryant, S., and Tao, Q. 2013. Towards a Frequency Distribution of Effective Permeabilities of Leaky Wellbores. *Energy Procedia* **37**: 5653-5660. <http://www.sciencedirect.com/science/article/pii/S1876610213007303>.
39. Chenevert, M. E. and Shrestha, B. K. 1991. Chemical Shrinkage Properties of Oilfield Cements (includes associated paper 23477). *SPE Drilling Engineering* **6** (01): 37-43. <https://doi.org/10.2118/16654-PA>.
40. Cheung, P. R. and Beirute, R. M. 1985. Gas Flow in Cements. *Journal of Petroleum Technology* **37** (06): 1041-1048. <https://doi.org/10.2118/11207-PA>.

41. Christian, W. W., Chatterji, J., and Ostroot, G. W. 1976. Gas Leakage in Primary Cementing - A Field Study and Laboratory Investigation. *Journal of Petroleum Technology* **28** (11): 1361-1369. <https://doi.org/10.2118/5517-PA>.
42. Cooke, C. E., Jr., Kluck, M. P., and Medrano, R. 1983. Field Measurements of Annular Pressure and Temperature During Primary Cementing. *Journal of Petroleum Technology* **35** (08): 1429-1438. <https://doi.org/10.2118/11206-PA>.
43. Corina, A. N., Opedal, N., Vrålstad, T. et al. 2019. Cement Plug Sealing Studies of Silica Cement Systems. *Proc.*, ASME 2019 38th International Conference on Ocean, Offshore and Arctic Engineering, Glasgow, Scotland, UK, 9–14 June. <https://doi.org/10.1115/OMAE2019-95928>.
44. Corina, A. N., Opedal, N., Vrålstad, T. et al. 2020. The Effect of Casing-Pipe Roughness on Cement-Plug Integrity. *SPE Drilling & Completion Preprint* (Preprint): 15. <https://doi.org/10.2118/194158-PA>.
45. Crow, W., Carey, J. W., Gasda, S. et al. 2010. Wellbore integrity analysis of a natural CO₂ producer. *International Journal of Greenhouse Gas Control* **4** (2): 186-197. <http://www.sciencedirect.com/science/article/pii/S1750583609001315>.
46. Davies, R. J., Almond, S., Ward, R. S. et al. 2014. Oil and gas wells and their integrity: Implications for shale and unconventional resource exploitation. *Marine and Petroleum Geology* **56**: 239-254. <https://doi.org/10.1016/j.marpetgeo.2014.03.001>.
47. Dean, G. D. and Brennen, M. A. 1992. A Unique Laboratory Gas Flow Model Reveals Insight To Predict Gas Migration in Cement. Presented at the SPE Western Regional Meeting, Bakersfield, California. 30 March - 1 April <https://doi.org/10.2118/24049-MS>.
48. Dubash, N. and Frigaard, I. 2004. Conditions for static bubbles in viscoplastic fluids. *Physics of Fluids* **16** (12): 4319-4330. <https://aip.scitation.org/doi/abs/10.1063/1.1803391>.
49. Fakoya, M., Patel, H., and Shah, S. 2018. Nanotechnology: innovative applications in the oil and gas industry. *Int J Global Adv Mater Nanotechnol* **1** (5): 16-30.
50. Feng, Y., Li, X., and Gray, K. E. 2017. Development of a 3D numerical model for quantifying fluid-driven interface debonding of an injector well. *International Journal of Greenhouse Gas Control* **62**: 76-90. <http://www.sciencedirect.com/science/article/pii/S1750583616307228>.
51. Forchheimer, P. 1901. Wasserbewegung durch boden. *Z Ver Deutsch, Ing* **45**: 1782-1788.

52. Ford, E. P., Moeinikia, F., Lohne, H. et al. 2017. Leakage Calculator for Plugged and Abandoned Wells. Presented at the SPE Bergen One Day Seminar, Bergen, Norway. 5 April 2017. <https://doi.org/10.2118/185890-MS>.
53. Gasda, S., Celia, M., Wang, J. S. Y. et al. 2013. Wellbore Permeability Estimates from Vertical Interference Testing of Existing Wells. *Energy Procedia* **37**: 5673-5680. <http://www.sciencedirect.com/science/article/pii/S1876610213007327>.
54. Gomez, S. P., Sobolik, S. R., Matteo, E. N. et al. 2017. Investigation of wellbore microannulus permeability under stress via experimental wellbore mock-up and finite element modeling. *Computers and Geotechnics* **83**: 168-177. <http://www.sciencedirect.com/science/article/pii/S0266352X16302300>.
55. Goodwin, K. J. and Crook, R. J. 1992. Cement Sheath Stress Failure. *SPE Drilling Engineering* **7** (04): 291-296. <https://doi.org/10.2118/20453-PA>.
56. Grinrod, M., Vassoy, B., and Dingsoyr, E. O. 1988. Development and Use of a Gas-Tight Cement. Presented at the IADC/SPE Drilling Conference, Dallas, Texas. 28 February-2 March. <https://doi.org/10.2118/17258-MS>.
57. Huerta, N., Checkai, D., and Bryant, S. 2009. Utilizing Sustained Casing Pressure Analog to Provide Parameters to Study CO₂ Leakage Rates Along a Wellbore. Presented at the SPE International Conference on CO₂ Capture, Storage, and Utilization, San Diego, California, USA. 2-4 November. <https://doi.org/10.2118/126700-MS>.
58. Huerta, N. J., Hesse, M. A., Bryant, S. L. et al. 2013. Experimental Evidence for Self-Limiting Reactive Flow through a Fractured Cement Core: Implications for Time-Dependent Wellbore Leakage. *Environmental Science & Technology* **47** (1): 269-275. <https://doi.org/10.1021/es3013003>.
59. Ichim, A. 2017. *Experimental determination of oilfield cement properties and their influence on well integrity*. Masters Thesis, University of Oklahoma (December 2017).
60. ISO 16530-1, *Petroleum and natural gas industries—Well integrity—Part 1, Life cycle governance*, 2017. Geneva, Switzerland: International Organization for Standardization
61. Jackson, P. B. and Murphey, C. E. 1993. Effect of Casing Pressure on Gas Flow Through a Sheath of Set Cement. Presented at the SPE/IADC Drilling Conference, Amsterdam, Netherlands. 23-25 February. <https://doi.org/10.2118/25698-MS>.

62. Jafarzade, G. 2014. *Leakage of CO₂ along Annular Well Cement*. Master's Thesis, Norwegian University of Science and Technology (August 2014).
63. Jannot, Y. and Lasseux, D. 2012. A new quasi-steady method to measure gas permeability of weakly permeable porous media. *Review of Scientific Instruments* **83** (1): 015113. <https://aip.scitation.org/doi/abs/10.1063/1.3677846>.
64. Jones, R. R. and Carpenter, R. B. 1991. New Latex, Expanding Thixotropic Cement Systems Improve Job Performance and Reduce Costs. Presented at the SPE International Symposium on Oilfield Chemistry, Anaheim, California. 20-22 February. <https://doi.org/10.2118/21010-MS>.
65. Kang, M., Baik, E., Miller, A. et al. 2015. Effective Permeabilities of Abandoned Oil and Gas Wells: Analysis of Data from Pennsylvania. *Environmental Science & Technology* **49** (7): 4757-4764. <https://doi.org/10.1021/acs.est.5b00132>.
66. Khalifeh, M., Saasen, A., Hodne, H. et al. 2018. Geopolymers as an alternative for oil well cementing applications: A review of advantages and concerns. *Journal of Energy Resources Technology* **140** (9): 092801. <https://doi.org/10.1115/OMAE2017-61227>.
67. Kimanzi, R., Patel, H., Khalifeh, M. et al. 2019. Potentials of nano-designed plugs: implications for short and long term well integrity. *Proc., 38th International Conference on Ocean, Offshore & Arctic Engineering* Glasgow, Scotland, UK, 9-14 June <https://doi.org/10.1115/OMAE2019-95589>.
68. Kiran, R., Teodoriu, C., Dadmohammadi, Y. et al. 2017. Identification and evaluation of well integrity and causes of failure of well integrity barriers (A review). *Journal of Natural Gas Science and Engineering* **45**: 511-526. <https://doi.org/10.1016/j.jngse.2017.05.009>.
69. Koenders, E. A. B. and van Breugel, K. 1997. Numerical modelling of autogenous shrinkage of hardening cement paste. *Cement and Concrete Research* **27** (10): 1489-1499. <http://www.sciencedirect.com/science/article/pii/S0008884697001701>.
70. Kristiansen, T., Dyngeland, T., Kinn, S. et al. 2018. Activating Shale to Form Well Barriers: Theory and Field Examples. Presented at the SPE Annual Technical Conference and Exhibition, Dallas, Texas, USA. 24-26 September. <https://doi.org/10.2118/191607-MS>.
71. Kwatia, G. O. 2018. *Studying “fitness for service” of the sealing assemblies and cement system*. Master's Thesis, University of Oklahoma, Norman, Oklahoma (May 2018).

72. Kwatia, G. O., Al Ramadan, M., Salehi, S. et al. 2019. Enhanced Cement Composition for Preventing Annular Gas Migration. *Proc.*, ASME 2019 38th International Conference on Ocean, Offshore and Arctic Engineering, Glasgow, Scotland, UK, June 9–14. <https://doi.org/10.1115/OMAE2019-95589>.
73. Ladva, H. K. J., Craster, B., Jones, T. G. J. et al. 2005. The Cement-to-Formation Interface in Zonal Isolation. *SPE Drilling & Completion* **20** (03): 186-197. <https://doi.org/10.2118/88016-PA>.
74. Lavrov, A. and Torsæter, M. 2016. Formation Stresses, Casing Pressure, and Annular Cement. In *Physics and Mechanics of Primary Well Cementing*, ed. Alexandre Lavrov and Malin Torsæter, 75-91. Cham: Springer International Publishing.
75. Lee, W. J. and Wattenbarger, R. A. 1996. *Gas reservoir engineering*, Vol. 5, 80-82. United State: Society of Petroleum Engineers.
76. Moore, M. J., Campo, D. B., Hockaday, J. et al. 2002. Expandable Liner Hangers: Case Histories. Presented at the Offshore Technology Conference, Houston, Texas. 6-9 May <https://doi.org/10.4043/14313-MS>.
77. Murray, S. J., Williamson, M. D., Gilham, S. et al. 1995. Well Design for Shallow Gas. Presented at the SPE/IADC Drilling Conference, Amsterdam, Netherlands. 28 February-2 March. <https://doi.org/10.2118/29343-MS>.
78. Nelson, E. B. and Guillot, D. 2006. *Well Cementing*, Second edition. Sugar Land, Texas 77478: Schlumberger.
79. Nishikawa, S. 1999. *Mechanism of Gas Migration after Cement Placement and Control of Sustained Casing Pressure*. Master's Thesis, Louisiana State University, Baton Rouge, Louisiana (May 1999).
80. NORSOK D-010, *Well integrity in drilling and well operations, rev. 4*, 2013. Lysaker, Norway: Standard Norway.
81. Nygaard, R., Salehi, S., Weideman, B. et al. 2014. Effect of Dynamic Loading on Wellbore Leakage for the Wabamun Area CO₂-Sequestration Project. *Journal of Canadian Petroleum Technology* **53** (01): 69-82. <https://doi.org/10.2118/146640-PA>.
82. Oil & Gas UK, *Guidelines for the Abandonment of Wells, 5th edition*, 2015. London, UK: Oil & Gas UK. <https://oilandgasuk.co.uk/product/op071/>.

83. Omosebi, O. A. 2016. *Mechanical Degradation of Well Cement in HPHT Carbonic Acid Environment: Experimental Studies and Mathematical Modeling*. PhD dissertation, University of Oklahoma, Norman, Oklahoma (June 2016).
84. Opedal, N., Corina, A. N., and Vrålstad, T. 2018. Laboratory Test on Cement Plug Integrity. *Proc.*, ASME 2018 37th International Conference on Ocean, Offshore and Arctic Engineering. <https://doi.org/10.1115/OMAE2018-78347>.
85. Parrott, L. J. 1995. Influence of cement type and curing on the drying and air permeability of cover concrete. *Magazine of Concrete Research* **47** (171): 103-111. <https://www.icevirtuallibrary.com/doi/abs/10.1680/mac.1995.47.171.103>.
86. Patel, H. 2016. *Effect of Nanoparticles and Solvent Based Emulsion on Heavy Oil Viscosity*. Master's Thesis, University of Oklahoma, Norman, OK (May 2016).
87. Patel, H. and Salehi, S. 2019. Development of an Advanced Finite Element Model and Parametric Study to Evaluate Cement Sheath Barrier. *Journal of Energy Resources Technology* **141** (9). <https://doi.org/10.1115/1.4043137>.
88. Patel, H., Salehi, S., and Teodoriu, C. 2019. Assessing Mechanical Integrity of Expanding Cement. Presented at the SPE Oklahoma City Oil and Gas Symposium, Oklahoma City, Oklahoma, USA. 9-10 April. <https://doi.org/10.2118/195225-MS>.
89. Phi, T., Elgaddafi, R., Al Ramadan, M. et al. 2019. Well Integrity Issues: Extreme High-Pressure High-Temperature Wells and Geothermal Wells a Review. Presented at the SPE Thermal Well Integrity and Design Symposium, Banff, Alberta, Canada. 19-21 November. <https://doi.org/10.2118/198687-MS>.
90. Pinto, G., Martins, A., Rocha, J. et al. 2012. New methodology for gas migration prediction before oilwell cementing. *Brazilian Journal of Petroleum and Gas* **6** (2).
91. PSA. 2013. Principles for Barrier Management in The Petroleum Industry, Norwegian Petroleum Safety Authority https://www.ptil.no/contentassets/11851dc03a84473e8299a2d80e656356/principles-for-barrier-management-in-the-petroleum-industry_2013.pdf.
92. Rocha-Valadez, T., Hasan, A. R., Mannan, S. et al. 2014. Assessing Wellbore Integrity in Sustained-Casing-Pressure Annulus. *SPE Drilling & Completion* **29** (01): 131-138. <https://doi.org/10.2118/169814-PA>.

93. Sabins, F. L., Tinsley, J. M., and Sutton, D. L. 1982. Transition Time of Cement Slurries Between the Fluid and Set States. *Society of Petroleum Engineers Journal* **22** (06): 875-882. <https://doi.org/10.2118/9285-PA>.
94. Salehi, S. 2013. Modeling Near Wellbore Leakage Pathways in Shale Gas Wells: Investigating Short and Long Terms Wellbore Integrity. *Proc.*, US EPA Technical Workshop on Well Construction/Operation and Subsurface Modelling, Research Triangle Park, North Carolina, April, Research Triangle Park, North Carolina.
95. Salehi, S., Khattak, M., Ali, N. et al. 2017. Study and Use of Geopolymer Mixtures for Oil and Gas Well Cementing Applications. *Journal of Energy Resources Technology* **140** (1). <https://doi.org/10.1115/1.4037713>.
96. Sarkar, S., Toksoz, M., and Burns, D. 2004. Fluid flow modeling in fractures, Massachusetts Institute of Technology. Earth Resources Laboratory.
97. Stewart, R. B. and Schouten, F. C. 1988. Gas Invasion and Migration in Cemented Annuli: Causes and Cures. *SPE Drilling Engineering* **3** (01): 77-82. <https://doi.org/10.2118/14779-PA>.
98. Stiles, D. 2006. Annular Formation Fluid Migration. In *Well Cementing*, ed. Erik B. Nelson and Dominique Guillot. Sugar Land, Texas: Schlumberger.
99. Stormont, J. C., Ahmad, R., Ellison, J. et al. 2015. Laboratory Measurements of flow Through Wellbore Cement-Casing Microannuli. Presented at the 49th US Rock Mechanics/Geomechanics Symposium, San Francisco, California. 28 June-1 July. onepetro.org/conference-paper/ARMA-2015-294.
100. Stormont, J. C., Fernandez, S. G., Taha, M. R. et al. 2018. Gas flow through cement-casing microannuli under varying stress conditions. *Geomechanics for Energy and the Environment* **13**: 1-13. <https://doi.org/10.1016/j.gete.2017.12.001>.
101. Sutton, D., Paul, R., and Sabins, F. L. 1984. New evaluation for annular gas-flow potential. *Oil Gas J;(United States)* **82** (51).
102. Talabani, S., Hareland, G., and Islam, M. R. 1997. Gas Migration Eliminated Through Correct Cement Design Including Elastomers. Presented at the SPE/IADC Middle East Drilling Technology Conference, Bahrain. 23-25 November. <https://doi.org/10.2118/39279-MS>.

103. Tao, Q., Checkai, D., and Bryant, S. 2010a. Permeability Estimation for Large-Scale Potential CO₂ Leakage Paths in Wells Using a Sustained-Casing-Pressure Model. Presented at the SPE International Conference on CO₂ Capture, Storage, and Utilization, New Orleans, Louisiana, USA. 10-12 November. <https://doi.org/10.2118/139576-MS>.

104. Tao, Q., Checkai, D., Huerta, N. et al. 2010b. Model To Predict CO₂ Leakage Rates Along a Wellbore. Presented at the SPE Annual Technical Conference and Exhibition, Florence, Italy. 19-22 September. <https://doi.org/10.2118/135483-MS>.

105. Teodoriu, C., Kosinowski, C., Amani, M. et al. 2013. Wellbore integrity and cement failure at HPHT conditions. *International Journal of Engineering* **2** (2): 2305-8269.

106. Teodoriu, C., Reinicke, K. M., Fichter, C. et al. 2010. Investigations on Casing-Cement interaction with application to Gas and CO₂ Storage Wells. Presented at the SPE EUROPEC/EAGE Annual Conference and Exhibition, Barcelona, Spain. 14-17 June. <https://doi.org/10.2118/131336-MS>.

107. Tinsley, J. M., Miller, E. C., Sabins, F. L. et al. 1980. Study of Factors Causing Annular Gas Flow Following Primary Cementing. *Journal of Petroleum Technology* **32** (08): 1427-1437. <https://doi.org/10.2118/8257-PA>.

108. Torbergsen, H. E. B., Haga, H. B., Sangesland, S. et al. 2012. An Introduction to Well Integrity. Presented at the Norwegian Oil and Gas Association's Well Integrity Forum (WIF), Norwegian University of Science and Technology (NTNU), Universitet i Stavanger (UIS). December 2012.

109. Vignes, B. 2011. Qualification Of Well Barrier Elements - Long-Term Integrity Test, Test Medium And Temperatures. Presented at the SPE European Health, Safety and Environmental Conference in Oil and Gas Exploration and Production, Vienna, Austria. 22-24 February. <https://doi.org/10.2118/138465-MS>.

110. Vignes, B. and Aadnoy, B. 2008. Well-Integrity Issues Offshore Norway. Presented at the IADC/SPE Drilling Conference, Orlando, Florida, USA. 4-6 March. <https://doi.org/10.2118/112535-MS>.

111. Watters, L. T. and Sabins, F. L. 1980. Field Evaluation Of Method To Control Gas Flow Following Cementing. Presented at the SPE Annual Technical Conference and Exhibition, Dallas, Texas. 21-24 September. <https://doi.org/10.2118/9287-MS>.

112. Webster, W. W. and Eikerts, J. V. 1979. Flow After Cementing : A Field And Laboratory Study. Presented at the SPE Annual Technical Conference and Exhibition, Las Vegas, Nevada. 23-26 September. <https://doi.org/10.2118/8259-MS>.
113. Wilkins, R. P. and Free, D. 1989. A New Approach to the Prediction of Gas Flow After Cementing. Presented at the SPE/IADC Drilling Conference, New Orleans, Louisiana. 28 February-3 March. <https://doi.org/10.2118/18622-MS>.
114. Witherspoon, P. A., Wang, J. S. Y., Iwai, K. et al. 1980. Validity of Cubic Law for fluid flow in a deformable rock fracture. *Water Resources Research* **16** (6): 1016-1024. <https://agupubs.onlinelibrary.wiley.com/doi/abs/10.1029/WR016i006p01016>.
115. Xu, R. 2002. *Analysis of diagnostic testing of sustained casing pressure in wells*. PhD Dissertation, Louisiana State University, Baton Rouge, Louisiana (December 2002).
116. Xu, R. and Wojtanowicz, A. K. 2001. Diagnosis of Sustained Casing Pressure from Bleed-off/Buildup Testing Patterns. Presented at the SPE Production and Operations Symposium, Oklahoma City, Oklahoma. 24-27 March. <https://doi.org/10.2118/67194-MS>.
117. Xu, R. and Wojtanowicz, A. K. 2003. Diagnostic Testing of Wells With Sustained Casing Pressure-An Analytical Approach. Presented at the Canadian International Petroleum Conference, Calgary, Alberta. 10-12 June. <https://doi.org/10.2118/2003-221>.
118. Xu, R. and Wojtanowicz, A. K. 2017. Pressure buildup test analysis in wells with sustained casing pressure. *Journal of Natural Gas Science and Engineering* **38**: 608-620. <http://www.sciencedirect.com/science/article/pii/S1875510016309337>.
119. Yodsudjai, W. and Wang, K. 2013. Chemical shrinkage behavior of pastes made with different types of cements. *Construction and Building Materials* **40**: 854-862. <http://www.sciencedirect.com/science/article/pii/S0950061812008896>.

Appendix A: Microannulus Gap Sizes in The Experimental Investigation

The analytical model presented in Chapter 4 was used to investigate the microannulus gap size in all the tests presented in chapter 3. Gas flow was assumed to occur only through microannulus. To estimate the microannulus gap size using the model developed by Stormont et al. (2018) (Equation 4.1), the obtained flow rate from each test was used. Then, the gas velocity was calculated based on the flow rate and microannulus area. After that, the Reynold's number was calculated based in the obtained velocity and microannulus gap size. The Reynold's number was less 2000 for all the tests conducted; hence, the gas flow was laminar in all the tests. The microannulus gap sizes ranges from 1.45 μm to 7.54 μm . Selection of microannulus gap sizes in the analytical investigation was based on the range obtained from the experimental investigation. Table A-1 to A-3, show the calculated data for all the tests in Specimen 1, Specimen 2, and Specimen 3, respectively.

Table A-1: Microannulus gap sizes in Specimen 1

Cement Age	q	q	Rm	h	v	Re	
Days	cc/sec	m ³ /s	m	μm	m ³ /s	-	
<i>1</i>	2.63E-03	2.63E-09	0.0571515	1.45	5.04E-03	0.002	Laminar
<i>2</i>	2.76E-03	2.76E-09	0.0571515	1.48	5.20E-03	0.003	Laminar
<i>11</i>	2.78E-03	2.78E-09	0.0571515	1.48	5.23E-03	0.003	Laminar
<i>12</i>	3.67E-03	3.67E-09	0.0571516	1.62	6.28E-03	0.003	Laminar
<i>13</i>	4.01E-03	4.01E-09	0.0571517	1.67	6.67E-03	0.004	Laminar

Table A-2: Microannulus gap sizes in Specimen 2

Cement Age	q	q	Rm	h	v	Re	
Days	cc/sec	m ³ /s	m	μm	m ³ /s	-	
<i>0.5</i>	0.057	5.70E-08	0.0571541	4.06	3.91E-02	0.054	Laminar
<i>8.5</i>	0.003395	3.39E-09	0.0571516	1.58	5.97E-03	0.003	Laminar
<i>9.5</i>	0.003531	3.53E-09	0.0571516	1.60	6.13E-03	0.003	Laminar

Table A-3: Microannulus gap sizes in Specimen 3

Cement Age	q	q	Rm	h	v	Re	
Days	cc/sec	m³/s	m	μm	m³/s	-	
<i>1</i>	0.095	9.49E-08	0.0571548	4.81	5.50E-02	0.09	Laminar
<i>3</i>	0.180	1.80E-07	0.0571559	5.95	8.42E-02	0.17	Laminar
<i>8</i>	0.241	2.41E-07	0.0571566	6.55	1.02E-01	0.23	Laminar
<i>9</i>	0.299	2.99E-07	0.0571570	7.04	1.18E-01	0.28	Laminar
<i>10</i>	0.367	3.67E-07	0.0571575	7.54	1.35E-01	0.35	Laminar

Appendix B: Data used to Generate the Leakage Scenarios in the Analytical Investigation

Here are the data used to develop the leakage scenarios in all the cases. Chapter 4 includes a full description on how these data were generated. All the leakage scenarios have a Reynold's number less than 2000; hence, this implies that the gas flow was laminar in all of the leakage scenarios. The data used to develop the first case are shown in Table B-1 to Table B-4, where a 250 psi of differential pressure was assumed. The leakage scenarios in the second case were developed using the data shown in Table B-5 to Table B-8, with the assumption of 500 psi differential pressure. Table B-9 to Table B-12 were used to construct the leakage scenarios in the third case where a differential pressure of 1000 psi was assumed. The fourth case was developed with an assumption of 1500 psi differential pressure, and the data for the leakage scenarios are exhibited in Table B-13 to Table B-16. The fifth case was developed with varying differential pressures at a permeability of 0.5 mD. The data for this case are shown in Table B-4, Table B-8, Table B-12, and Table B-16.

Table B-1: Data generated for 250 psi differential pressure and permeability of 0.01 mD

Lc	q	t	v	Re
ft	m³/s	hrs	m/s	
500	3.90E-10	294.14	0.0001	7.86E-04
450	4.33E-10	238.25	0.0002	8.74E-04
400	4.87E-10	188.25	0.0002	9.83E-04
350	5.57E-10	144.13	0.0002	1.12E-03
300	6.50E-10	105.89	0.0002	1.31E-03
250	7.80E-10	73.54	0.0003	1.57E-03
200	9.75E-10	47.06	0.0004	1.97E-03
150	1.30E-09	26.47	0.0005	2.62E-03
100	1.95E-09	11.77	0.0007	3.93E-03
50	3.90E-09	2.94	0.0014	7.86E-03

Table B-2: Data generated for 250 psi differential pressure and permeability of 0.1 mD

Lc	q	t	v	Re
ft	m³/s	hrs	m/s	
500	3.90E-09	29.41	0.0014	0.017
450	4.33E-09	23.83	0.0016	0.019
400	4.87E-09	18.83	0.0018	0.021
350	5.57E-09	14.41	0.0021	0.024
300	6.50E-09	10.59	0.0024	0.028
250	7.80E-09	7.35	0.0029	0.034
200	9.75E-09	4.71	0.0036	0.042
150	1.30E-08	2.65	0.0048	0.056
100	1.95E-08	1.18	0.0072	0.085
50	3.90E-08	0.29	0.0144	0.169

Table B-3: Data generated for 250 psi differential pressure and permeability of 0.3 mD

Lc	q	t	v	Re
ft	m³/s	hrs	m/s	
500	1.17E-08	9.80	0.0043	0.07
450	1.30E-08	7.94	0.0048	0.08
400	1.46E-08	6.28	0.0054	0.09
350	1.67E-08	4.80	0.0062	0.10
300	1.95E-08	3.53	0.0072	0.12
250	2.34E-08	2.45	0.0086	0.15
200	2.92E-08	1.57	0.0108	0.18
150	3.90E-08	0.88	0.0144	0.24
100	5.85E-08	0.39	0.0216	0.37
50	1.17E-07	0.10	0.0432	0.73

Table B-4: Data generated for 250 psi differential pressure and permeability of 0.5 mD

Lc	q	t	v	Re
ft	m³/s	hrs	m/s	
500	1.95E-08	5.88	0.0072	0.14
450	2.17E-08	4.77	0.0080	0.16
400	2.44E-08	3.77	0.0090	0.18
350	2.78E-08	2.88	0.0103	0.21
300	3.25E-08	2.12	0.0120	0.24
250	3.90E-08	1.47	0.0144	0.29
200	4.87E-08	0.94	0.0180	0.36
150	6.50E-08	0.53	0.0240	0.48
100	9.75E-08	0.24	0.0360	0.72
50	1.95E-07	0.06	0.0720	1.45

Table B-5: Data generated for 500 psi differential pressure and permeability of 0.01 mD

Lc	q	t	v	Re
ft	m³/s	hrs	m/s	
<i>500</i>	6.88E-10	166.63	0.0003	1.81E-03
<i>450</i>	7.65E-10	134.97	0.0003	2.01E-03
<i>400</i>	8.60E-10	106.64	0.0003	2.26E-03
<i>350</i>	9.83E-10	81.65	0.0004	2.59E-03
<i>300</i>	1.15E-09	59.99	0.0004	3.02E-03
<i>250</i>	1.38E-09	41.66	0.0005	3.62E-03
<i>200</i>	1.72E-09	26.66	0.0006	4.53E-03
<i>150</i>	2.29E-09	15.00	0.0008	6.03E-03
<i>100</i>	3.44E-09	6.67	0.0013	9.05E-03
<i>50</i>	6.88E-09	1.67	0.0025	1.81E-02

Table B-6: Data generated for 500 psi differential pressure and permeability of 0.1 mD

Lc	q	t	v	Re
ft	m³/s	hrs	m/s	
<i>500</i>	6.88E-09	16.66	0.0025	0.039
<i>450</i>	7.65E-09	13.50	0.0028	0.043
<i>400</i>	8.60E-09	10.66	0.0032	0.049
<i>350</i>	9.83E-09	8.16	0.0036	0.056
<i>300</i>	1.15E-08	6.00	0.0042	0.065
<i>250</i>	1.38E-08	4.17	0.0051	0.078
<i>200</i>	1.72E-08	2.67	0.0064	0.098
<i>150</i>	2.29E-08	1.50	0.0085	0.130
<i>100</i>	3.44E-08	0.67	0.0127	0.195
<i>50</i>	6.88E-08	0.17	0.0254	0.390

Table B-7: Data generated for 500 psi differential pressure and permeability of 0.3 mD

Lc	q	t	v	Re
ft	m³/s	hrs	m/s	
<i>500</i>	2.06E-08	5.55	0.0076	0.17
<i>450</i>	2.29E-08	4.50	0.0085	0.19
<i>400</i>	2.58E-08	3.55	0.0095	0.21
<i>350</i>	2.95E-08	2.72	0.0109	0.24
<i>300</i>	3.44E-08	2.00	0.0127	0.28
<i>250</i>	4.13E-08	1.39	0.0152	0.34
<i>200</i>	5.16E-08	0.89	0.0191	0.42
<i>150</i>	6.88E-08	0.50	0.0254	0.56
<i>100</i>	1.03E-07	0.22	0.0381	0.84
<i>50</i>	2.06E-07	0.06	0.0762	1.69

Table B-8: Data generated for 500 psi differential pressure and permeability of 0.5 mD

Lc	q	t	v	Re
ft	m³/s	hrs	m/s	
<i>500</i>	3.44E-08	3.33	0.0127	0.33
<i>450</i>	3.82E-08	2.70	0.0141	0.37
<i>400</i>	4.30E-08	2.13	0.0159	0.42
<i>350</i>	4.92E-08	1.63	0.0181	0.48
<i>300</i>	5.73E-08	1.20	0.0212	0.56
<i>250</i>	6.88E-08	0.83	0.0254	0.67
<i>200</i>	8.60E-08	0.53	0.0318	0.83
<i>150</i>	1.15E-07	0.30	0.0423	1.11
<i>100</i>	1.72E-07	0.13	0.0635	1.67
<i>50</i>	3.44E-07	0.03	0.1270	3.33

Table B-9: Data generated for 1000 psi differential pressure and permeability of 0.01 mD

Lc	q	t	v	Re
ft	m³/s	hrs	m/s	
<i>500</i>	1.17E-09	97.79	0.0004	4.39E-03
<i>450</i>	1.30E-09	79.21	0.0005	4.87E-03
<i>400</i>	1.47E-09	62.59	0.0005	5.48E-03
<i>350</i>	1.68E-09	47.92	0.0006	6.27E-03
<i>300</i>	1.95E-09	35.20	0.0007	7.31E-03
<i>250</i>	2.35E-09	24.45	0.0009	8.77E-03
<i>200</i>	2.93E-09	15.65	0.0011	1.10E-02
<i>150</i>	3.91E-09	8.80	0.0014	1.46E-02
<i>100</i>	5.86E-09	3.91	0.0022	2.19E-02
<i>50</i>	1.17E-08	0.98	0.0043	4.39E-02

Table B-10: Data generated for 1000 psi differential pressure and permeability of 0.1 mD

Lc	q	t	v	Re
ft	m³/s	hrs	m/s	
<i>500</i>	1.17E-08	9.78	0.0043	0.094
<i>450</i>	1.30E-08	7.92	0.0048	0.105
<i>400</i>	1.47E-08	6.26	0.0054	0.118
<i>350</i>	1.68E-08	4.79	0.0062	0.135
<i>300</i>	1.95E-08	3.52	0.0072	0.157
<i>250</i>	2.35E-08	2.44	0.0087	0.189
<i>200</i>	2.93E-08	1.56	0.0108	0.236
<i>150</i>	3.91E-08	0.88	0.0144	0.315
<i>100</i>	5.86E-08	0.39	0.0216	0.472
<i>50</i>	1.17E-07	0.10	0.0433	0.945

Table B-11: Data generated for 1000 psi differential pressure and permeability of 0.3 mD

Lc	q	t	v	Re
ft	m³/s	hrs	m/s	
500	3.52E-08	3.26	0.0130	0.41
450	3.91E-08	2.64	0.0144	0.45
400	4.40E-08	2.09	0.0162	0.51
350	5.03E-08	1.60	0.0186	0.58
300	5.86E-08	1.17	0.0216	0.68
250	7.04E-08	0.81	0.0260	0.82
200	8.79E-08	0.52	0.0325	1.02
150	1.17E-07	0.29	0.0433	1.36
100	1.76E-07	0.13	0.0649	2.04
50	3.52E-07	0.03	0.1299	4.09

Table B-12: Data generated for 1000 psi differential pressure and permeability of 0.5 mD

Lc	q	t	v	Re
ft	m³/s	hrs	m/s	
500	5.86E-08	1.96	0.0216	0.81
450	6.51E-08	1.58	0.0240	0.90
400	7.33E-08	1.25	0.0271	1.01
350	8.38E-08	0.96	0.0309	1.15
300	9.77E-08	0.70	0.0361	1.35
250	1.17E-07	0.49	0.0433	1.62
200	1.47E-07	0.31	0.0541	2.02
150	1.95E-07	0.18	0.0721	2.69
100	2.93E-07	0.08	0.1082	4.04
50	5.86E-07	0.02	0.2164	8.08

Table B-13: Data generated for 1500 psi differential pressure and permeability of 0.01 mD

Lc	q	t	v	Re
ft	m³/s	hrs	m/s	
<i>500</i>	1.57E-09	72.92	0.0006	7.39E-03
<i>450</i>	1.75E-09	59.07	0.0006	8.21E-03
<i>400</i>	1.97E-09	46.67	0.0007	9.24E-03
<i>350</i>	2.25E-09	35.73	0.0008	1.06E-02
<i>300</i>	2.62E-09	26.25	0.0010	1.23E-02
<i>250</i>	3.14E-09	18.23	0.0012	1.48E-02
<i>200</i>	3.93E-09	11.67	0.0015	1.85E-02
<i>150</i>	5.24E-09	6.56	0.0019	2.46E-02
<i>100</i>	7.86E-09	2.92	0.0029	3.70E-02
<i>50</i>	1.57E-08	0.73	0.0058	7.39E-02

Table B-14: Data generated for 1500 psi differential pressure and permeability of 0.1 mD

Lc	q	t	v	Re
ft	m³/s	hrs	m/s	
<i>500</i>	1.57E-08	7.29	0.0058	0.159
<i>450</i>	1.75E-08	5.91	0.0065	0.177
<i>400</i>	1.97E-08	4.67	0.0073	0.199
<i>350</i>	2.25E-08	3.57	0.0083	0.228
<i>300</i>	2.62E-08	2.63	0.0097	0.265
<i>250</i>	3.14E-08	1.82	0.0116	0.319
<i>200</i>	3.93E-08	1.17	0.0145	0.398
<i>150</i>	5.24E-08	0.66	0.0194	0.531
<i>100</i>	7.86E-08	0.29	0.0290	0.796
<i>50</i>	1.57E-07	0.07	0.0581	1.593

Table B-15: Data generated for 1500 psi differential pressure and permeability of 0.3 mD

Lc	q	t	v	Re
ft	m³/s	hrs	m/s	
<i>500</i>	4.72E-08	2.43	0.0174	0.69
<i>450</i>	5.24E-08	1.97	0.0194	0.77
<i>400</i>	5.90E-08	1.56	0.0218	0.86
<i>350</i>	6.74E-08	1.19	0.0249	0.98
<i>300</i>	7.86E-08	0.88	0.0290	1.15
<i>250</i>	9.43E-08	0.61	0.0348	1.38
<i>200</i>	1.18E-07	0.39	0.0435	1.72
<i>150</i>	1.57E-07	0.22	0.0581	2.30
<i>100</i>	2.36E-07	0.10	0.0871	3.45
<i>50</i>	4.72E-07	0.02	0.1742	6.89

Table B-16: Data generated for 1500 psi differential pressure and permeability of 0.5 mD

Lc	q	t	v	Re
ft	m³/s	hrs	m/s	
<i>500</i>	7.86E-08	1.46	0.0290	1.36
<i>450</i>	8.74E-08	1.18	0.0323	1.51
<i>400</i>	9.83E-08	0.93	0.0363	1.70
<i>350</i>	1.12E-07	0.71	0.0415	1.95
<i>300</i>	1.31E-07	0.53	0.0484	2.27
<i>250</i>	1.57E-07	0.36	0.0581	2.72
<i>200</i>	1.97E-07	0.23	0.0726	3.40
<i>150</i>	2.62E-07	0.13	0.0968	4.54
<i>100</i>	3.93E-07	0.06	0.1451	6.81
<i>50</i>	7.86E-07	0.01	0.2903	13.62

Appendix C: Governing Equations for the Numerical Model

The diffusivity equation was used to develop the leakage model in cement column. In this model, square pressure method was used to solve it numerically. In this section, a brief description on how this equation was utilized to model the leakage of gas. Diffusivity equation for linear flow on cartesian coordinates is given by:

$$\frac{\partial}{\partial x} \left(k_x \frac{\partial P^2}{\partial x} \right) + \frac{\partial}{\partial y} \left(k_y \frac{\partial P^2}{\partial y} \right) + \frac{\partial}{\partial z} \left(k_z \frac{\partial P^2}{\partial z} \right) = \varphi c_t \mu \frac{\partial P^2}{\partial t} \quad (C-1)$$

For simplification, only the discretization in the x-direction is going to be explained in detail. The other terms in the other directions follow the same steps. First of all, the solution domain is defined as it is shown below in Figure C-1.

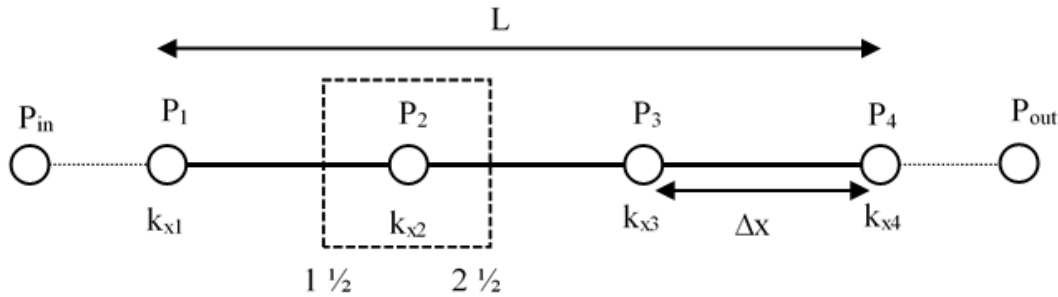


Figure C-1: Solution domain with a control volume on the second grid point

The number of grids (N_x) is given by:

$$N_x = \frac{L}{D_x} \quad (C-2)$$

where L is the length of x-direction, and D_x is the distance between two grids. To solve for the diffusivity equation, it will be discretized using finite volume method. Pressure distribution along

the points in x-direction will be solved implicitly. Now, P_2 inside the control volume in the dashed square will be solved. The diffusivity equation is to be integrated over the control volume as following:

$$\int \frac{\partial}{\partial x} \left(k_x \frac{\partial P}{\partial x} \right) dx = \int \varphi c_t \mu \frac{\partial P}{\partial t} dx \quad (C-3)$$

$$\left(k_x \frac{\partial P}{\partial x} \right) \Big|_{i=2\frac{1}{2}} - \left(k_x \frac{\partial P}{\partial x} \right) \Big|_{i=1\frac{1}{2}} = \varphi c_t \mu \Delta x \left(\frac{P_p^{n+1} - P_p^n}{\Delta t} \right) \quad (C-4)$$

At this point each term is solved individually as following:

$$\frac{\partial P}{\partial x} \Big|_{i=2\frac{1}{2}} = \frac{P_E - P_p}{\Delta x} \quad (C-5)$$

where P_E represent the pressure at the east direction, and it is P_3 for this point. P_p represent the pressure at this middle of this grid, which is P_2 .

$$\frac{\partial P}{\partial x} \Big|_{i=1\frac{1}{2}} = \frac{P_p - P_w}{\Delta x} \quad (C-6)$$

where P_w represent the pressure at the west direction, and it is P_1 for this point. Then, the permeability is for each point is calculated based on the geometric average:

$$k_{x\ 2\frac{1}{2}} = \frac{2 \Delta x}{\frac{\Delta x}{k_{x2}} + \frac{\Delta x}{k_{x3}}} \quad (C-7)$$

$$k_{x\ 1\frac{1}{2}} = \frac{2 \Delta x}{\frac{\Delta x}{k_{x1}} + \frac{\Delta x}{k_{x2}}} \quad (C-8)$$

After that, equations (C-5), (C-6), (C-7), and (C-8) are substituted in equation (C-4):

$$\frac{2 \Delta x}{\frac{\Delta x}{k_{x2}} + \frac{\Delta x}{k_{x3}}} \left(\frac{P_E^{n+1} - P_p^{n+1}}{\Delta x} \right) - \frac{2 \Delta x}{\frac{\Delta x}{k_{x1}} + \frac{\Delta x}{k_{x2}}} \left(\frac{P_p^{n+1} - P_w^{n+1}}{\Delta x} \right) = \frac{\varphi c_t \mu \Delta x}{\Delta t} (P_p^{n+1} - P_p^n) \quad (C-9)$$

where P^{n+1} is the pressure at the new time step, while P^n is the pressure at the previous time step.

Then, more simplification by rearranging the previous equation is done:

$$-a_w P_w^{n+1} + (a_w + a_E + a_{p_o}) P_p^{n+1} - a_E P_E^{n+1} = a_{p_o} P_p^n \quad (C-10)$$

$$a_w = \frac{2}{\frac{\Delta x}{k_{x1}} + \frac{\Delta x}{k_{x2}}} \quad (C-11)$$

$$a_E = \frac{2}{\frac{\Delta x}{k_{x2}} + \frac{\Delta x}{k_{x3}}} \quad (C-12)$$

$$a_{p_o} = \frac{\varphi c_t \mu}{\Delta t} \quad (C-13)$$

To simplify equation (C-10) new terms are introduced:

$$a_p = a_w + a_E + a_{p_o} \quad (C-14)$$

$$S = a_{p_o} P_p^n \quad (C-15)$$

where S represents the source term. The final equation is going to look like the following:

$$-a_w P_w^{n+1} + a_p P_p^{n+1} - a_E P_E^{n+1} = S \quad (C-16)$$

This procedure is valid for all the interior grid points. For the example shown here, this procedure is only valid for P_2 and P_3 . The procedure is quite different for the grid points adjacent to the boundary which are P_1 and P_4 in this example. To solve for the grid point, P_w will be equal to P_{in} , and P_E will be equal to P_2 as shown in Figure C-2. P_{in} is a constant in this situation, that is why the number of unknowns for this grid is going to reduce from three to two unknowns. In addition, since P_{in} is out of the domain, the permeability will go to infinity. Once this value is substituted in the geometric averaging equation, the average permeability will be:

$$k_{x\frac{1}{2}} = 2k_{x1} \quad (C-17)$$

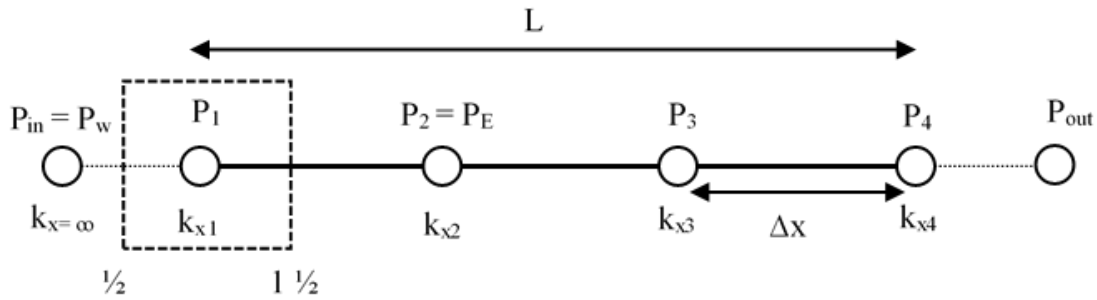


Figure C-2: Solution domain with a control volume on the first grid point

Then the a_w and the source terms become:

$$a_w = \frac{2k_{x1}}{\Delta x} \quad (C-18)$$

$$P_w = P_{in} \quad (C-19)$$

$$\hat{S} = a_w P_{in} + a_{p_o} P_p^n \quad (C-20)$$

$$\dot{S} = a_w P_{in} + S \quad (C-21)$$

Then, the final equation for the first grid point is going to be:

$$a_P P_p^{n+1} - a_E P_E^{n+1} = \dot{S} \quad (C-22)$$

After finding all the coefficients for each grid, it becomes easier to find the pressure distribution for all the grid points at different time steps. These coefficients are assigned to a matrix (A) and the source terms are assigned to a matrix (S) as following:

$$A = \begin{bmatrix} a_P & -a_E & 0 & 0 \\ -a_w & a_P & -a_E & 0 \\ 0 & -a_w & a_P & -a_E \\ 0 & 0 & -a_w & a_P \end{bmatrix} \quad (C-23)$$

$$S = \begin{bmatrix} \dot{S}_1 \\ S_2 \\ S_3 \\ \dot{S}_4 \end{bmatrix} \quad (C-24)$$

$$\begin{bmatrix} a_P & -a_E & 0 & 0 \\ -a_w & a_P & -a_E & 0 \\ 0 & -a_w & a_P & -a_E \\ 0 & 0 & -a_w & a_P \end{bmatrix} \begin{bmatrix} P_1 \\ P_2 \\ P_3 \\ P_4 \end{bmatrix} = \begin{bmatrix} \dot{S}_1 \\ S_2 \\ S_3 \\ \dot{S}_4 \end{bmatrix} \quad (C-25)$$

Finally, the pressure at each grid point can be calculated by inverting the matrix as following:

$$P = A \setminus S \quad (C-26)$$

All the procedure presented in this section is for 1D diffusivity equation. For 2D and 3D, the procedure will be the same for the other directions. Each direction will have two new coefficients. In the model presented in this report, 2D diffusivity equation was used. For the y-direction, (a_N) and (a_S) were used as the coefficients for this direction, where (a_N) and (a_S) stand for north and south coefficients, respectively. (a_T) and (a_B) were used for the z-direction, where (a_T) and (a_B) stand for top and bottom coefficients, respectively.

Appendix D: Leakage Scenarios Developed by the Numerical Model

The leakage scenarios presented in this appendix were developed using the input data listed in Table 5-6. These leakage scenarios were summarized in Figure 5-16.

For Microannulus gap size of 50 μm :

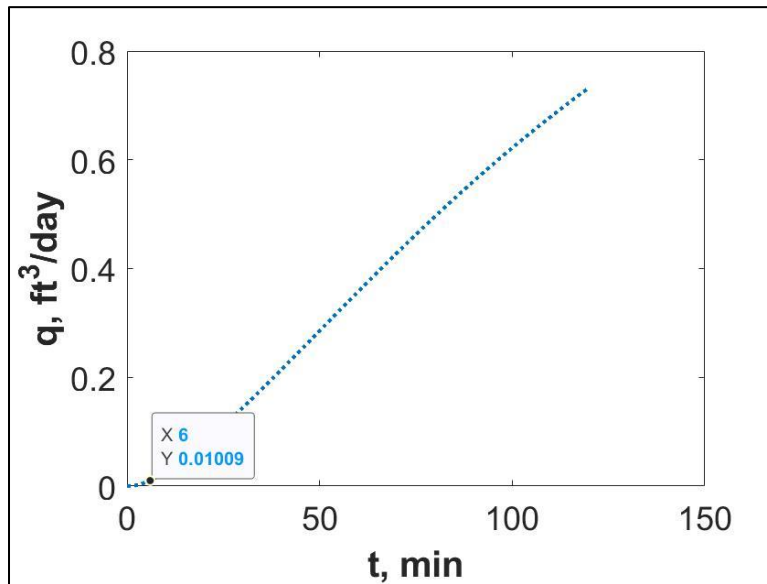


Figure D-1: Leakage scenario for 50 ft of casing-liner overlap (flow rate at 1000 psi and 110 °F)

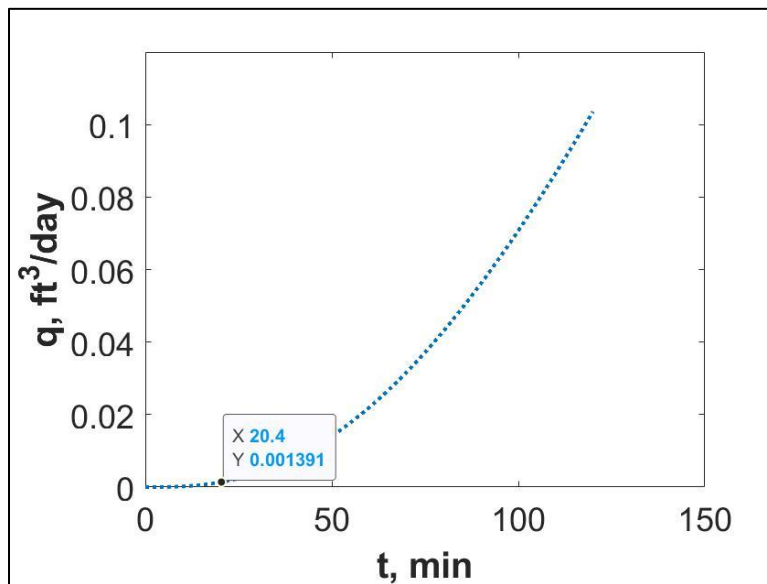


Figure D-2: Leakage scenario for 100 ft of casing-liner overlap (flow rate at 1000 psi and 110 °F)

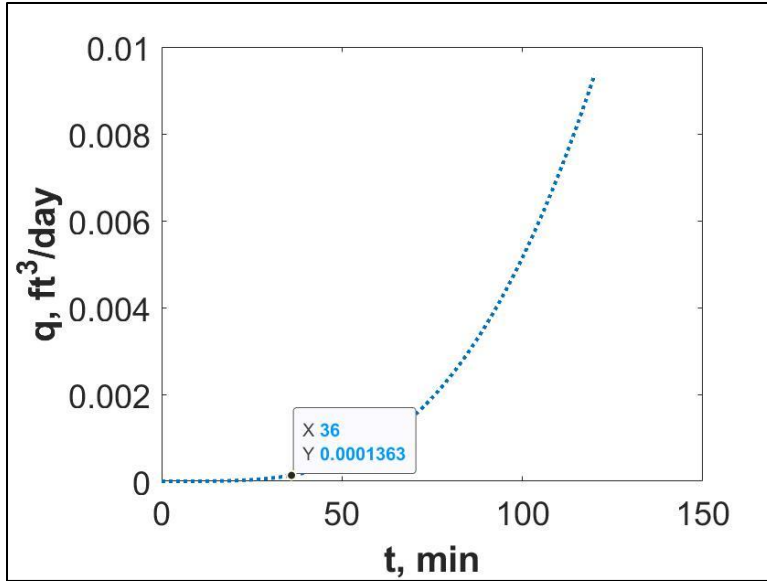


Figure D-3: Leakage scenario for 150 ft of casing-liner overlap (flow rate at 1000 psi and 110 °F)

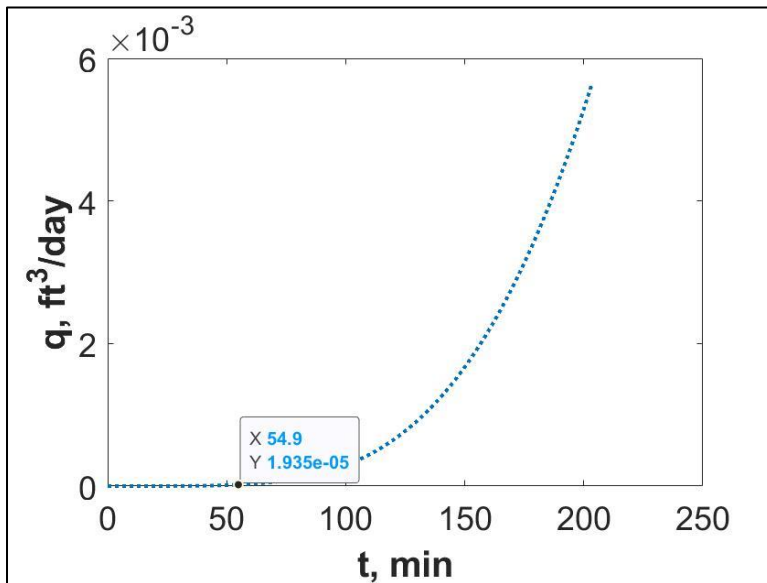


Figure D-4: Leakage scenario for 200 ft of casing-liner overlap (flow rate at 1000 psi and 110 °F)

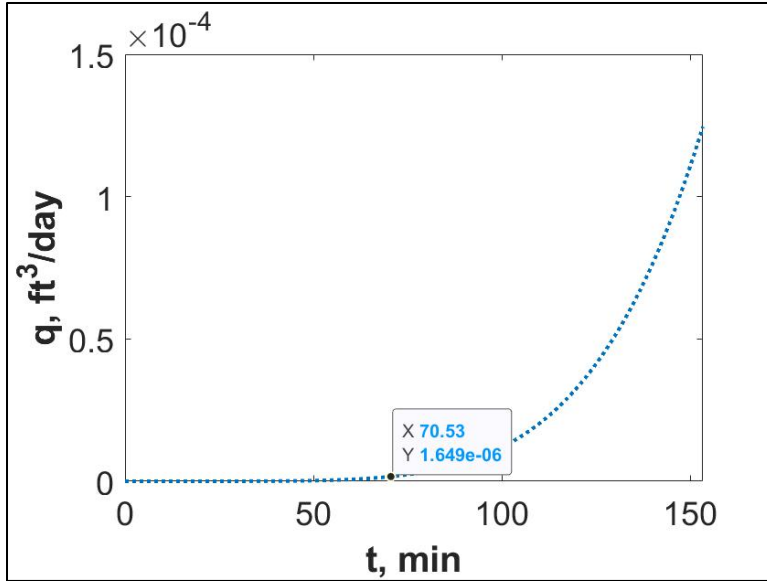


Figure D-5: Leakage scenario for 250 ft of casing-liner overlap (flow rate at 1000 psi and 110 °F)

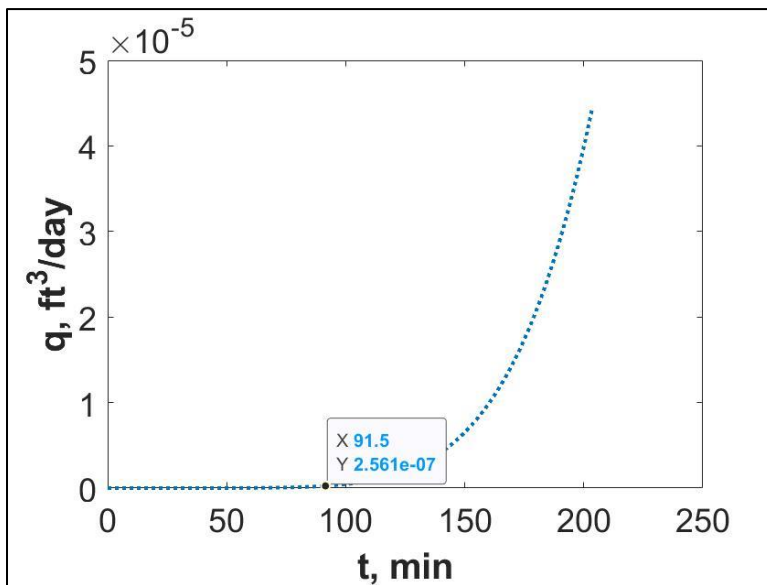


Figure D-6: Leakage scenario for 300 ft of casing-liner overlap (flow rate at 1000 psi and 110 °F)

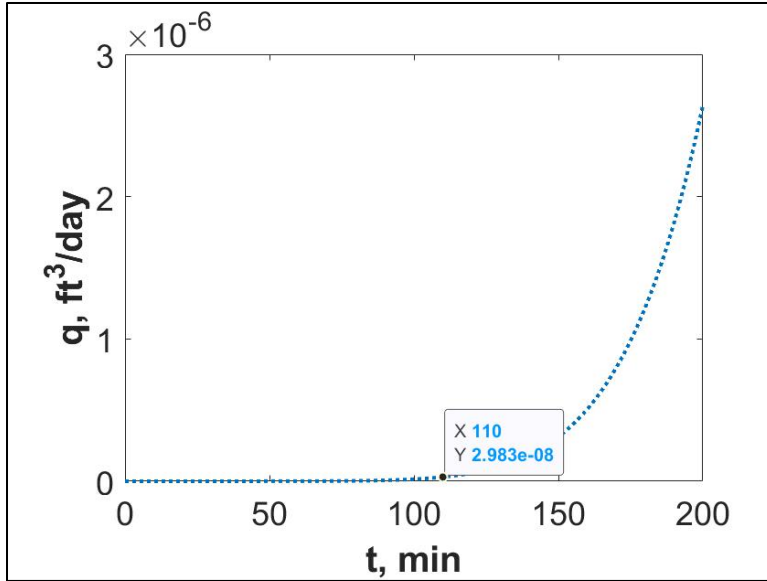


Figure D-7: Leakage scenario for 350 ft of casing-liner overlap (flow rate at 1000 psi and 110 °F)

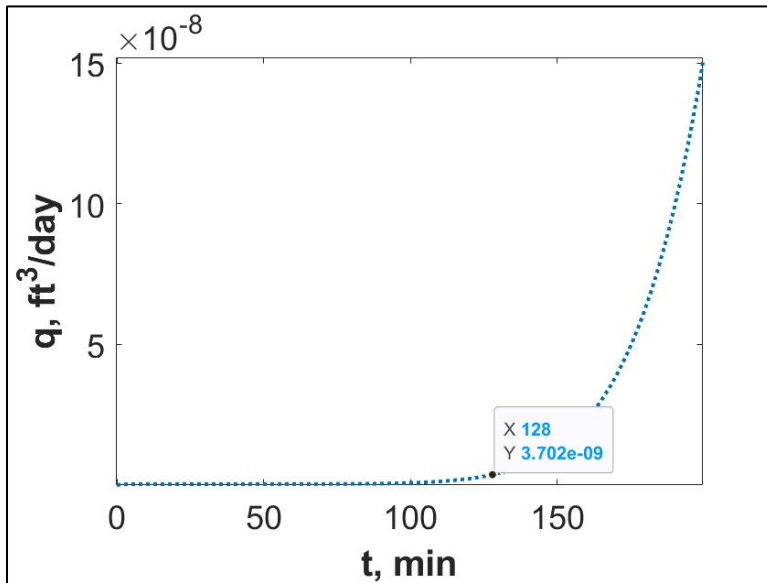


Figure D-8: Leakage scenario for 400 ft of casing-liner overlap (flow rate at 1000 psi and 110 °F)

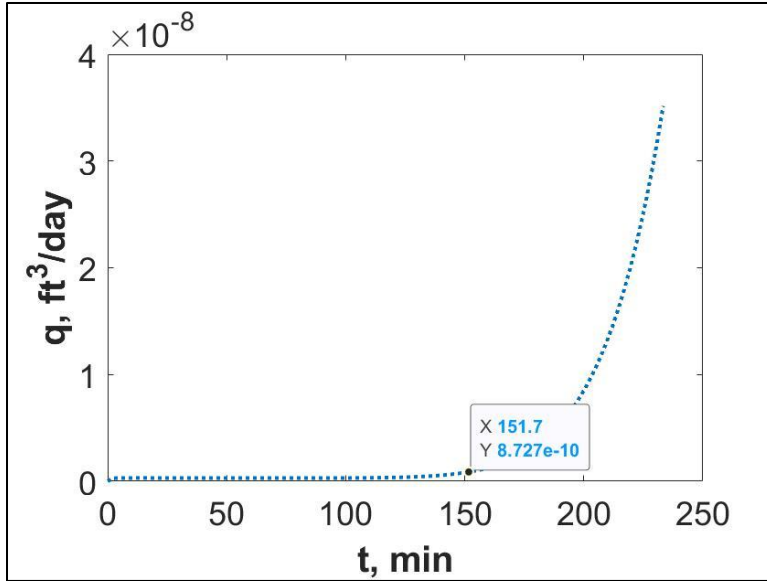


Figure D-9: Leakage scenario for 450 ft of casing-liner overlap (flow rate at 1000 psi and 110 °F)

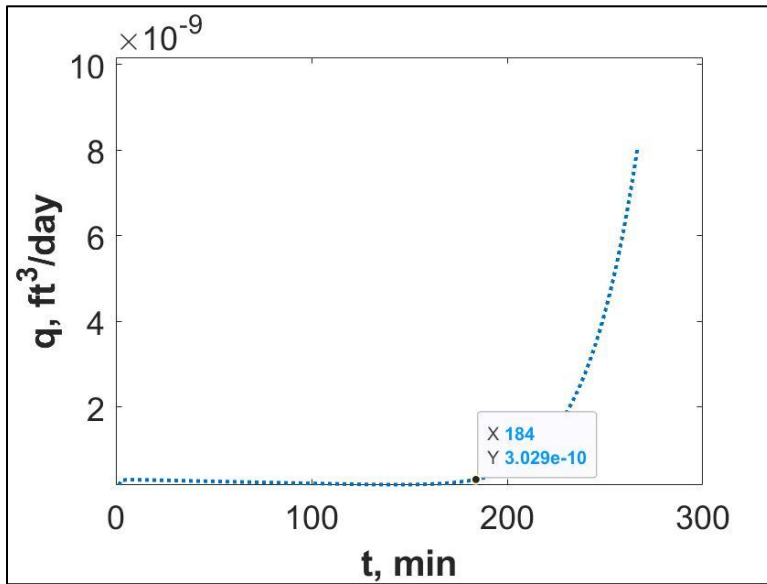


Figure D-10: Leakage scenario for 500 ft of casing-liner overlap (flow rate at 1000 psi and 110 °F)

For Microannulus gap size of 75 μm :

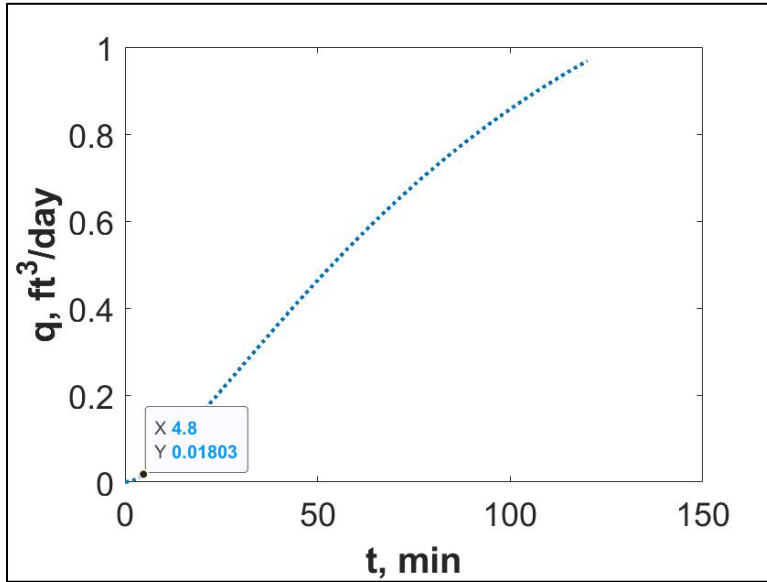


Figure D-11: Leakage scenario for 50 ft of casing-liner overlap (flow rate at 1000 psi and 110 °F)

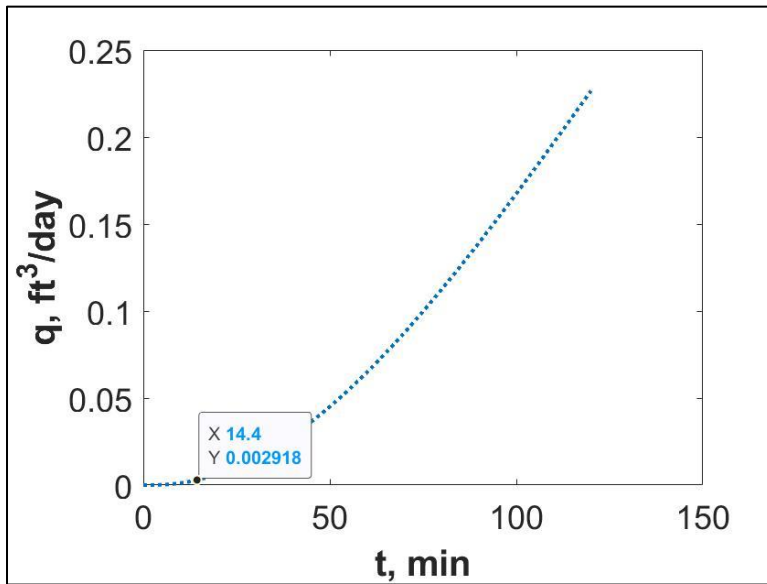


Figure D-12: Leakage scenario for 100 ft of casing-liner overlap (flow rate at 1000 psi and 110 °F)

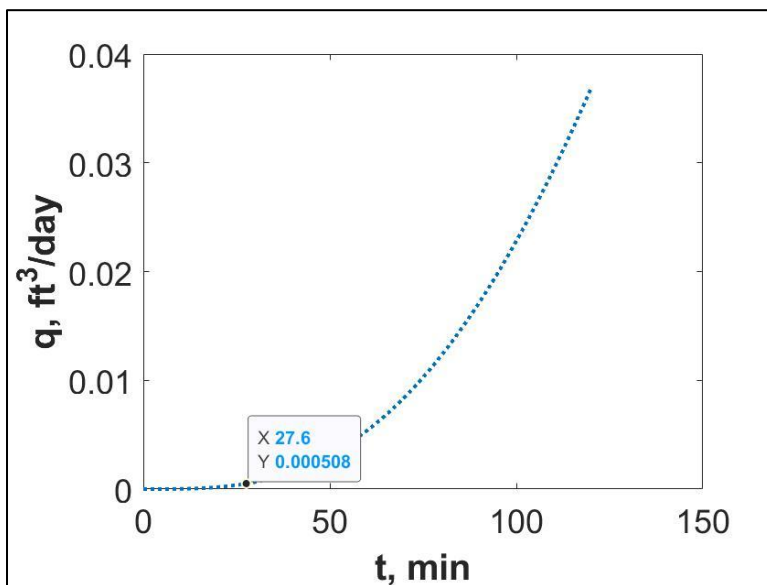


Figure D-13: Leakage scenario for 150 ft of casing-liner overlap (flow rate at 1000 psi and 110 °F)

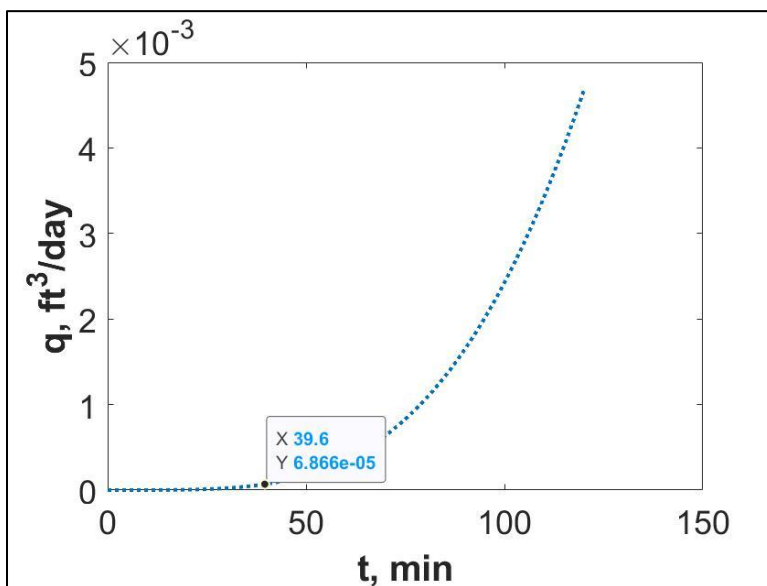


Figure D-14: Leakage scenario for 200 ft of casing-liner overlap (flow rate at 1000 psi and 110 °F)

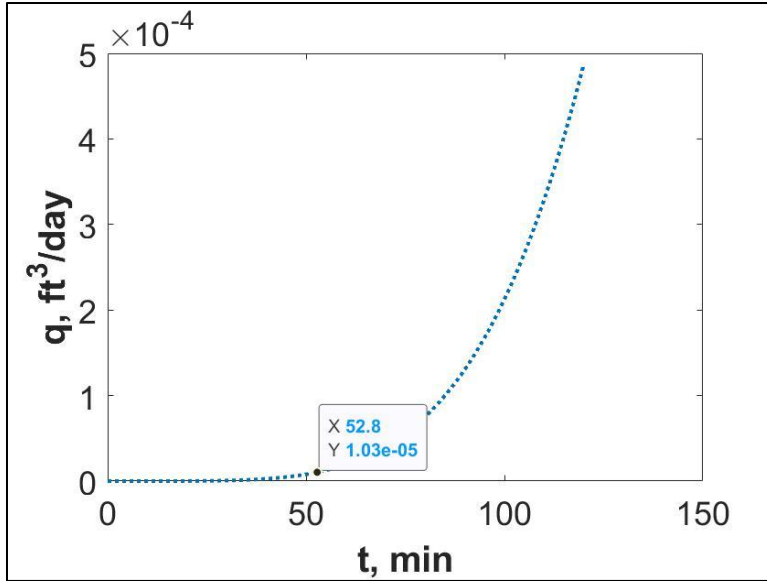


Figure D-15: Leakage scenario for 250 ft of casing-liner overlap (flow rate at 1000 psi and 110 °F)

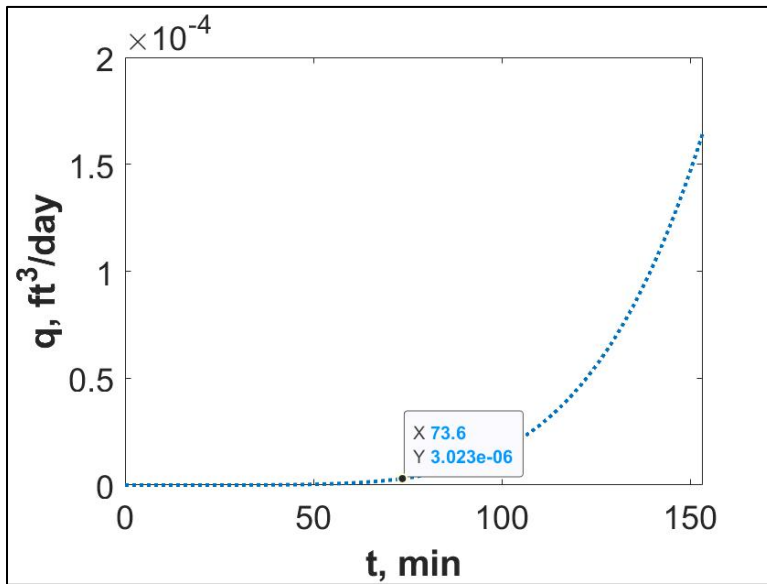


Figure D-16: Leakage scenario for 300 ft of casing-liner overlap (flow rate at 1000 psi and 110 °F)

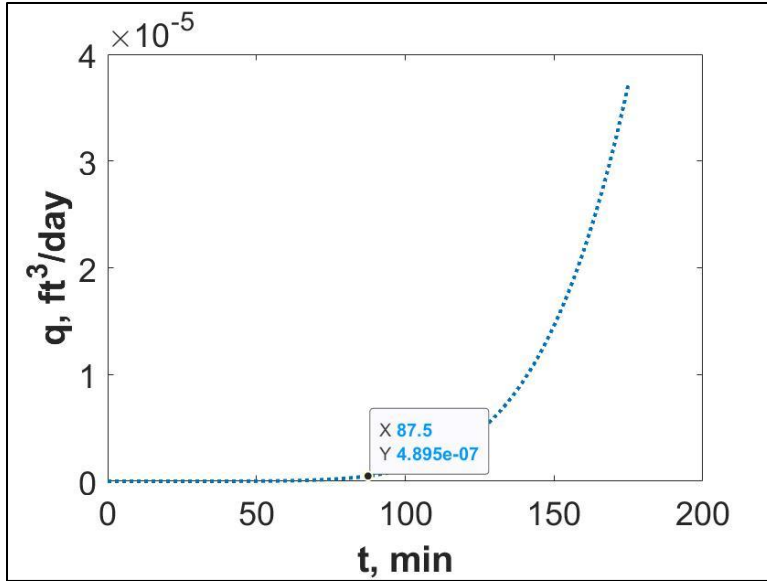


Figure D-17: Leakage scenario for 350 ft of casing-liner overlap (flow rate at 1000 psi and 110 °F)

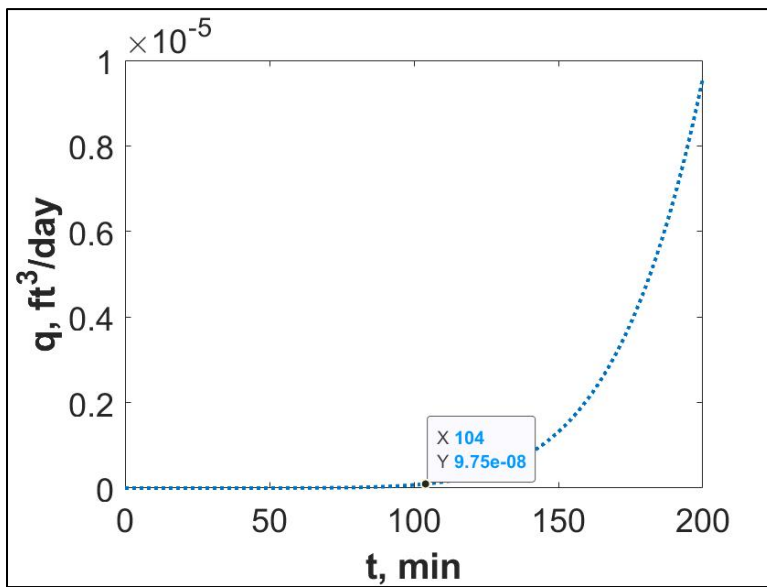


Figure D-18: Leakage scenario for 400 ft of casing-liner overlap (flow rate at 1000 psi and 110 °F)

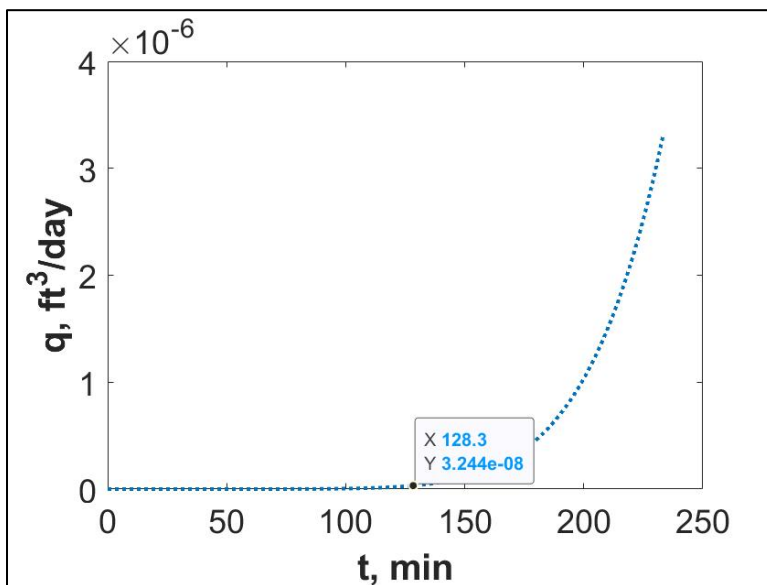


Figure D-19: Leakage scenario for 450 ft of casing-liner overlap (flow rate at 1000 psi and 110 °F)

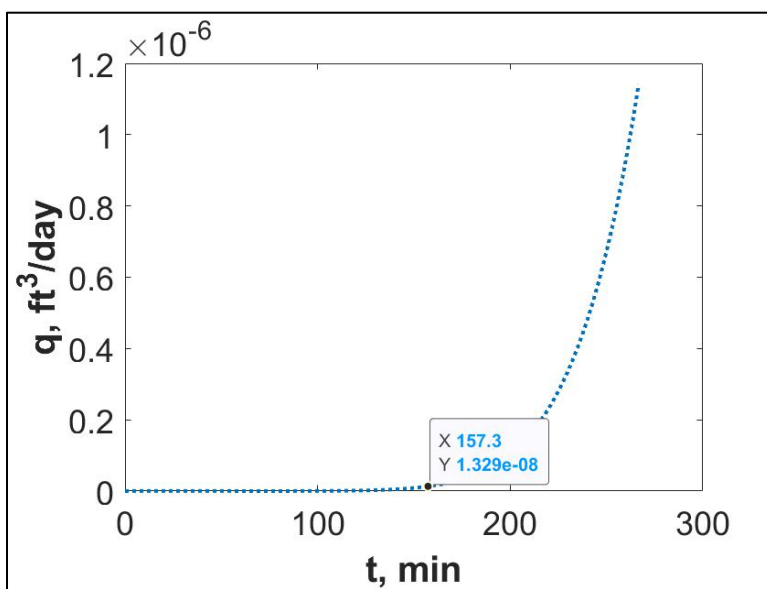


Figure D-20: Leakage scenario for 500 ft of casing-liner overlap (flow rate at 1000 psi and 110 °F)

For Microannulus gap size of 75 μm :

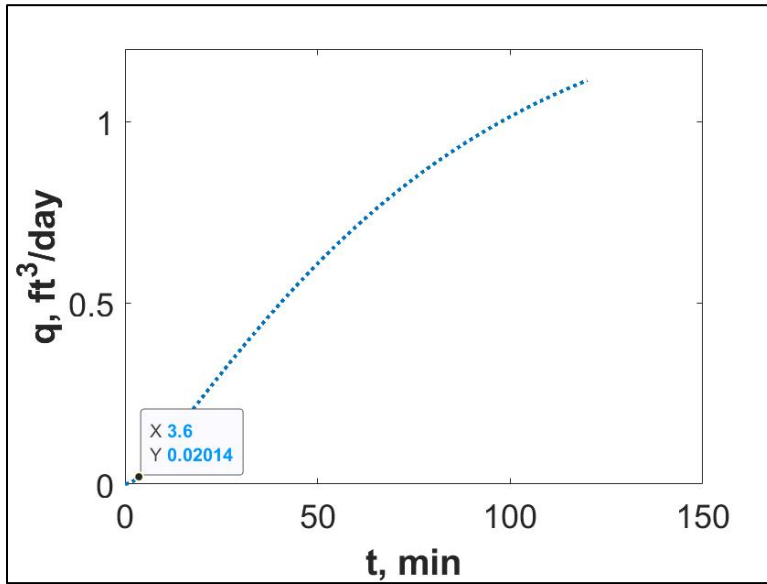


Figure D-21: Leakage scenario for 50 ft of casing-liner overlap (flow rate at 1000 psi and 110 °F)

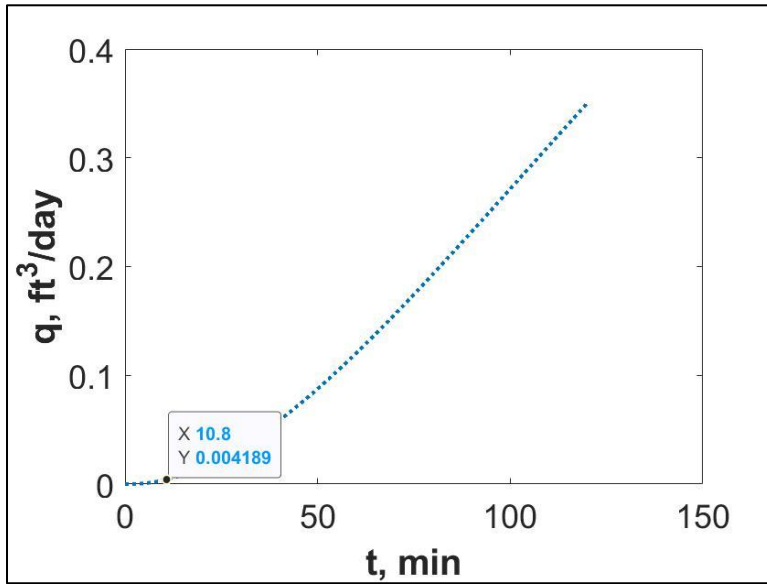


Figure D-22: Leakage scenario for 100 ft of casing-liner overlap (flow rate at 1000 psi and 110 °F)

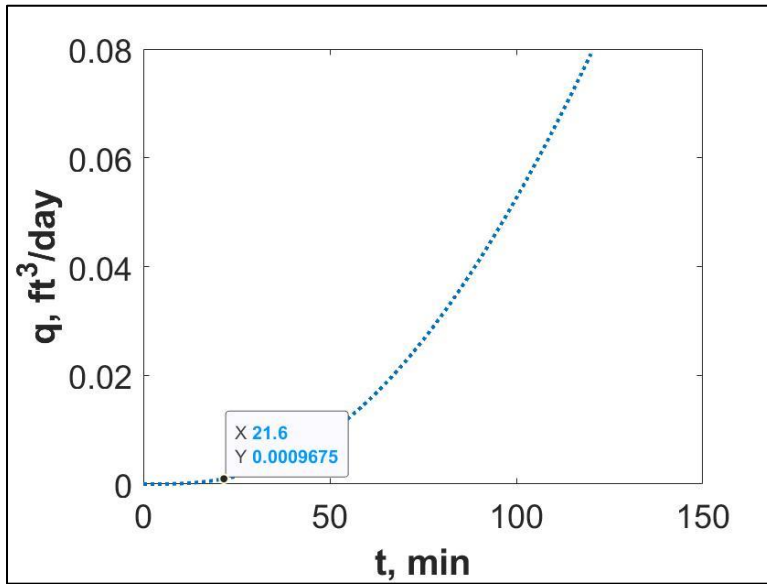


Figure D-23: Leakage scenario for 150 ft of casing-liner overlap (flow rate at 1000 psi and 110 °F)

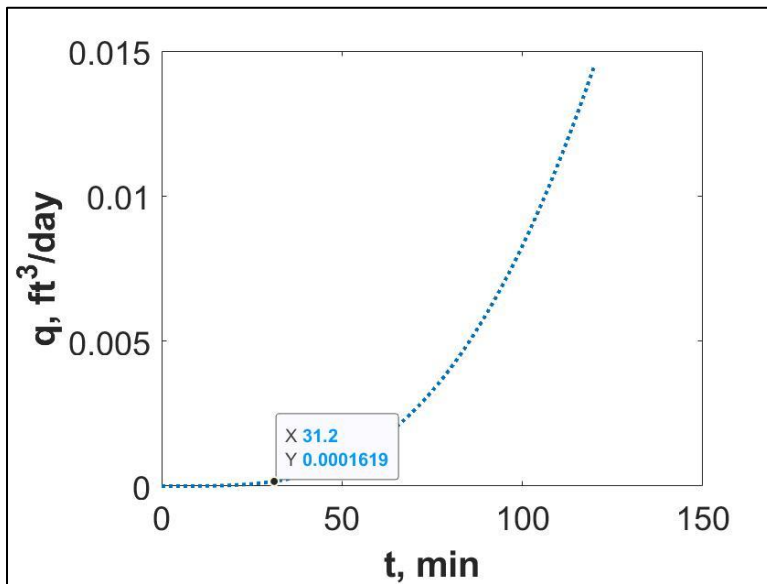


Figure D-24: Leakage scenario for 200 ft of casing-liner overlap (flow rate at 1000 psi and 110 °F)

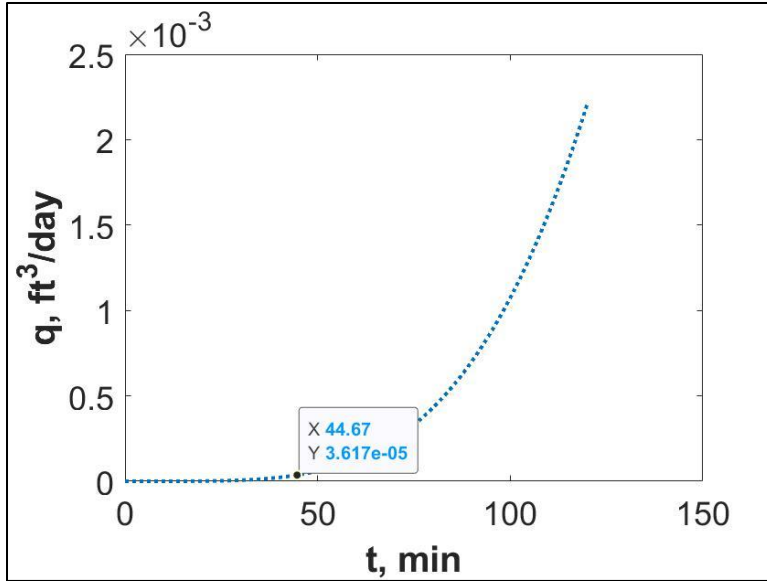


Figure D-25: Leakage scenario for 250 ft of casing-liner overlap (flow rate at 1000 psi and 110 °F)

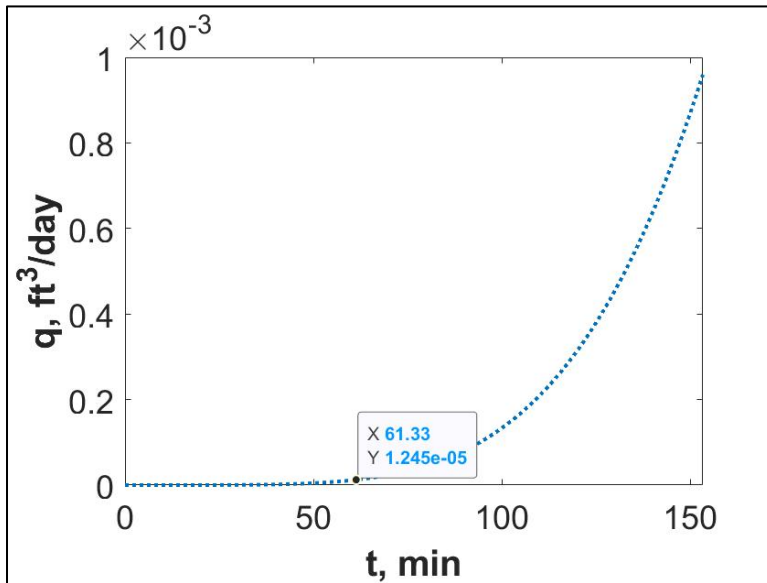


Figure D-26: Leakage scenario for 300 ft of casing-liner overlap (flow rate at 1000 psi and 110 °F)

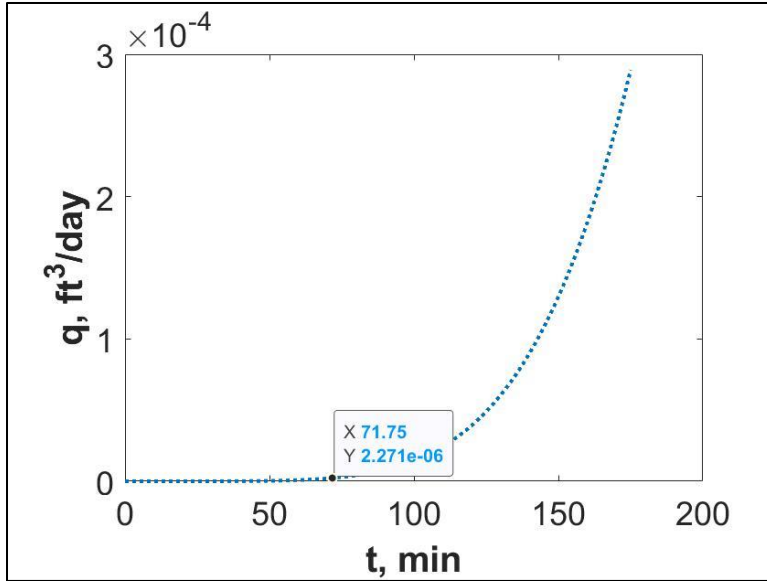


Figure D-27: Leakage scenario for 350 ft of casing-liner overlap (flow rate at 1000 psi and 110 °F)

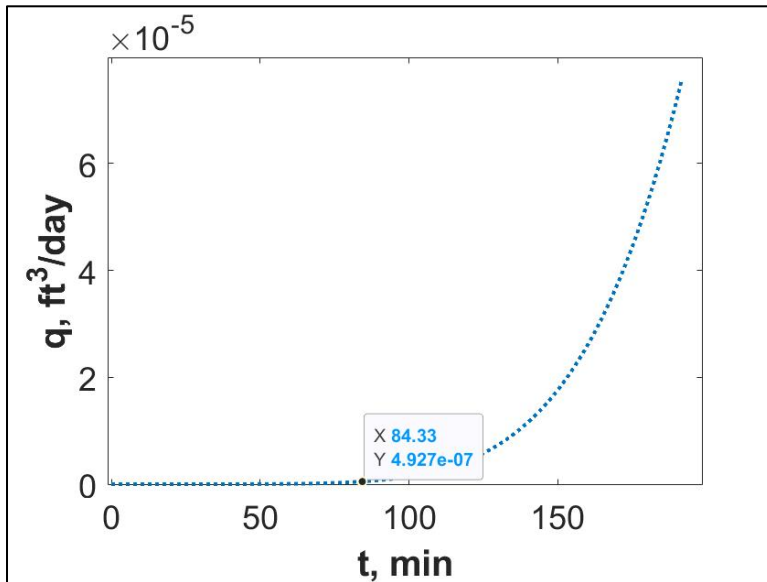


Figure D-28: Leakage scenario for 400 ft of casing-liner overlap (flow rate at 1000 psi and 110 °F)

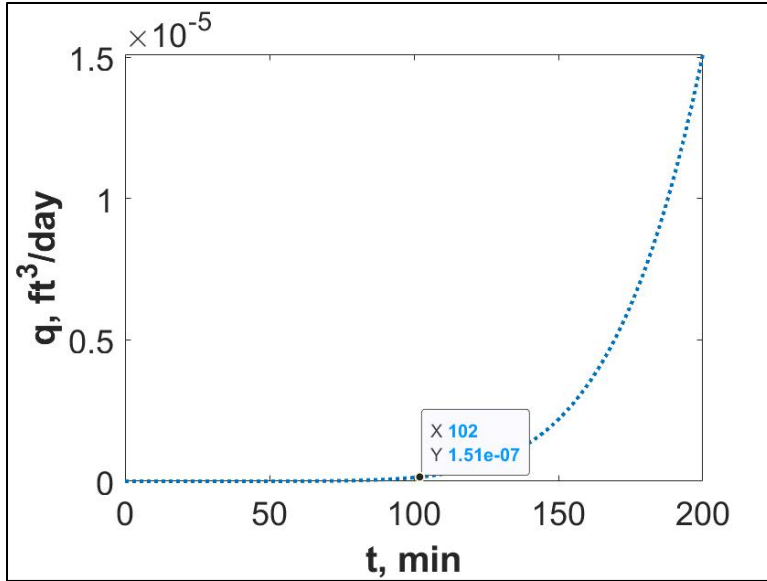


Figure D-29: Leakage scenario for 450 ft of casing-liner overlap (flow rate at 1000 psi and 110 °F)

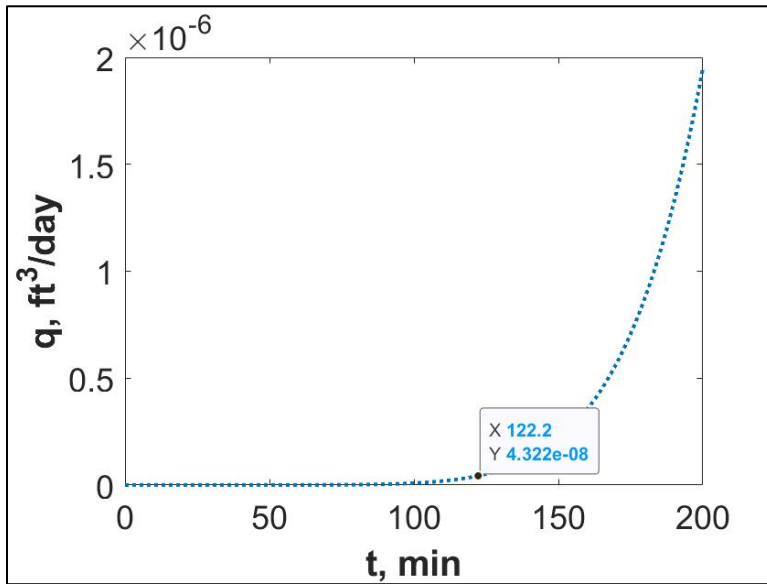


Figure D-30: Leakage scenario for 500 ft of casing-liner overlap (flow rate at 1000 psi and 110 °F)